BIOLOGICAL AND MECHANICAL PERFORMANCE OF TI-6AL-4V IMPLANT SUPERPLASTICALLY EMBEDDED WITH HYDROXYAPATITE IN ANIMAL

HIDAYAH BINTI MOHD KHALID

FACULTY OF ENGINEERING
UNIVERSITY OF MALAYA
KUALA LUMPUR

2018

BIOLOGICAL AND MECHANICAL PERFORMANCE OF TI-6AL-4V IMPLANT SUPERPLASTICALLY EMBEDDED WITH HYDROXYAPATITE IN ANIMAL

HIDAYAH BINTI MOHD KHALID

THESIS SUBMITTED IN FULFILMENT OF THE REQUIREMENTS FOR THE DEGREE OF DOCTOR OF PHILOSOPHY

FACULTY OF ENGINEERING
UNIVERSITY OF MALAYA
KUALA LUMPUR

2018

UNIVERSITY OF MALAYA

ORIGINAL LITERARY WORK DECLARATION

Name of Candidate: HIDAYAH BINTI MOHD KHALID

Matric No: KHA110117

Name of Degree: DOCTOR OF PHILOSOPHY

Title of Project Paper/Research Report/Dissertation/Thesis ("this Work"):

BIOLOGICAL AND MECHANICAL PERFORMANCE OF TI-6AL-4V IMPLANT SUPERPLASTICALLY EMBEDDED WITH HYDROXYAPATITE IN ANIMAL

Field of Study: ADVANCED MATERIALS/NANOMATERIALS

I do solemnly and sincerely declare that:

(1) I am the sole author/writer of this Work;
(2) This Work is original;
(3) Any use of any work in which copyright exists was done by way of fair dealing and for permitted purposes and any excerpt or extract from, or reference to or reproduction of any copyright work has been disclosed expressly and sufficiently and the title of the Work and its authorship have been acknowledged in this Work;
(4) I do not have any actual knowledge nor do I ought reasonably to know that the making of this work constitutes an infringement of any copyright work;
(5) I hereby assign all and every rights in the copyright to this Work to the University of Malaya ("UM"), who henceforth shall be owner of the copyright in this Work and that any reproduction or use in any form or by any means whatsoever is prohibited without the written consent of UM having been first had and obtained;
(6) I am fully aware that if in the course of making this Work I have infringed any copyright whether intentionally or otherwise, I may be subject to legal action or any other action as may be determined by UM.

Candidate's Signature Date:

Subscribed and solemnly declared before,

Witness's Signature Date:

Name:

Designation:

UNIVERSITI MALAYA

PERAKUAN KEASLIAN PENULISAN

Nama: HIDAYAH BINTI MOHD KHALID

No. Matrik: KHA110117

Nama Ijazah: IJAZAH SARJANA KEDOKTORAN

Tajuk Kertas Projek/Laporan Penyelidikan/Disertasi/Tesis ("Hasil Kerja ini"):

KEUPAYAAN BIOLOGI DAN MEKANIKAL IMPLAN TI-6AL-4V YANG DI TANAM DENGAN HYDROXYAPATITE SECARA SUPERPLASTIC DI DALAM HAIWAN

Bidang Penyelidikan: BAHAN TERMAJU/ BAHAN NANO

Saya dengan sesungguhnya dan sebenarnya mengaku bahawa:

(1) Saya adalah satu-satunya pengarang/penulis Hasil Kerja ini;
(2) Hasil Kerja ini adalah asli;
(3) Apa-apa penggunaan mana-mana hasil kerja yang mengandungi hakcipta telah dilakukan secara urusan yang wajar dan bagi maksud yang dibenarkan dan apa-apa petikan, ekstrak, rujukan atau pengeluaran semula daripada atau kepada mana-mana hasil kerja yang mengandungi hakcipta telah dinyatakan dengan sejelasnya dan secukupnya dan satu pengiktirafan tajuk hasil kerja tersebut dan pengarang/penulisnya telah dilakukan di dalam Hasil Kerja ini;
(4) Saya tidak mempunyai apa-apa pengetahuan sebenar atau patut semunasabahnya tahu bahawa penghasilan Hasil Kerja ini melanggar suatu hakcipta hasil kerja yang lain;
(5) Saya dengan ini menyerahkan kesemua dan tiap-tiap hak yang terkandung di dalam hakcipta Hasil Kerja ini kepada Universiti Malaya ("UM") yang seterusnya mula dari sekarang adalah tuan punya kepada hakcipta di dalam Hasil Kerja ini dan apa-apa pengeluaran semula atau penggunaan dalam apa jua bentuk atau dengan apa juga cara sekalipun adalah dilarang tanpa terlebih dahulu mendapat kebenaran bertulis dari UM;
(6) Saya sedar sepenuhnya sekiranya dalam masa penghasilan Hasil Kerja ini saya telah melanggar suatu hakcipta hasil kerja yang lain sama ada dengan niat atau sebaliknya, saya boleh dikenakan tindakan undang-undang atau apa-apa tindakan lain sebagaimana yang diputuskan oleh UM.

Tandatangan Calon Tarikh:

Diperbuat dan sesungguhnya diakui di hadapan,

Tandatangan Saksi Tarikh:

Nama:

Jawatan:

BIOLOGICAL AND MECHANICAL PERFORMANCE OF TI-6AL-4V IMPLANT SUPERPLASTICALLY EMBEDDED WITH HYDROXYAPATITE IN ANIMAL ABSTRACT

The bioactivity, biocompatibility and durability of two types of Ti-6Al-4V implants embedded with hydroxyapatite (HA), i.e. superplastic embedment (SPE) and superplastic deformation (SPD) implants are studied and compared with the as-received titanium. The samples were implanted subcutaneously on the backs of Sprague Dawley (SD) rat models for 1, 5 and 12 weeks. Wear tests were conducted to evaluate the durability of the HA layers. The HA layer thickness for the SPE and SPD samples increased from 249.1±0.6 nm to 874.8±13.7 nm, and from 206.1±5.8 nm to 1162.7±7.9 nm respectively, after 12 weeks of implantation. The SPD sample exhibited much faster growth of newly formed HA compared to SPE. The growth of the newly formed HA was strongly dependent on the degree of HA crystallinity in the initial HA layer. After 12 weeks of implantation, the surface hardness value of the SPE and SPD samples decreased from 661±0.4 HV to 586±1.3 HV and from 585±6.6 HV to 425±86.9 HV respectively. The decrease in surface hardness values was due to the newly formed HA layer that was more porous than the initial HA layer. However, the values were still higher than the substrate surface hardness of 321±28.8 HV. According to a histological evaluation, the SPD sample exhibited the best biocompatibility where the space left by the removed implant was almost completely filled with fibrous tissue. This suggests that more bioactive HA layer accelerated the body system's response to the SPD sample. The wear test indicates that to some extent both SPE and SPD samples were able to withstand the durability test. The SPD sample adequately strengthened the newly-formed HA layer, indicating the best durability test result. This study confirms that the

bioactivity, biocompatibility and durability results demonstrate the potential of the SPD sample for medical implant applications.

Keywords: Biomaterials; Implantation; Bioactivity; Biocompatibility; Mechanical properties

KEUPAYAAN BIOLOGI DAN MEKANIKAL BAGI IMPLAN TI-6AL-4V YANG DI TANAM DENGAN HYDROXYAPATITE SECARA SUPERPLASTIC DI DALAM HAIWAN

ABSTRAK

Kadar tindakbalas bioaktif , keserasian biologi dan ketahanan dua jenis implan Ti-6Al-4V yang ditanam dengan hydroxyapatite (HA) iaitu jenis superplastically embedded(SPE) dan superplastically deformed (SPD) telah dikaji dan dibuat perbandingan dengan Titanium asli. Sampel-sampel telah ditanam secara subcutaneous pada belakang tikus jenis Sprague Dawley dengan kadar 1,5, dan 12 minggu. Ujian kehausan telah dijalankan bagi membuat penilaian terhadap ketahanan lapisan HA. Ketebalan lapisan HA bagi kedua-dua sampel jenis sampel SPE dan SPD telah bertambah selepas ditanam selama 12 minggu iaitu masing-masing daripada 249.1±0.6 nm kepada 874.8±13.7 nm dan 206.1±5.8 nm kepada 1162.7±7.9 . Sampel jenis SPD telah menunjukkan kadar pertumbuhan HA baru yang lebih tinggi daripada sampel jenis SPE. Kadar pertumbuhan HA baru adalah bergantung kepada tahap ketulenan lapisan HA yang awal. Selepas tempoh penanaman 12 minggu , kadar kekerasan permukaan sampel SPE dan SPD masing-masing telah berkurangan 661±0.4 HV kepada 586±1.3 HV dan daripada 585±6.6 HV kepada 425±86.9 HV. Pengurangan kekerasan permukaan ini adalah disebabkan wujudnya lapisan HA baru yang lebih berliang(poros) daripada lapisan HA yang awal.Walaubagaimanapun , nilai ini adalah lebih tinggi daripada kekerasan substrat iaitu 321±28.8 HV. Berdasarkan penilaian histologi, sampel SPD menunjukkan kadar keserasian biologi. Berdasarkan kepada penilaian histologi, sampel SPD menunjukkan keserasian biologi pada bahagian di mana implan telah dikeluarkan dan dipenuhi dengan tisu gentian. Perkara ini menunjukkan lapisan HA yang lebih bioaktif mempercepat kadar tindakbalas badan kepada sampel SPD. Ujian

kehausan menunjukkan kedua-dua sampel SPE dan SPD mampu bertahan darjah ujian ketahanan yang tertentu. Sampel SPD telah meneguhkan dengan kadar yang secukupnya lapisan HA yang baru dibentuk dan menunjukkan keputusan yang lebih baik. Kajian ini membuktikan tindakbalas bioaktif, keserasian biologi dan keputusan ketahanan menunjukkan potensi penggunaan implan SPD bagi tujuan perubatan.

Kata kunci: Biomaterials; Implantation; tindakbalas bioaktif; keserasian biologi; Mechanical properties

ACKNOWLEDGEMENTS

All Praise be to Allah S.W.T for granting me the knowledge, health, patience and perseverance which enabled me to complete this thesis.

My sincere gratitude goes to my supervisor, Dr.Isawadi bin Jauhari, for his persistent guidance, advice, help, and support which leads to the successful completion of this thesis. Special thanks to veterinary at Animal Experimental Unit (AEU), Faculty of Medicine, Dr. Haryanti Azura binti Mohamad Wali, for granting me the opportunity to gain invaluable experience, as well as for sharing her knowledge and guidance during the surgery session.

My warmest appreciation goes to Mrs. Latifah from Histopathology lab of University Putra Malaysia, Mr. Nazarul Zaman from FESEM lab of University of Malaya and all staff from AEU for their technical assistance in this dissertation.

My deepest gratitude goes to my family, especially my husband, my children and my parents, for their endless prayers and support in my study. I am also indebted to my beloved siblings, for their love and moral support.

My heartfelt thanks to my lab members, for their moral support and encouragement in the “thick and thin”. I am also grateful to all the unnamed people, who have directly or indirectly helped me in completing my research.

Last but not least, I would like to express my appreciation to UM for financing my research project, under the PPP Fund (Project No. PG076-2014B). I am also indebted to MyPhD scheme for granting me the scholarship.

TABLE OF CONTENTS

LIST OF FIGURES

LIST OF TABLES

LIST OF SYMBOLS AND ABBREVIATIONS

Symbols

σ	:	Flow stress
K	:	Constant
$\acute{\varepsilon}$	:	Strain rate
m	:	Strain-rate sensitivity
ε	:	Strain
β	:	Beta
α	:	Alpha
ω	:	Widmenstätten
p	:	Probability

Abbreviations

Ti-6Al-4V	:	Titanium alloy
HA	:	Hydroxyapatite
SPE	:	Superplastic embedment
SPD	:	Superplastic deformation
SD	:	Sprague dawley
Zn-Al	:	Zinc aluminium
Cd-Zn	:	Cadmium zinc
Bi-Sn	:	Bismuth tin
GBS	:	Grain boundary sliding
SPF-DB	:	Superplastic forming diffusion bonding
HCP	:	Hexagonal-close-packed
BCC	:	Body-centered-cubic
CP	:	Commercially pure
TMP	:	Thermo-mechanical processing
Ti	:	Titanium
Al_2O_3	:	Aluminium oxide
ZrO_2	:	Zirconia
Si_3N_4	:	Silicon nitride
SiC	:	Silicon carbide
B_4C	:	Boron carbide
UHMWPE	:	Ultra-high molecular weight polyethylene
PTFE	:	Polytetrafluoroethylene
HCL	:	Hydrochloric acid
HF	:	Hydrogen flouride
HNO_3	:	Nitric acid

AAALAC	:	Association for Assessment and Accreditation of Laboratory Animal Care
RO	:	Reverse osmosis
IACUC	:	Institutional Animal Care and Use Committee
CO_2	:	Carbon dioxide
NBF	:	Neutral-buffered formalin
FESEM	:	Field emission scanning electron microscopy
EDX	:	Energy-dispersive X-ray spectroscopy
XRD	:	X-ray diffraction
FE	:	Field emission

LIST OF APPENDICES

CHAPTER 1: INTRODUCTION

1.1 Background

Orthopaedic and dental applications have amplified significantly in current years owing to osteoporosis, bone damage from car/sport accidents and cancer, together with the need for dental/facial reconstruction (Balazic, Kopac, Jackson, & Ahmed, 2007). Thus, artificial hard tissue replacement implants should integrate well into the musculoskeletal system without causing fibrosis of the connective tissue in the system . For this reason, since the early 1960s concurrent studies have focused on the development of bioactive materials used bare (without coating) or sometimes with a coating layer (Hieda et al., 2014; Watari et al., 2004). The ultimate goal of the successful fixation of cementless implants used for joint reconstruction is to obtain life-long, secure implant anchoring in the native surrounding bone (Lakstein et al., 2009).

Titanium (Ti) and its alloys have been utilized as medical devices, with Ti-6Al-4V being among the most commonly employed. This is due to its excellent combination of biocompatibility and good mechanical properties (Bigi et al., 2008; J. Chen et al., 2007; X.-h. Wang, Li, Hu, Kou, & Zhou, 2013). Nevertheless, the incidence of bone implant interface failure due to ineffective osteointegration with the host tissue is still high (Liang, Shi, Fairchild, & Cale, 2004; Lin et al., 2007) and the accumulation of metal ions in the surrounding tissue is reported in long-term implantation, which adversely affects bone tissue growth (Fukuda et al., 2011). Bioactivity is widely viewed as an essential requirement for an artificial biomaterial to exhibit chemical bonding to living host tissues upon bone formation, like apatite layer formation on the material's surface in any simulated body environment (Forsgren, Svahn, Jarmar, & Engqvist, 2007; Yoshida et al., 2012). A bioactive surface can be achieved by coating the metal surface with a thin film of bioactive ceramic such as hydroxyapatite (HA). HA exhibits extended responsiveness as a coating material on titanium surfaces because its

roughness increases the surface contact 5-fold compared to smooth implants, and it closely resembles the natural minerals in bones and teeth (Cheng, Chen, & Nie, 2013; Darimont, Cloots, Heinen, Seidel, & Legrand, 2002; Nandi et al., 2015). HA coating has been applied extensively on metallic prostheses with the aims of improving bone apposition, implant fixation and reducing healing time (Bigi et al., 2008; H. Wang et al., 2006; Yoshida et al., 2012).

Numerous methods have been established to enhance the surface compatibility of implants with bone. Plasma spraying is very commonly used because of its versatility, ability to attain coating fixation and economic feasibility (Jiyong Chen, Tong, Cao, Feng, & Zhang, 1997; Kaya, 2008; Liang et al., 2004; Nandi et al., 2015). However, it suffers some drawbacks, such as difficulty with even HA coating and high-temperature processing. Furthermore, it has been reported that the mechanical stability of the interface between the HA coating and titanium alloy substrate could be problematic either during the surgical operation or after implantation (Collier et al., 1993; Nie, Leyland, & Matthews, 2000). Plasma spraying is also not effective for preparing a bioactive surface on the inner surface of implants, such as cages or other complex structures. Several ideas to overcome these drawbacks have been suggested (Jamlus, Jauhari, & Khalid, 2014; H. Wang et al., 2006).

The superplastic phenomenon of materials has enabled forming complex part geometries requiring particularly high levels of ductility with minimal internal stress (Garriga-Majo et al., 2004). The superplastic deformation in titanium alloy has widely been exploited in many industries, including bio-medical, automotive, electronics and airspace. The application of superplastic deformation in industry offers advantages mainly related to the possibility of producing elements with complex shapes, since its polycrystalline materials can exhibit very high strain values. In medicine, superplastic

deformation is now an interesting alternative method for forming biomaterials and producing implants. In our previous study, an HA layer with good bonding strength was successfully produced when HA was superplastically embedded (SPE) into Ti-6Al-4V alloy. The superplastic deformed titanium substrate can support the embedded HA layer strongly (Mohamad Dom, Jauhari, Yazdanparast, & Khalid, 2010; Ramdan, Jauhari, Hasan, & Masdek, 2008; Yazdan Parast, Jauhari, & Asle Zaeem, 2011). Other studies on this subject indicate that the superplastically embedded HA layer remains strongly intact on the substrate surface even after the substrate is further deformed (SPD) at high temperatures without HA structure deterioration (Jamlus et al., 2014).

The HA layers after SPE and SPD in *in vitro* condition were also evaluated in our prior study. Results from the *in vitro* study of the HA layers after SPE and SPD suggest that newly formed apatite layers can grow within a week of immersion in simulated body fluid (SBF). The HA layer can also withstand a relatively high load applied to the surface (Jamlus et al., 2014). However, the performance of SPE and SPD implants in *in vivo* condition has not yet been studied. Therefore, in this work, SPE and SPD samples are implanted subcutaneously on the backs of SD rats in order to evaluate their bioactivity. At the same time, the biocompatibility and durability of the samples are also evaluated through histological test and wear tests. The as-received Ti-6Al-4V alloy is also investigated for comparison.

1.2 Objectives

i) To prepare SPE and SPD implants using the superplastic method.

ii) To analyse the bioactivity of the implants in SD rats.

iii) To evaluate the biocompatibility of the implants.

iv) To evaluate the mechanical performance (hardness and wear) of the implants.

1.3 Thesis outlines

This thesis is outlined as follows:

(1) Introduction

A brief background of the research, the research objectives as well as layout of the thesis is presented in Chapter 1.

(2) Literature review

The theories and concepts pertaining to superplasticity, implant preparation and performance of implant in *in vivo* condition were reviewed from journals, dissertations, theses, Internet websites and reference books. A summary of the literature review is presented in Chapter 2.

(3) Experimental procedure

The experimental procedure for two types of Ti-6Al-4V-HA implants (SPE and SPD implants) preparation and *in vivo* of the implant subcutaneously on the backs of SD rat models is presented in Chapter 3. The microstructures, embedded coating thickness an d morphologies of the HA layer before and after implantation were imaged by Field Emission Scanning Electron Microscopy (Zeiss FESEM). Phase identification of the HA layer formed before and after implantation was carried out using Bruker D8 Advance X-ray diffractometer (XRD). The hardness of the HA layerwas measured using Vickers microhardness tester Mitutoyo. The biocompatibility of the implants was examined with a light microscope (Nikon 50i). The adhesion strength of the HA layer formed and interfacial strength between the HA layer and substrate before and after implantation were tested for wear under 10% neutral-buffered formalin (NBF).

(4) Results and discussion

The data, results and discussions from characterization techniques are compiled and documented in Chapter 4.

(5) Conclusions and recommendations

Conclusions of the current study and recommendations for future works are presented in Chapter 5

CHAPTER 2: LITERATURE REVIEW

2.1 Superplasticity

The word superplasticity is derived from Latin and Greek words, with the prefix *super* meanings excess and *plastikos* meanings to give form, respectively. In materials science, superplasticity is known as a state in which solid crystalline materials can exhibit large plastic deformation beyond the usual breaking points. Such state is normally achievable under specific microstructural and deformation conditions (G. Wang & Fu, 2007).

In 1945, the term "superplasticity" was coined by Bochvar and Sviderskaya to describe the extended ductility observed in Zn-Al alloys (Pilling & Ridley, 1989). Miguel Lagos explained the theory of superplasticity by using data on several alloys from a wide range of conditions. The physicist proposed that the movement of atomic vacancies creates a "rolling action," which allows microcrystals to slide past one another as the material stretches (Brown, 2000).

Examples of superplastic materials are some fine-grained metals and ceramics. Other non-crystalline materials (amorphous), such as silica glass ("molten glass") and polymers also deform similarly, but are not called superplastic, because they are not crystalline; rather, and their deformation is rather described as Newtonian fluid. One of the advantages of superplastic materials is that they exhibit plastic deformation even under small shear stress in a certain temperature range below melting temperature. In addition, they display large atomic diffusion along grain boundaries (Hefti, 2007; Matsushita, Ogiyama, Suko, & Matsuda, 2009).

Superplastic behaviour was initially observed in the late 1920s, with a maximum of 361% for Cd-Zn eutectic at 20°C and a strain rate of ~10-8/s, and 405% at 120°C and a strain rate of ~10-6/s. In 1934, Pearson detected tensile elongation of 1950% without failure for a Bi-Sn alloy while working on eutectics, Pearson also examined the bulging characteristics of the materials using internally pressurized tubular specimens (Pilling & Ridley, 1989). Structural superplasticity is only observed in alloys with extremely fine grain sizes, when deformed at elevated temperatures and in certain strain rates rangess. Elongations ranging from two hundred to several thousand per-cent has been obtained (Giuliano, 2008; Srinivasa Raghavan, 1984). The world record for superplastic ductility of over 9000%; was reportedly observed in titanium alloys (Ti-6Al-4V) treated with protium, as shown in Figure 2.1 (Nakahigashi & Yoshimura, 2002).

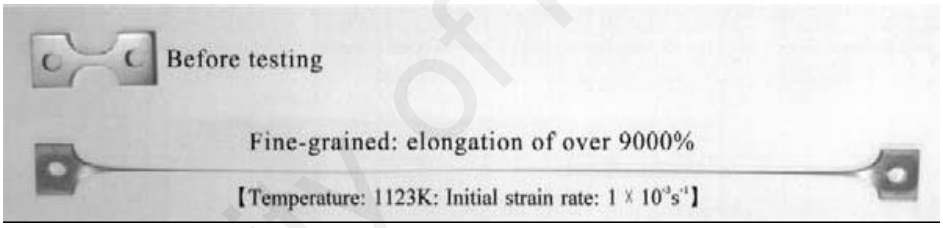

Figure 2.1: Appearance of a superplastically elongated specimen of fine-grained material (Nakahigashi & Yoshimura, 2002)

2.1.1 Superplasticity Characteristics and Mechanism

Three conditions are required for a material to undergo superplasticity: (i) the presence of a stable microcrystalline structure (usually less than 10 μm), (ii) deformation temperature exceeding $0.5T_m$ and (iii) a specific strain rate range (within 10^{-5} to 10^{-1} s^{-1}) (Giuliano, 2008; Pilling & Ridley, 1989; Vanderhasten, Rabet, & Verlinden, 2008).

Among the factors affecting superplasticity, grain size is the most important since stable microcrystalline structure is an essential condition for attaining structural

superplasticity. The grain size of superplastic materials should be as small as possible, but it normally ranges from 2 to 10 μm, although limited superplasticity is still observed for grain sizes up to 20 μm or even greater. In the presence of suitable microstructure, superplasticity occurs over a narrow temperature range and generally above $0.5T_m$. Overall, increasing the temperature or decreasing the material grain size has a similar effect on the variation of flow stress with strain rate. The strain rates at which superplasticity is normally observed are in the range of 10^{-5} to 10^{-1}/s, although it is more often between $2x10^{-4}$ and $2x10^{-3}$/s. These strain rates are less than those used in conventional hot deformation processes.

However, the most important mechanical characteristics of superplastic materials are strongly dependent on their strain rate sensitivity of flow stress which can be defined by the Backofen equation as follows:

$$\sigma = K\dot{\varepsilon}^m \tag{2.1}$$

where σ is the flow stress, ε̇ is the strain rate, *m* is the strain -rate sensitivity exponent and *K* is a material-related constant. Among these, *m* is a very important parameter in superplastic formation and represents the resistance to necking during testing (Giuliano, 2008; Pilling & Ridley, 1989). Generally, the greater the *m* value, the better the resistance to necking and the better the superplasticity. Since *m* is dependent on strain rate, the maximum *m* value has a corresponding strain rate, which is the optimal strain rate from a superplasticity deformation perspective (G. Wang & Fu, 2007).

For superplastic behaviour, the *m* value exceeds about 0.3 and is less than 1.0. However, for most superplastic materials, *m* lies in the range of 0.4 to 0.8. The presence of a neck in a material subject to tensile straining leads to a locally high strain rate and for a high *m* value, it leads to a sharp increase in the flow stress within the neck region. Hence, the neck undergoes strain rate hardening, which inhibits its further development.

Thus, high strain rate sensitivity confers high resistance to neck development and results in high tensile elongations characteristics of superplastic materials (Pilling and Ridley, 1989).

A unique feature of superplastic materials is the mechanism, of grain movement during deformation. The material's integrity during superplastic deformation is assured by the intervention of grain boundary accommodation mechanisms, which are known intergranular diffusion, grain boundary diffusion and dislocation climb. With larger grain size, the effectiveness of these mechanisms is lower, because the volume to be accommodated becomes larger, thus resulting in increasing flow stress (Vanderhasten et al., 2008). In principle, the superplasticity mechanism is similar to the classical creeps of metals. Creep includes grain boundary sliding (GBS), dislocation movement, dynamic recovery and the recrystallization process. It is known that GBS is the predominant deformation mechanism in superplastic materials and can be facilitated by evenly distributing the second material phase. Moreover, reducing the material grain size (<10μm) can also encourage grain boundary sliding (Cheong, Lin, & Ball, 2001). The deformation mechanism of superplasticity is displayed in Figure 2.2.

Upon the application of a small load, the motion of individual grains or grain clusters relative to each other accumulates strain by sliding or rolling. Grains are observed to change their neighbours and emerge at the free surface from the interior. This indicates that a group of grains with favourable orientation moves as a block relative to its neighbours. The stress concentration in the grain in which the slip plane exists and which acts as a slip barrier produces new dislocations that once again cause a slip through the grain, stopping at the next grain boundary and leading to a dislocation pile-up. The rising stress then causes a slip to initiate and proceeds through the blocking grain, while the mobility of dislocations increases due to the climb mechanism.

If grain boundary sliding occurs in a completely rigid system of grains, then a neighbouring grain is inserted between the individual grains as shown in Figure 2.3. Therefore, grain boundary slip is a result of the diffusion controlled mass transport along the grain boundary or through the grain volume (Pilling & Ridley, 1989; Siegert & Werle, 1994)

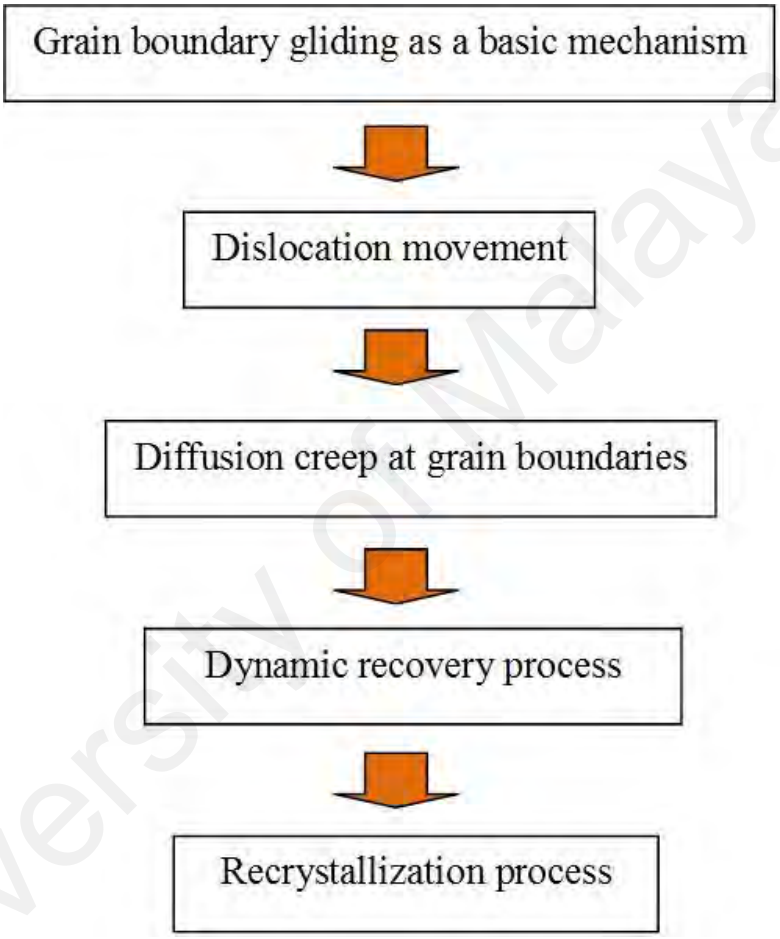

Figure 2.2: Flow mechanism of superplasticity

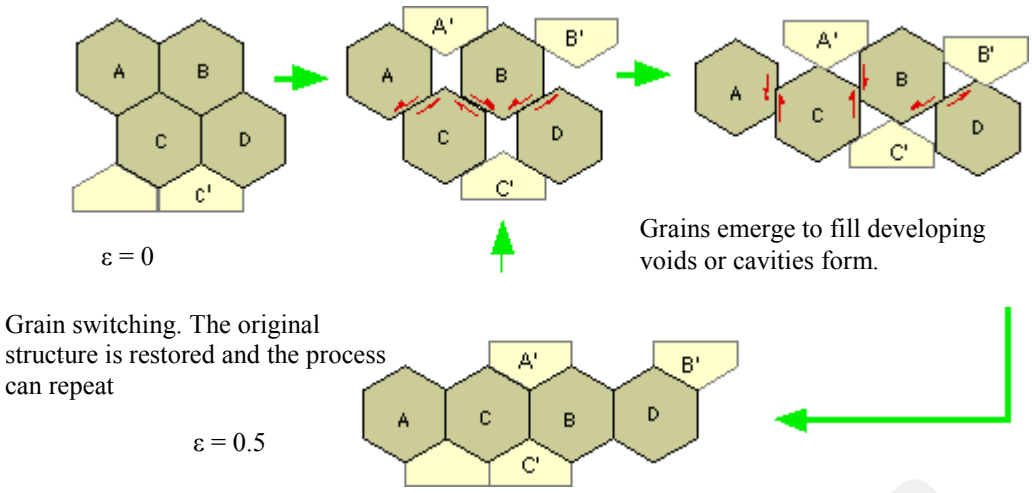

Figure 2.3: Grain movement in superplastic materials (Pilling & Ridley, 1989)

2.1.2 Application of Superplasticity

Since superplasticity permits the formation of complex geometries that require extremely high degrees of ductility with minimal internal stress it can be exploited in the production of complex architecture components. Examples include the aerospace, defence, biomedical, sports and automotive sectors. Most commercial applications of superplastics are found in metallic systems, for example those based on titanium alloy, aluminium, magnesium and zinc. It has also been reported in some ceramics and geological materials. However, titanium alloy (Ti-6Al-4V) has attracted a great deal of attention in the last few decades due to its broad application in the aerospace, transportation and biomedical areas (Alabort, Putman, & Reed, 2015; Guo, Liu, Tan, & Chua, 2014; G. Wang & Fu, 2007).

Superplasticity is normally applied in two processes, which are superplastic formation or superplastic deformation (SPF or SPD), and superplastic forming and diffusion bonding (SPF-DB). SPF is a process that allows the formation of unique, complex shapes as well as the fabrication of components from a single piece of material. This process can be used to produce parts that are otherwise impossible to

form with conventional techniques. Once a state of superplasticity is reached, pressure is applied to the metal to create a complex form. For this reason, SPF has been widely utilized in many industries, including bio-medical, aerospace, and automotive and electronics. In the SPF process, the *m* value is a critical parameter that represents the material's superplasticity. Wang and Fu (2007) noted there are three critical matters that need to be addressed in the SPF process. They are the dynamic measurement of deformation velocity and loading, calculating the *m* value, and the simultaneous control of deformation velocity (G. Wang & Fu, 2007).

Diffusion bonding is such a process, whereby two matched surfaces are held together at a temperature ranging between 0.5 of the material's absolute melting temperature and room temperature under low pressure without causing macroscopic plastic deformation in the materials. The process is dependent on various parameters, particularly time, applied pressure, and bonding temperature, to promote microscopic atomic movement and ensure complete metallurgical bonding (H.-S. Lee et al., 2007). SPF-DB is another process with the combined benefits of the SPF and DB processes. A concurrent formation and bonding process can save energy and reduce manufacturing costs, since the method combines the benefits of each process in producing components with superior structural integrity and properties. Previous studies have shown that through SPF-DB, the advantages of two unusual properties of titanium alloys (superplasticity and diffusion bondability) result in significant cost and weight savings compared with conventional titanium manufacturing methods (Kim, Lee, & Hong, 2001; Y.-S. Lee, Lee, & Lee, 2001; Nieh & Wadsworth, 1997).

Recently, Guo et al. introduced a new process that benefits from hot drawing (mechanical pre-forming) together with gas forming. The process is known as superplastic-like forming and is more efficient than the conventional SPF process. The

forming time in superplastic-like forming can be significantly shorter as the hot-drawing step would have produced a pre-formed component prior to gas forming. A schematic of the superplastic-like forming process is shown in Figure 2.4. During the hot drawing stage, the punch is actuated to mechanically pull a desired amount of the flange material into the die cavity. Subsequently, argon gas pressure is applied onto the pre-formed sheet to complete gas forming at a targeted strain rate (Guo et al., 2014).

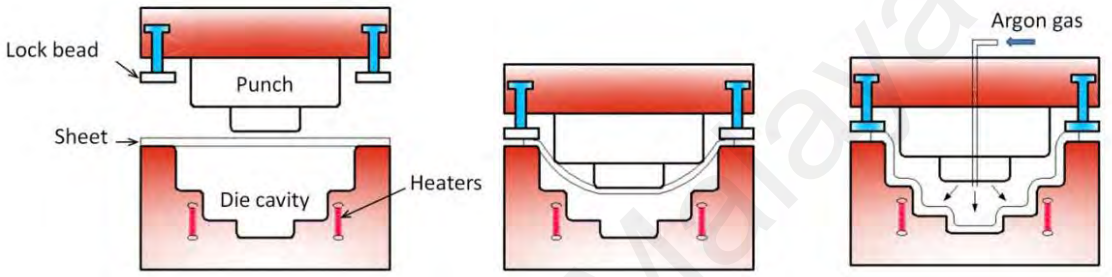

Figure 2.4: Schematic of the superplastic-like forming process: (a) heating and clamping; (b) hot drawing and sealing; (c) gas forming (Guo et al., 2014)

2.2 Titanium and its Alloys

Titanium is a transition metal that is silver in colour. Great Britain, by William Gregor discovered it in 1791 in Cornwall, Great Britain, and Martin Heinrich Klaproth f named it Titanium after the Titans from Greek mythology. Titanium occurs in several minerals including rutile and ilmenite, which are well-dispersed over the Earth's crust (Britannica, 2016). It was discovered much later than other commonly utilized materials, and its commercial application started in the late 1940s, mainly as a structural material. Even though titanium is as strong as some steels, its density is 40% lighter than steel and 60% heavier than aluminium. This combination of high strength and low weight encourages its broad use in a variety of applications, including aerospace, sporting equipment, power generation, and the automotive, dental and medical industries. Table 2.1 illustrates the properties of titanium (D. & Callister, 2003).

Titanium is rather difficult to fabricate because of its susceptibility to oxygen, nitrogen and hydrogen impurities, which cause it to become more brittle. Elevated temperature processing must be used under special conditions in order to avoid the diffusion of these gasses into titanium. To overcome such restrictions, commercial pure titanium is substituted with titanium alloy (Efunda, 2016). The alloying behaviour of titanium is readily discussed in terms of the effect of different solutes on the allotropic transformation temperature of pure metal. Allotropic transformation occurs at 882°C. Below this temperature, a hexagonal-close-packed (HCP) crystal structure is,otherwise known as α-phase is exhibited, whereas a body-centered-cubic (BCC) structure would form as a β-phase at higher temperature.

Table 2.1: Properties of titanium

Property	Typical value
Density	4510 kg/m^3
Melting Point	1668 °C
Elastic Modulus	107 GPa
Tensile Strength	234 MPa

(D. & Callister, 2003)

The possibility to add alloying elements stabilizes one or the other of these forms, thereby raising or lowering the β-transus temperature. The elements that stabilize the low-temperature form are termed α-stabilizers and those that stabilize the high-temperature form are termed β-stabilizers (Leyens & Peters, 2003). Table 2.2 shows the effects of several elements.

Table 2.2: Alloying elements and their effects on structure

Alloying Element	Effect
Aluminum	α-stabilizer
Tin	α-stabilizer
Vanadium	β-stabilizer
Molybdenum	β-stabilizer
Chromium	β-stabilizer
Zirconium	α and β strengtheners

2.2.1 Classification of Titanium Alloys

Titanium has a wide range of alloys owing to its ability to dissolve so many different elements. Controlling the α- and β- phases adding alloying elements and through thermo-mechanical processing is the basis for titanium alloy use in industries today. It is also a primary method of classifying of titanium alloys. Titanium alloying elements fall into three classes, namely; alpha, beta, or alpha-beta (a mixture of the two structures). A partial phase diagram of titanium with β-stabiliser elements is depicted in Figure 2.5.

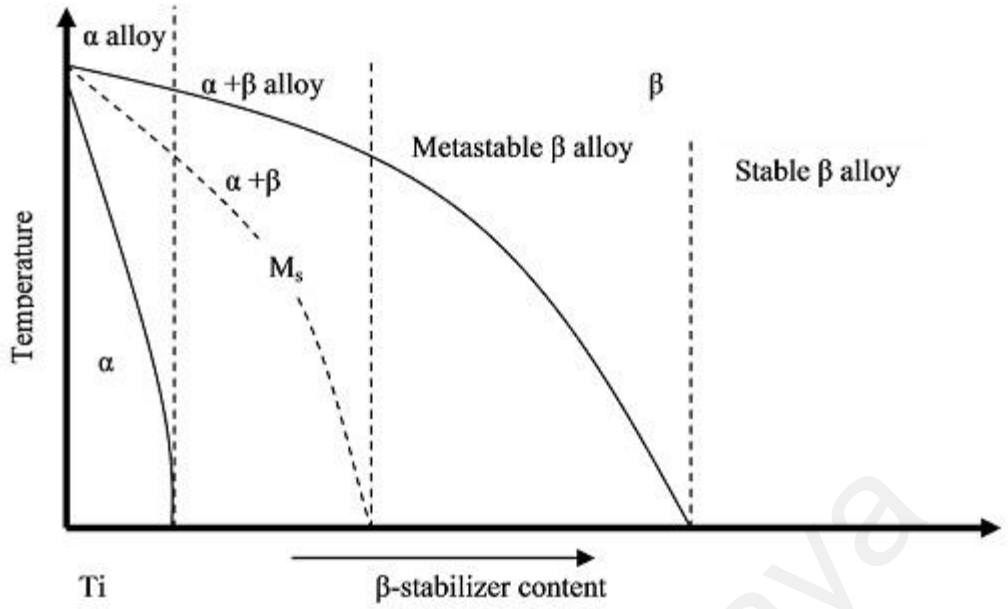

Figure 2.5: Partial phase diagram of titanium and a β-stabilizer element (Balazic et al., 2007)

Alpha titanium alloys are principally formed with commercially pure (CP) titanium and alloys with α-stabiliser elements, which present only the α-phase at room temperature. Such alloys exhibit high creep resistance and are thus suitable for high-temperature servicing. Since no metastable phase remains after cooling from high temperature, no major modification in terms of microstructure and mechanical properties is possible using heat treatments. Finally, as the α-phase is not subjected to ductile-brittle transition, these alloys are proper for very low-temperature applications. Regarding mechanical and metallurgical properties, α-alloys present a reasonable level of mechanical strength, high elastic modulus, good fracture toughness and low forgeability, owing to the HCP crystal structure.

Beta titanium alloys are obtained when high amounts of β-stabiliser elements are added to titanium, which decrease the temperature of the allotropic transformation (α/βtransition) of titanium. If the β-stabiliser content is sufficiently high to reduce the

martensitic start temperature (M_s) to below room temperature, α-phase nucleation and growth will be very restricted, and hence, metastable β will be retained at room temperature under rapid cooling as depicted in Figure 2.5. This titanium alloy may be hardened using heat treatment procedures. In some cases, depending upon composition and heat treatment parameters, ω-phase precipitation is possible. However, the ω-phase may cause a titanium alloy to become brittle and generally, its precipitation must be avoided. Beta titanium alloys are very brittle at cryogenic temperatures and are not meant to be applied at high temperatures as they display low creep resistance.

Finally, α+β alloys include alloys with enough α and β-stabilisers to expand the α+β field to room temperature. The αβ phase combination allows attaining an optimum balance of properties. The characteristics of both α and β-phases may be tailored by applying adequate heat treatments and thermos-mechanical processing. A significantly greater assortment of microstructures may be obtained compared to α-type alloys. Ti-6Al-4V is an example of α+β type alloy. Due to its large availability, very good workability and enhanced mechanical behaviour and based on these characteristics this alloy is still largely applied as a biomaterial, mainly in orthopaedic implant devices (Balazic et al., 2007).

2.2.2 Ti-6Al-4V

In the 1950's, the first commercial α+β titanium alloys was Ti-6Al-4V. Although it does not excel in terms of at any particular property, it has a good combination of strength and workability. This alloy is also lower in cost owing to its larger-scale production (Efunda, 2016). Ti-6Al-4V denotes that the titanium alloy has a composition of 6% aluminium and 4% vanadium. The addition of aluminium to titanium stabilizes the α-phase, while adding vanadium stabilized the β-phase (BCC structure).

The combination of 6% aluminium and 4% vanadium facilitate both allotropic modifications at room temperature. Therefore, this alloy is classified as a two-phase α-β material with a β-transus temperature of 995°C. The alloying additions also contribute to augmented strength by solid-solution strengthening mechanisms. There are two basic microstructural morphologies that control the fundamental mechanical behaviour of these alloys: the lamellar transformed-β microstructure and the primary (equiaxed) α. The lamellar transformed-β structure (sometimes called the colony structure or lenticular) is the easiest to attain by the solidification of ingots/shape castings melts, or by hot-working (forging) above the β-transus temperature, or by solution treatment above the β-transus temperature. This morphology has a natural resistance to both creep and hot-working from hot-temperature deformation, because of its large "grain" size. It has good resistance to fatigue crack propagation as well as and also high fracture toughness owing to its lamellar structure. The primary (equiaxed) alpha microstructure is the result of hot-working in the alpha+beta field, sufficiently below T_β to cause recrystallization of the lamellar alpha-phase inherited from the ingot casting stage. Despite the time consuming process, a material is formed with excellent hot work ductility (25% elongation), strength, and high cycle fatigue strength on account of its fine grain size. Both the complex metallurgical transformations, and relative amounts of α and β-phases present in the material, can affect the mechanical properties.

The mechanical properties of Ti-6Al-4V (Table 2.3) compare favorably with other metal alloys. The yield strength is approximately the same as that of surgical quality 316L stainless steel and almost twice that of the familiar cast Co-Cr-Mo alloy used in orthopaedic implants. The elastic modulus is approximately half that of other popular metal alloys used in surgery. The low modulus results in a material that is less rigid and deforms elastically under applied loads. These properties may have significant roles in the development of orthopaedic products, where a close match between the elastic

properties of long bone and surgical implants is needed. The fatigue strength of this alloy is approximately twice that of stainless steel or cast Co-Cr-Mo alloy (*Encyclopedia of Materials Science and Engineering: Co - E*, 1986).

Table 2.3: Typical mechanical properties of Ti-6Al-4V alloy

Ultimate tensile strength (MPa)	965
Yield strength (MPa)	895
Young's modulus (GPa)	110
Elongation (%)	12
Fatigue endurance limit at 10^7 cycles (MP)	515

2.2.3 Solution Heat Treatment of Ti-6Al-4V

The mechanical properties and microstructure development of titanium and its alloys are exceedingly dependent on the processing and heat treatment they undergo (Gallagher, 2004). The purposes of heat treating titanium and its alloys are to reduce residual stresses developing during fabrication, to produce an optimum combination of ductility, machinability, and dimensional and structural stability, and to increase strength (Henkel & Pense, 2002). Heat treatment is dependent on the cooling rate from the solution temperature and can be affected by component size.

It is recognised that two basic microstructural morphologies control the fundamental mechanical behaviour of these alloys. The primary α can exist in various forms from elongated plates to globular sections depending on whether the material is lightly or heavily worked. The transformed β regions are those of the β-phase at working temperature, which vary depending on cooling rates.

Previous studies have shown that the thermo-mechanical processing (TMP) of α + β titanium alloy above β-transus temperature leads to a 'lamellar' microstructural morphology, consisting of α platelets with an inter-platelet β-phase. The 'lamellar' structure varies with cooling rate, ranging from colonized plate-like α at low cooling rates to, a basket-weave morphology at an intermediate cooling rate, to Widmanstätten at high cooling rates, to martensite, when quenched in water. When processed below β-transus temperature, Ti-6Al-4V exhibits an (α + β) structure with the prior α-phase retained to room temperature and the β-phase partially transformed (Ding, Guo, & Wilson, 2002). The heat treatment process for the common titanium alloy, Ti-6Al-4V is shown in Figure 2.6.

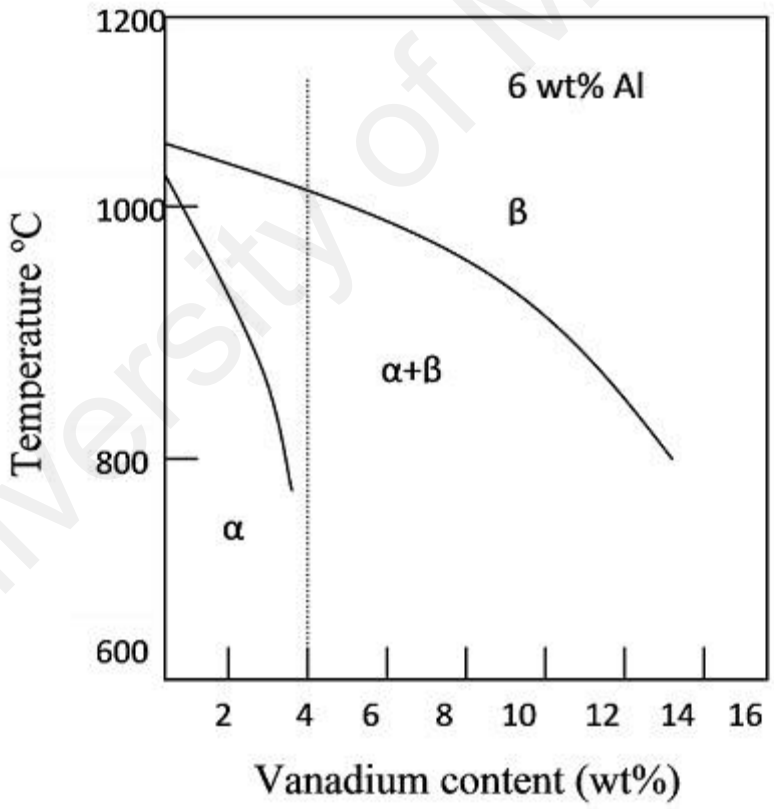

Figure 2.6: Microstructural development of Ti-6Al-4V (Gallagher, 2004)

In addition to processing temperature, other hot-working parameters, such as strain and strain rate, also affect the microstructure, e.g. the volume fractions of the α and β-phases, and the phase size and 'lamellar' dimensions of the α-phase. The aspect ratio of the α-lamella phase is also a very important factor influencing the mechanical properties of Ti6Al4V alloy (Froes & Bomberger, 2012). Previous studies have indicated that dynamic or metadynamic recrystallization may occur for Ti-6Al-4V during isothermal forging and hot compression (Park, Ko, Park, & Lee, 2008).

2.3 Superplastic behaviour in Ti-6Al-4V

Superplastic behaviour has been demonstrated in several aluminium and titanium alloys. One of the most extensively studied titanium alloys in terms of superplasticity is Ti-6Al-4V. The formability of this material is greatly improved through the superplastic forming process, resulting in weight reduction and cost savings. Accordingly, many efforts have been made in establishing rules to enhance the superplastic behaviour of materials. Edington et al. reported that enhanced superplasticity is obtainable through the most efficient grain refinement methods (Edington, Melton, & Cutler, 1976). In addition, a previous study reported that a stable and fine-grained Ti-6Al-4V alloy was achieved through dynamic globularization, which entails the conversion of the transformed β microstructure to a fine equiaxed microstructure (Park et al., 2008). It was mentioned in section 2.1.1 that a fine grain size of less than 10 μm is essential for the occurrence of GBS, which is the predominant deformation mechanism in superplastic materials.

An abundance of articles regarding the superplasticity of Ti-6Al-4V materials have emerged in the literature. According to a study (Ghosh & Hamilton, 1979), the Ti-6Al-4V alloy is superplastic at approximately between 750°C and 950°C, and at strain rates between 10^{-4} s^{-1} and 5×10^{-3} s^{-1}. Nieh et al. showed that superplastic behaviour of Ti-

6Al-4V alloy can be achieved above 900˚C at low strain rates (usually lower than $10^{-3}s^{-1}$) (Nieh & Wadsworth, 1997). In addition, Vanderhasten et al. stated that in their study, at above 750 ˚C and for strain rates over 10^{-3} s^{-1} at this temperature, softening is sufficiently fast to balance the rate of work hardening and mechanisms like dynamic recrystallization and dynamic recovery (Vanderhasten et al., 2008). Alabort et al. reported that the superplasticity regime in Ti-6Al-4V was pinpointed in the range of 850-900˚C at strain rates between 0.001 s^{-1} and 0.0001s^{-1} (Alabort et al., 2015).

2.4 Hydroxyapatite (HA)

Hydroxyapatite with the chemical formula $Ca_5(PO_4)_3(OH)$ is a natural mineral form of calcium apatite that is also called hydroxylapatite. The Ca/P molar ratio is between 1.67 and 1.5. In 1963, the first HA powder was chemically precipitated by Hayek and Newesely. It is acknowledged that up to 50% (by volume) and 70% (by weight) of human bone is a modified form of hydroxyapatite (bone mineral). Bone mineral consists of tint hydroxyapatite crystals in the nanoregime . Fathi et al. expected nanostructured hydroxyapatite to have better bioactivity than coarser crystals. Stoichiometric HA is biocompatible, osteoconductive, nontoxic, non-inflammatory, a nonimmunogenic agent and bioactive with the ability to form direct chemical bonds with living tissues (Fathi, Hanifi, & Mortazavi, 2008). Moreover, its chemical composition that is similar to the inorganic components of bone and teeth makes it a good candidate for bone substitutes. It is thus widely used as a bioceramic in reconstructive surgery, dentistry as well as drug delivery materials.

Even though many clinical tests have proven that HA is compatible with the tissue of vertebrates, it has been noted that the bending strength and fracture toughness of this bioceramic are inferior to human bone. It is only applicable where no significant stress needs to be borne. In order to overcome this drawback, HA has been applied as a

surface coating on mechanically strong implant materials in load-bearing implant applications in order to combine the mechanical strength of metals with the excellent biological properties of HA ceramics. Typically, the metals used can be titanium, Ti-6Al-4V, and stainless steel 316L (de Jonge et al., 2010; Yip, Khor, Loh, & Cheang, 1997). Developing a composite that comprises of Ti alloy and HA could mitigate this problem too. However, in recent years, titanium and its alloys have been the most widely employed materials for load-bearing orthopaedic implants, mainly due to their superior biocompatibility and low density.

2.5 Combinations of Ti-6Al-4V with Hydroxyapatite (HA)

It has been proven in previous research work that titanium alloys are potentially very suitable materials for load-bearing medical devices, such as components for total joint replacements or osteosynthesis plates because of their excellent mechanical properties and biocompatibility (Apachitei, Lonyuk, Fratila-Apachitei, Zhou, & Duszczyk, 2009; de Jonge et al., 2010; Nie et al., 2000; Yao et al., 2010; Yip et al., 1997). Unfortunately, the applications of titanium and its alloys are limited by their low surface hardness, high friction coefficient and poor wear resistance. It currently reported that surgical implants undergo degradation after use for a certain time due to wear and corrosion failures. Moreover, like most metals, it is not capable of establishing the formation of tight, chemical bonds with bone tissue, something known as poor osteoinductivity (Yildiz, Yetim, Alsaran, & Efeoglu, 2009).

Thus, this drawback has generally been improved in many studies by coating the metal with a layer of bioceramic HA, which is the main component of bone and thus a very good osteoinductor. In this case, biocompatibility is assured by HA, while the metal substrate contributes the mechanical properties. It has been established that HA coating can endorse more rapid fixation and stronger bonding between the host bone

and the implant. Moreover, HA coating offers protection to the titanium substrate against corrosion in a biological environment, and acts as a barrier against the release of metal ions from the substrate into the environment (Nie et al., 2000; J. Wang, Chao, Wan, Zhu, & Yu, 2009). More inspiring acknowledged that HA coating enhances bone growth across a gap of 1 mm between the bone and the implant and is capable of limiting the formation of any fibrous membrane and converting a motion-induced fibrous membrane into a bony anchorage (J. Wang et al., 2009).

There are a variety of surface coating techniques for depositing HA-based coatings, ranging from the conventional press-and-sinter method to more sophisticated approaches such as ion beam sputtering, chemical vapour deposition, dip coating, electrophoresis and electrochemical deposition. Among these techniques, plasma-sprayed calcium phosphate coating is one of the most extensively examined methods, and its efficiency has been confirmed in many reports (Takemoto et al., 2005). However, it has also been reported that with the plasma-spraying method, the mechanical stability of the interface between the HA coating and titanium alloy substrate could be problematic either during surgical operation or after implantation. Additionally, its poor step coverage hinders the preparation a bioactive cover on the inner surface of an implant such as cage or other complex structure, making it difficult to control the HA composition, structure and high deposition temperature that may affect the substrate (Forsgren et al., 2007; Gu, Khor, & Cheang, 2003; Song, Jun, Han, & Hong, 2004; Takemoto et al., 2005).

One alternative has been suggested to overcome these inherent deficiencies, which is to conduct HA deposition using the continuous pressing method at elevated temperature. This is known as superplastic embedment (SPE) or superplastic deformation (SPD) method. It has been shown that beside diffusion occurring from the

high-temperature condition in the process, the additional pressing work can provide additional energy that forces the bio-apatite to move inside the substrate, leading to dense HA/Ti composite formation and, improving the HA adherent strength. Moreover, surface asperities of the Ti-6Al-4V substrate can be plastically deformed easily by continuous pressing, which accelerates HA powder and substrate embedment (Mohamad Dom et al., 2010; Ramdan et al., 2008; Yazdan Parast et al., 2011).

Since its introduction in the 1980s, hydroxyapatite (HA) coating on orthopaedic implants has gained wide acceptance in orthopaedic surgery. In a review by Liang H. et al. with focus on joint replacement, it was mentioned there is a list of implants that have a major role in replacing or improving the function of every major body system, such as the skeletal, circulatory or nervous system. Materials employed in such replacements are by definition biomaterials. A summary of common biomaterials is given in Table 4.1. These conventional materials fit the specific needs of bio-applications (Liang et al., 2004; H. Wang et al., 2006).

Table 2.4: Summary of common biomaterials

Materials	Applications	Major properties description
Metals: brass, stainless steel, nickel plating, nickel-plated steel, zinc-plated steel	Inserts	
Alloys: titanium alloys, titanium aluminium vanadium alloy, cobalt chromium alloy, cobalt chromium molybdenum alloy	Total joint replacements	Wear and corrosion resistance
Inorganic: diamond-like carbon	Biocompatible coatings,	Reduced friction and increased wear resistance
Ceramics : Al_2O_3, ZrO_2, Si_3N_4, SiC, B_4C, quartz, bioglass (Na_2O–CaO–SiO_2–P_2O_5),Sintered hydroxyapatite ($Ca_{10}(PO_4)_6(OH)_2$)	Bone joint coatings	Wear and corrosion resistance

Materials	Applications	Major properties description
Polymers: Ultra-high molecular weight polyethylene (UHMWPE), Polytetraflouroethylene (PTFE)	Joint sockets	Wear, abrasion and corrosion resistance
	Interpositional temporomandibular joint(jaw) implants	Low coefficient of friction
Polyglycolic acid	Joint bones	Elastic with less wear
Polyurethane	Leaflet heart valves	Highly biocompatible,high strength, and dynamic ranges of breathability
Composites: Specialized silicone polymers	Bone joints (Liang et al., 2004)	Wear, corrosion, and fatigue resistance

Some common implants include orthopaedic devices, such as total knee, hip, shoulder, and ankle joint replacements, spinal implants, and bone fixators; cardiac implants, such as artificial heart valves and pacemakers; soft tissue implants, such as breast implants and injectable collagen for soft tissue augmentation; and dental implants to replace teeth/root systems and bony tissue in the oral cavity. Figure 2.1Figure 2.7 shows the most frequently performed in joint replacements (Liang et al., 2004).

Figure 2.7: Joints of hips, knees, shoulders, and artificial ankle and foot (Liang et al., 2004)

2.6 Goals and Surface Characteristics of Implants

A number of implants with different surfaces have been used over the last 30 years, with the primary objective of increasing both the quality and quantity of bone contact. The chemical and physical properties of implant surfaces have critical roles in achieving satisfactory bone response and viable implantation. The ultimate goal of the successful fixation of cementless implants used for joint reconstruction is to obtain life-long secure anchoring of implants in the native surrounding bones (Bigi et al., 2008; de Jonge et al., 2010; Lakstein et al., 2009). Furthermore, focus is also on improving implant design features in an attempt to accelerate bone healing early after implantation.

Generally, the success of an endosseous implant in achieving adequate bone regeneration, stability, and optimal required function is greatly dependent on the nature and surface characteristics of the biomaterial. The surface characteristic of an implants is very important because it is the first part of an implant that interacts with the host (J. Chen et al., 2011; Surmenev, Surmeneva, & Ivanova, 2014). Therefore, bioactivity is well accepted as an essential requirement to exhibit chemical bonding with living tissues upon the formation of a bone-like apatite layer on the surface. This apatite layer chemically bonds to the bioactive surface and acts as an intermediate layer between new

bone and the implant. Since an implant with a bioactive surface is achievable by coating with osteoconductive HA, the coating's performance factors should be highlighted (Bohner & Lemaitre, 2009; Forsgren et al., 2007; Gu et al., 2003). In particular, the adhesion strength of the coating to the implant surface appears to be a property that needs to be maximized to avoid HA coat cracking, shearing off, and chipping during implant emplacement (Kurzweg, Heimann, Troczynski, & Wayman, 1998). Besides, rough and porous implant surfaces are also sought as ideal bone substitutes. In a previous study, it was found that for implants coated with HA, the roughness increased the surface contact 5 times compared to smooth implants. Moreover, interconnected pores permit tissue ingrowth and thus anchor the prosthesis to the surrounding bone, preventing loosening of the implant. For consistent performance, HA coatings should also a moderate to high crystallinity, and high chemical and phase stability in order to enhance direct contact with the host during implantation (Darimont et al., 2002; Lakstein et al., 2009; Nie et al., 2000; Takemoto et al., 2005).

2.6.1 Implant Failures

Despite the success of surgical implants with HA surface modifications according to many reported studies failure can still happen during or after implantation. Apparently, a major problems pertaining to HA-coated implants is their long-term functional service on account of coating failure. Prior studies have reported that fractures more often occur at the HA/substrate interface rather than the bone/HA interface from direct shear loading. Yang Y.C and Yang C.Y stressed that this occurs due to insufficient adhesion between the ceramic material and the substrate. In addition, in-plane compressive stress existing at the implant surface may induce a through-thickness tensile stress that is likely to weaken the adhesion between the HA coating and Ti substrate (Li, Khor, & Cheang, 2007; Yang & Yang, 2013).

Another failure is the macrophage response to phagocytosis of particulate wear debris that happens in the interaction between cement and bone. Metal wear debris may induce inflammatory reactions, which is a principal causative factor in osteolysis that, leads to periprosthetic bone loss and subsequent prosthesis loosening. Additionally, the smooth implant surface may lack the appropriate macropores for accommodating the permanent intervention of tissues. Without intervention, the bone tissue originally adhering to the implant surface but not integrating into the implant matrix can slowly fall off the implant surface over a period of 15 to 20 years. Liang H. et al. have summarized a number of common failures:

- Deficiencies in the design (size and shape) of the device for aparticular patient (e.g., an undersized uncemented stem)
- Surgical problems (e.g., problematic orientation or difficulty with wound healing)
- Host abnormalities or diseases (e.g., osteopenia)
- Infection
- Material fracture, wear, and corrosion.(Karanjai et al., 2008; Liang et al., 2004; Tian, 2008)

2.6.2 In Vivo Study of Implant Materials

In recent decades, numerous studies have elaborated on implant surface modifications to enhance the surface compatibility of implants with bone. Therefore, in order to examine the biocompatibility and osseointegration of implants with tissues upon implantation, *in vivo* studies have been accomplished.

In Latin, *in vivo* means within the living, while in common language, *in vivo* studies are those that test the effects of various biological entities on whole, living organisms,

usually animals including humans, and plants as opposed to partial or dead organisms. Examples of investigations *in vivo* include disease pathogenesis by comparing the effects of bacterial infection with the effects of purified bacterial toxins; the development of antibiotics, antiviral drugs, and new drugs in general; and new surgical procedures. Consequently, animal and clinical trials are major elements of *in vivo* research.

Based on the previous research, Bigi et al., de Jonge et al. and Lakstein et al. found that the main objective and problem in the implant application is concern on their duration for the functional service and establishment of a stable interface between the ceramic material and the substrate. Therefore, in this study, the biological and mechanical performances of the raw as-received and coated Ti-6Al-4V implants were evaluated depending to the implantation period. In addition, the embedment of HA on titanium alloy via superplastic method was introduced to improve the coating substrate surface.

CHAPTER 3: EXPERIMENTAL PROCEDURE

3.1 Materials, Samples, and Die and Punch Preparation

In this study, two types of materials were used as-received Ti-6Al-4V alloy and hydroxyapatite powder. Since the samples were not standard size, the die and punch were custom-made to follow the sample sizes. The die and punch were fabricated in one size fit both samples size.

3.1.1 Materials

Ti-6Al-4V alloy with an average grain size of 13 ± 0.5 μm served as the substrate material and its chemical composition is listed in Table 3.1. Hydroxyapatite powder with spherical shape and particle size of 4 +10 μm was supplied by Taihei Chemical Co. Ltd. Tokyo, Japan and was used as the embedment material.

Table 3.1: Chemical composition of Ti-6Al-4V

Element	Titanium, Ti	Aluminium, Al	Vanadium, V	Carbon, C
Wt%	88.05	6.73	3.9	2.12

3.1.2 Sample Preparation

In this study, the titanium alloy sample was machined into (17.5x3x3) mm^3 dimension from the as-received material using a lathe cutting machine, as shown in Figure 3.1. The lathe machine was used to smoothen and flatten the sample' edges in order to obtain precise sample sizes.

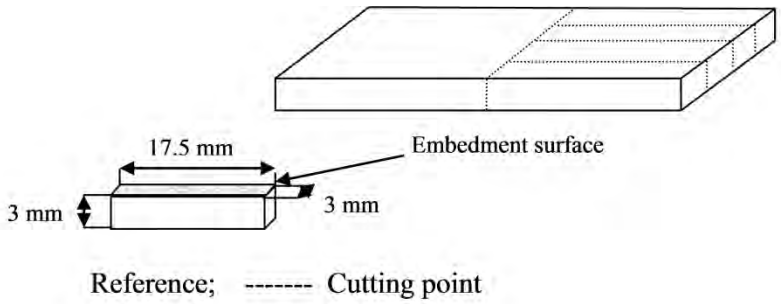

Figure 3.1: Sample dimensions before embedment

3.1.3 Die and Punch Preparation

A special die and punch was fabricated for embedment during the compression test. The material used for the jig and punch was heat resistant steel. This material is appropriate for titanium hot forming (Layman, 1961). The die and punch was fabricated using a power saw, lathe machine, drilling machine and milling machine. The dimensions and a picture of the die and punch are shown in Figure 3.2 and Figure 3.3, respectively.

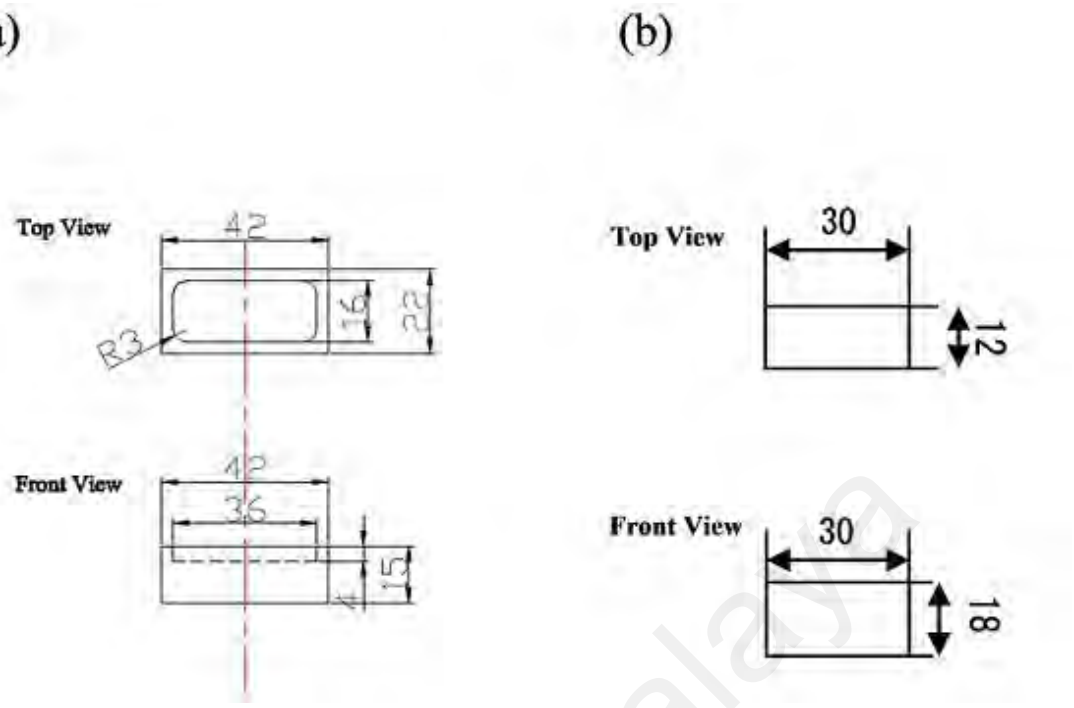

Figure 3.2: Dimensions of (a) die and (b) punch

Figure 3.3:Die and punch: (a) side view and (b) top view

3.2 Solution Heat Treatment

In this study, the as-received Ti-6Al-4V was solution-treated to achieve a full martensite (metastable phase) microstructure. The objective of this treatment was to obtain a suitable superplastic condition for the sample during the embedment process. The heat treatment process is shown in Figure 3.4.

To ensure thermal equilibrium and the formation of a full martensite microstructure during the quenching process, the samples were hung inside at furnace heated to 1373 K (beta-transus temperature at which alpha + beta → beta: ≈ 1250 K). The heating rate of the furnace is 12.1 K/min. Once the temperature reached 1373 K, the samples were held for 30 minutes for homogenization. Following this, the samples were ice quenched to room temperature. The samples were dropped immediately into a container with ice and water (~ 273 K) that was placed under the furnace. Figure 3.5 presents the set- up apparatus used for the heat treatment process.

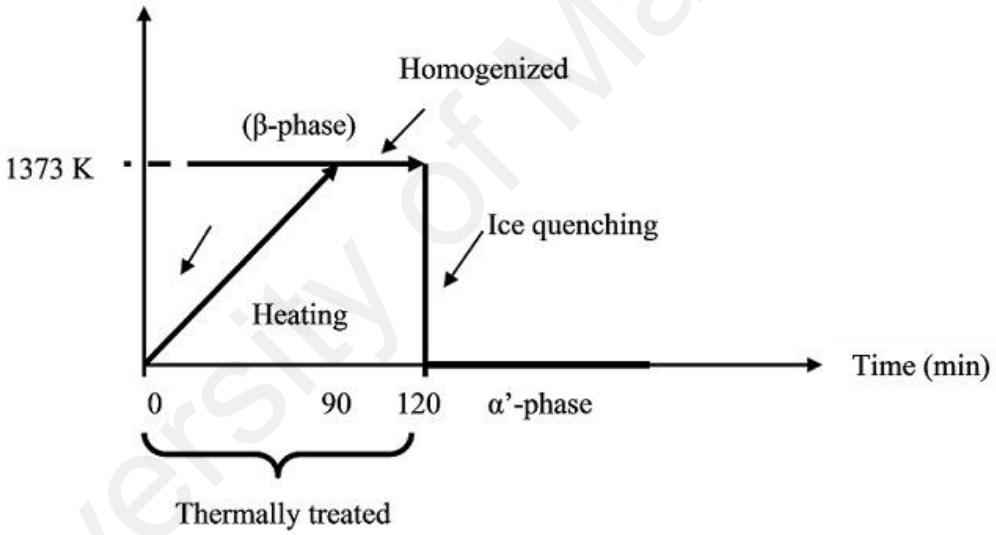

Figure 3.4: Heat treatment process for Ti-6Al-4V

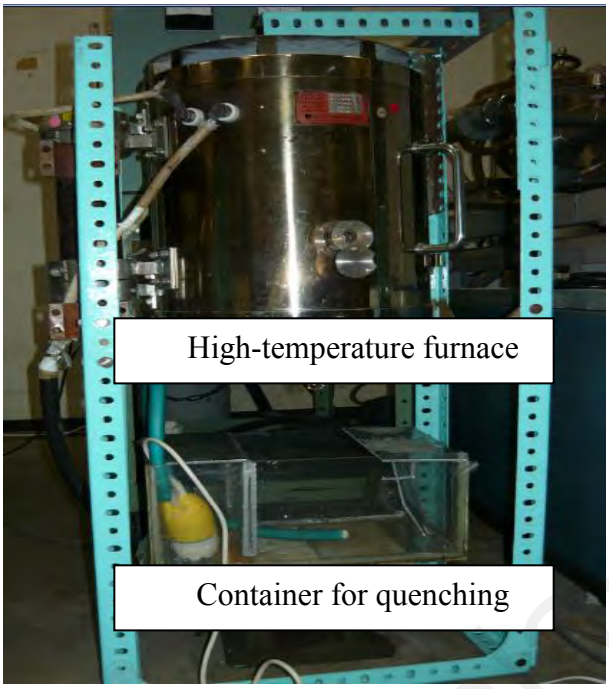

Figure 3.5: Apparatus used for the heat treatment process

3.3 Superplastic Embedment (SPE) and Superplastic Deformation (SPD) Process

In this work, SPE and SPD were conducted using a compression testing machine (Instron Corporation, Norwood, MA) equipped with a high-temperature furnace under controlled gas atmospheric condition at 1200 K. Argon gas was used throughout the process to prevent gas diffusion into titanium, which would cause the titanium to become more brittle. The samples prepared via SPE and SPD were labelled as superplastic embedment (SPE) and superplastic deformation (SPD), respectively

3.3.1 SPE Process

In the SPE process, hydroxyapatite (HA) bio ceramic was applied as embedding material due to its chemical similarity to the inorganic components of human bone. Prior to SPE processing, the heat-treated sample surfaces were polished using emery paper of up to 1200 grit size and cleaned with alcohol to remove oxide layers and

irregularities. A schematic diagram of the experimental setup and the position of the heat-treated Ti-6Al-4V with 2g of HA powder placed inside a specially designed die are shown in Figure 3.6. In this study, a puncher located on the sample was used to homogenize the embedment process. This assembly was heated from room temperature to embedment temperature and maintained for 1 h before being compressed under a strain rate of 1×10^{-4} s^{-1} until the material attained 54% thickness reduction. The strain and strain rate used in the SPE process follows the previous studies which the optimum condition for superplastic embedment was achieved (Jamlus et al., 2014). When the process was completed, the sample was cooled to room temperature in the furnace. The cross-sections of the embedded samples were ground and polished to attain mirror surfaces. The samples were then etched using Kroll's reagent (a mixture of 3 ml HCL (36%), 2 ml HF (48%) and 5 ml HNO3 (65%) in 190 ml of distilled water) for 10 s before physicochemical characterisation.

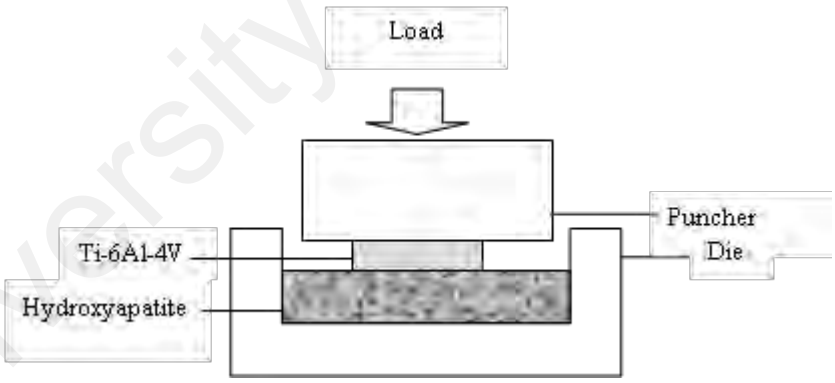

Figure 3.6: Schematic diagram of the experimental setup for the SPE process

3.3.2 SPD Process

In the SPD process, the sample prepared using SPE process (SPE sample) was reheated to 1200 K, held for 1 h for homogenization and compressed at a constant strain rate of 1.6×10^{-3} s^{-1} until 30% of height reduction respect to height after the SPE

process. The strain rate used is different with the SPE process because the purpose of the SPD process was only to deform the embedded sample similar to industrial application especially in complex structure. However, the strain rate is still within the range of superplastic condition. It is worth noting that the experimental setup for SPD was similar to that for SPE, except no HA powder was involved. Figure 3.7 illustrates a schematic diagram of the experimental setup for the SPD process. Upon process completion, the furnace was air-cooled to room temperature. Following the deformation process, the embedded coating thicknesses were measured and the morphologies of the embedded surfaces were evaluated for each condition.

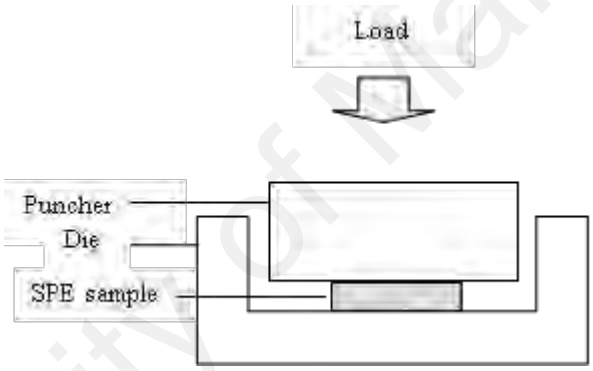

Figure 3.7: Schematic diagram of the experimental setup for the SPD process

3.4 Surgical Procedure

In this study, male albino rats of Sprague Dawley (SD) stock underwent a surgical procedure in order to identify the bioactivity and biocompatibility of the SPE and SPD samples besides as-received samples for comparison.

3.4.1 Animal Procedures

In this work, the behaviour and optimum time of the tissue reaction for the three different implants fabricated and body system were evaluated. Therefore, the samples were tested in an animal system (known as a mammalian system similar to the human

system). The response of the fabricated implant to the living system was identified. The samples were labelled as SPE and SPD. These were prepared using the SPE and SPD processes, respectively. As-received Ti-6Al-4V served for comparison. The samples were implanted subcutaneously on the backs of 45 male albino rats of Sprague Dawley (SD) stock. The SD rats weighed between 250 g and 300 g (mean 225 g).

The animals were housed at an Association for Assessment and Accreditation of Laboratory Animal Care (AAALAC) internationally accredited facility following standard conditions (23±1 ˚C and a 12 hour light/dark cycle). The rats were fed a standard pellet diet (Brand: Altromin) and reverse osmosis (RO) water. The guidelines for handling the animals are in accordance with the Guide for the Care and Use of Laboratory Animals: Eighth Edition (2011), and the protocols were approved by the Faculty of Medicine Institutional Animal Care and Use Committee (IACUC).

3.4.2 Implantation on the Backs of SD Rats

The three different samples with size of (17.5x3x3) mm^3 were implanted subcutaneously on the backs of the albino rats (dorsum area). The rats were anaesthetized by intraperitoneal injection with a mixture of Ketamine HCL (50 mg/kg body weight) and Xylazine (5 mg/kg body weight). The rat fur was shaved in the dorsum area, where betadine solution (10%) was subsequently applied. An incision (approximate length of 1 cm) was made about the mid-portion of the back, the subcutaneous layer was spread to create a pocket, and the respective sample was inserted into the incision, as shown in Figure 3.8. Each incision was closed with intermittent suturing 0.5 apart using surgical nylon thread and No. 4 suture. The animals were euthanized with CO_2 at the specified time intervals (1, 5 and 12 weeks) after surgery for analysis. The surgical process flow is shown in Appendix 1.

Figure 3.8: Sample implanted subcutaneously in the dorsum area of an SD rat

3.5 Histological Procedure

A histological procedure is known as the method of studying the structure of cells, and animal and plant tissues. Normally, thin slices of tissue are prepared first and then discerned with a microscope. A thin slice of tissue is called a histological section. Besides, the cells and tissues are observed by placing a suitable stain onto the section.

Immediately after excision, each tissue surrounding the implant was fixed in 25 ml of 10% formalin for 48 h to halt autolysis. Autolysis is a combination of postmortem changes due to rupture of cell homeostasis that leads to uncontrolled water and electrolytes dynamics in and out of the cell and of alteration of enzymatic activity. These changes are favorable conditions for bacterial and fungal growth and ultimately result in complete destruction of tissue structures. Once the tissue has been fixed, it must be processed into a form in which it can be made into thin microscopic sections. The usual way this was done is with paraffin. Wet fixed tissues (in aqueous solutions) cannot be directly infiltrated with paraffin. First, the water from the tissues must be removed by dehydration. This is usually done with a series of isopropyl alcohol (80%, 95% and

100%) for 1 h. Chloroform and paraffin (100%) treatment was finally used on each specimen for 1 h.

This process was done automatically via automatic vacuum tissue process (LEICA TP 1020). Subsequently, the specimens were processed for embedding using hot (60-65˚C, LEICA EG 1150 H) and cold (4˚C, LEICA 1150 C) embedding centres for 20 mins. After embedding, the specimens were sectioned (2 µm thickness) using a microtome (JUNG Multicut 2045) and stained with hematoxylin and eosin. The specimens were examined with a light microscope (Nikon 50i) by an expert pathologist to monitor the tissue reactions. The flow of the histological rat tissue process is illustrated in Figure 3.9.

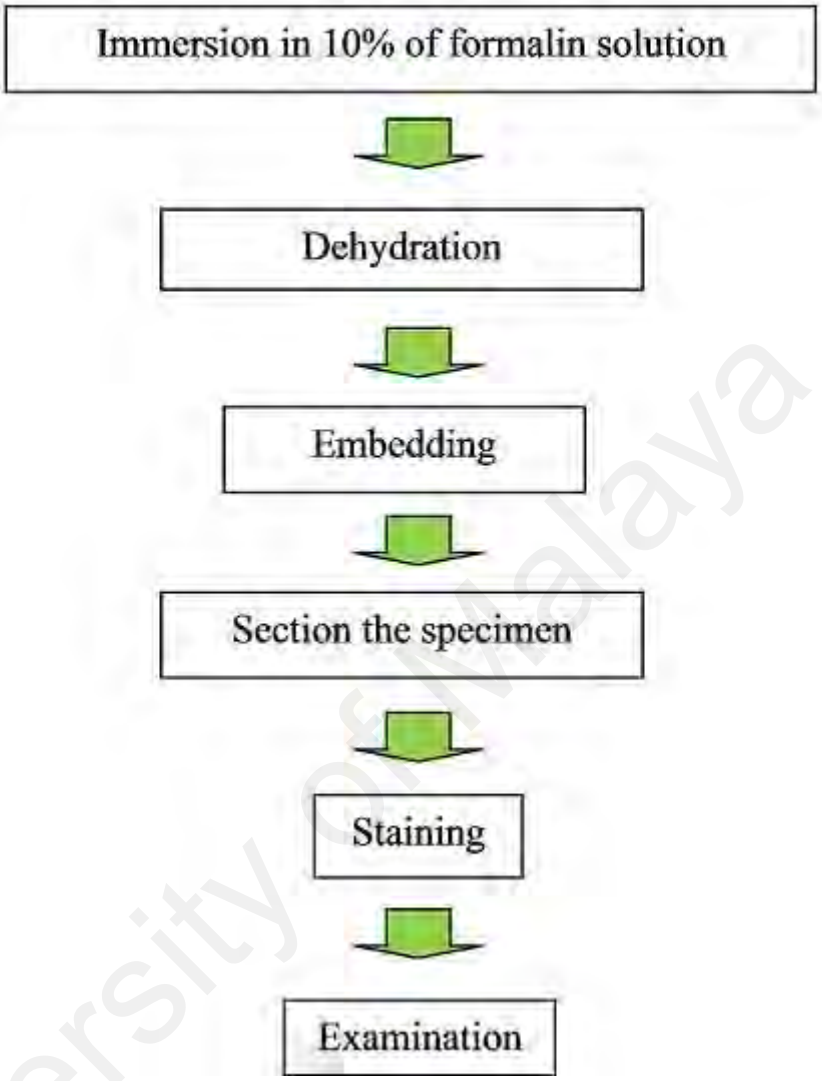

Figure 3.9: Flow chart of histological process

3.6 Mechanical Testing

Long-term mechanical performance is a fundamental requirement for HA coatings on metals. Critical factors, such as implant surface characteristics, adhesion strength of the coating to the implant surface, and in vivo and in vitro bioactivity require attention. For this reason, two types of testing were conducted in this study following the embedment process.

3.6.1 Wear Testing

In order to test the binding strength of the SPE and SPD HA layers after 1 and 12 weeks of implantation, wear tests were carried out against polishing cloths in 500 ml of 10% neutral-buffered formalin (NBF) solution at room temperature for 30 minutes. The tests were carried out using a modified polishing machine with rotational speed of 165 rpm under 0.5 MPa of pressure. A schematic diagram of the equipment used is shown in Figure 3.10. After the wear tests, the surface morphology and distribution of then Ca, P, and Ti elements was evaluated.

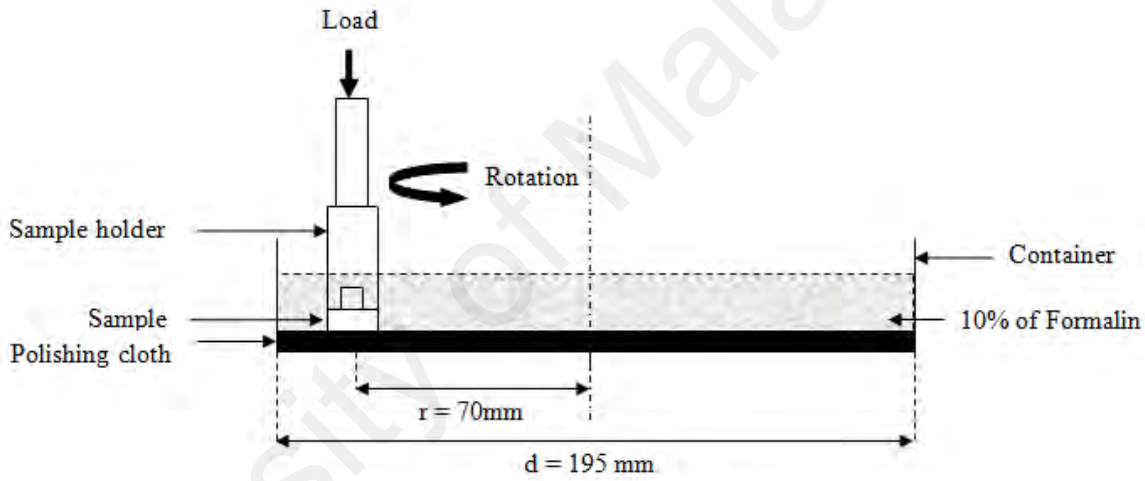

Figure 3.10: Schematic diagram of wear testing

3.6.2 Microhardness Tester

A microhardness tester is an apparatus used for hardness testing, which is available as a relatively simple alternative to tensile testing. The term 'microhardness test' usually refers to static indentations made with loads not exceeding 10 N. The indenter was a Vickers diamond pyramid. The testing procedure was very similar to the standard Vickers hardness test, except that it was carried out on a microscopic scale with higher

precision instruments. Precision microscopes used to measure indentations usually magnify to around 500× and have of ± 0.5 mm accuracy (Gordon England, 2008).

In this research, a Mitutuyo microhardness tester (model MVK-H2) fitted with a Vickers indenter under an applied load of 2 N and loading time of 10 s was used to measure the surface hardness of the HA embedded layer. Figure 3.11 presents the microhardness tester. The reader gives the hardness value automatically after the diamond size is measured.

Figure 3.11: Microhardness tester

3.7 Characterization Process

In this study, surface characterization was done using field emission scanning electron microscopy (FESEM), energy-dispersive X-ray spectroscopy (EDX) and X-ray diffraction (XRD). Thickness and elemental analyses of the HA layer were done with FESEM and EDX, respectively. In addition, the chemical composition of the HA layer was analysed using XRD.

3.7.1 Field Emission Scanning Electron Microscopy (FESEM)

FESEM is a very useful tool for high-resolution surface imaging in nanomaterials science. It is a microscope that functions with electrons (particles with a negative charge) that are liberated by a field emission (FE) source. The electrons are accelerated with a high electrical field gradient. Within the high vacuum column, these so-called primary electrons are focused and deflected by electronic lenses to produce a narrow scan beam that bombards the object. Consequently, secondary electrons are emitted from each spot on the object. The angle and velocity of these secondary electrons relate to the object's surface structure. A detector catches the secondary electrons and produces an electronic signal. This signal is amplified and transformed into a video scan-image that can be viewed on a monitor, or into a digital image that can be saved and processed further (Wikimedia Foundation Inc., 2011).

Zeiss Auriga FESEM with maximum 50000× enlargement was used in this study and connected by a Panasonic digital camera (model WV-CP410) to an image analyser SmartSEM V05.04 operating software. Figure 3.12 shows the FESEM machine.

Figure 3.12: FESEM machine

3.7.2 Energy Dispersive X-ray Spectroscopy (EDX)

EDX is an analytical technique used for elemental analysis or the chemical characterization of samples. EDX systems are most commonly found in scanning electron microscopes (SEM-EDX). In this study, the EDX system was coupled with FESEM. There are four primary components of EDX: beam source, X-ray detector, pulse processor and analyser (Materials Evaluation and Engineering, Inc., 2009). The EDX detector measures the relative abundance of emitted X-rays versus their energy. When an incident X-ray strikes the detector, it creates a charge pulse that is proportional to the energy of the X-ray. The charge pulse is converted to a voltage pulse by a charge-sensitive preamplifier. This information is sent to a pulse processor, which measures the signals and conveys them to an analyser for data display and analysis.

In this study, the elemental composition of an HA-embedded surface was identified by energy dispersive X-ray analysis (EDX). Line scanning was used with 20 kV voltage to Exhibit The Interdiffusion Of Ti Element From The HA Layer To The Substrate.

3.7.3 X-Ray Diffraction (XRD)

XRD is a non-destructive technique for identifying the chemical composition and crystallographic structure of natural and manufactured materials. The XRD results are displayed similar to fingerprints with different patterns. An XRD pattern is formed when X-rays directed to a crystalline material experience diffraction (constructive interface) as a result of their interaction with a series of parallel atomic planes according to Bragg's Law. This law states that the wavelength of electromagnetic radiation is related to the diffraction angle and lattice spacing in a crystalline sample. These diffracted X-rays are then detected, processed and counted (Dutrow and Clark, 2011).

In this study, a Bruker D8 Advance X-ray diffractometer (XRD) with Kα radiation of 40 kV and 40 mA was used to identify the type of crystal structure formed in every

condition. The scanning range (2θ) was within 20˚ to 80˚ at a scan speed of 0.1˚ sec^{-1} and step size of 0.02˚. The XRD machine employed is presented in Figure 3.13.

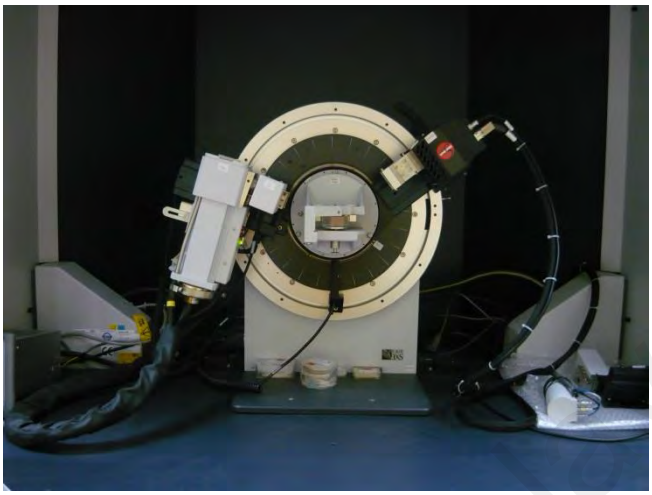

Figure 3.13: X-ray diffraction machine

CHAPTER 4: RESULTS AND DISCUSSION

4.1 Ti-6Al-4V – HA implants

In the present study, two types of Ti-6Al-4V implants embedded with hydroxyapatite (HA) were prepared. These are known as superplastic embedment (SPE) and superplastic deformation (SPD) implants. The as-received Ti-6Al-4V substrates were solution-treated prior to undergoing the embedment process.

4.1.1 Analysis of Heat-Treated Ti-6Al-4V

Figure 4.1 presents FESEM images of the as-received Ti-6Al-4V, which clearly display 13±0.5 μm of an equiaxed primary α-phase with secondary (platelet) α, and a small amount of intergranular β. Following the solution treatment process, α' martensite phase transformation was done. This phase consists of parallel-sided plates (lamella) or laths, as shown in Figure 4.2. The purpose of the treatment was to obtain an optimum condition for the subsequent embedment process via superplastic deformation. The reason is that the meta-stable microstructure (α' martensite) that formed after treatment had many dislocations both inside the grains and around the grain boundaries, thus creating a material with high grain boundary energy. The extra internal energy hastens grain refinement, and grain boundary sliding (GBS) occurs easily when a material deforms superplastically during SPE and SPD.

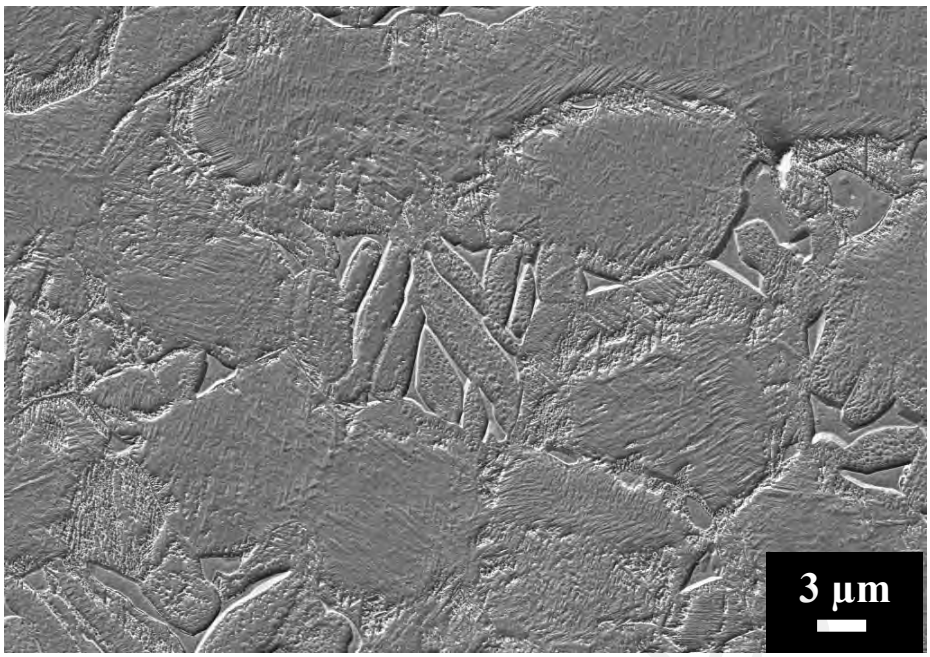

Figure 4.1: FESEM image of as-received Ti-6Al-4V

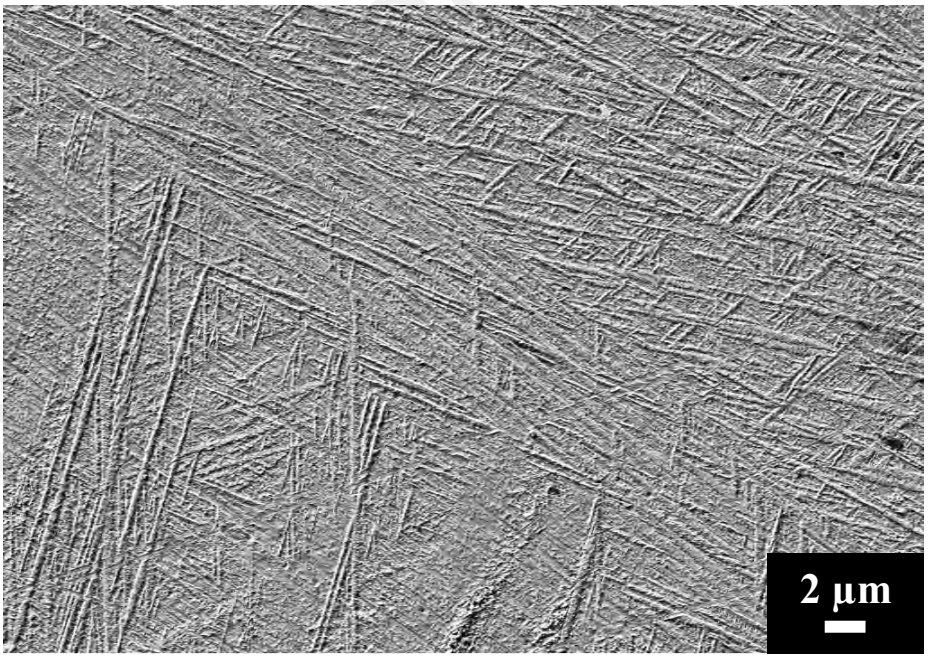

Figure 4.2: FESEM image of Ti-6Al-4V after solution treatment

4.1.2 Properties and Characterization of SPE and SPD

Figure 4.3 represents the stress versus strain curves obtained with the SPE and SPD processes. According to the figure, the SPE process exhibited a higher maximum stress (154±14.9 MPa) than SPD (112±7.7 MPa). The sample thicknesses reduced to 1.98±0.2 mm and 1.37±0.1 mm after SPE and SPD, respectively. Table 4.1 summarizes the properties of each process. No cracks were identified after both processes, indicating that the stress level experienced during the procedures was below the failure region. This also suggests that superplasticity occurred and had an important role in both processes through grain boundary sliding (GBS).

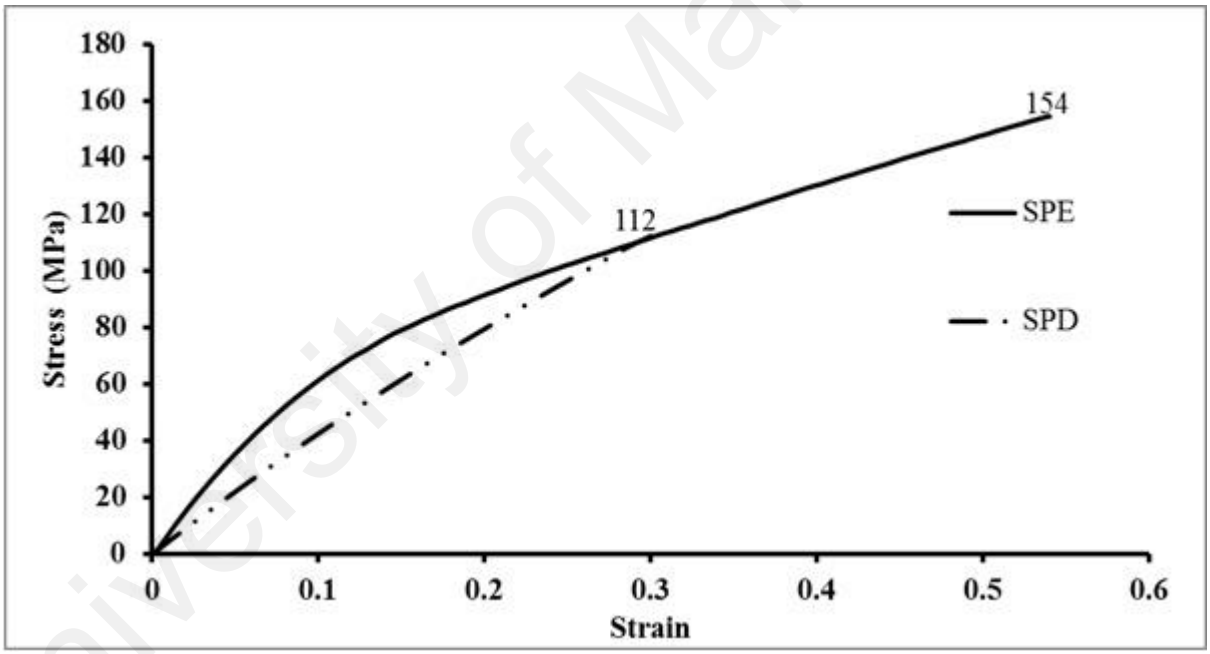

Figure 4.3: Stress-strain curves for Ti-6Al-4V alloy after superplastic embedment (SPE) and superplastic deformation (SPD)

Table 4.1: SPE and SPD properties. Each value is the average of five tests; values are given as mean± SD

Properties	Superplastic embedment (SPE)	Superplastic deformation (SPD)
Strain rate (s^{-1})	1×10^{-4}	1.6×10^{-3}
Maximum stress (MPa)	154 ±14.9	112 ± 7.7
Time (min)	90	3
Final samples thickness (mm)	1.98 ± 0.2	1.37 ± 0.1
HA layer thickness (nm)	249.1 ±0.5	206.1 ±4.9

The surface morphologies of the HA-embedded SPE and SPD samples and their cross-sectional images are depicted in Figure 4.4 to Figure 4.7. Following the SPE process, an embedded HA layer of approximately 249.1±0.6 nm (Figure 4.5) was obtained with a well-melted splat morphology (marked by black circles) and very fine globular morphology of un-melted HA (marked by white circles) (Figure 4.4). In contrast, after the SPD process (Figure 4.6) the surface was relatively rough, contained cracks and experienced delamination, and the HA layer was completely removed from the substrate's surface in certain areas. It is because; in the SPD process the sample has further experienced 30% deformation. Since the SPD sample known was a continuation from the SPE process, the embedded HA layer thickness after the SPD process was diminished, as shown in Figure 4.7. After SPD, the HA layer was approximately 206.1±5.8nm thick. The results are quite similar to previous works, where the embedded HA layer decreased when exposed to higher compression stress (Jamlus et al., 2014).

However, according to the cross-sectional view of SPD, the HA nanolayer remained intact and uniform on the substrate even after experiencing such large deformation.

The X-ray diffraction (XRD) image in Figure 4.8 illustrates that the HA structure was retained even after experiencing deformation. Moreover, the HA crystallinity improved with further heating to 1200K during the deformation process, as indicated by the strong HA line peaks, especially at around 40˚in SPD sample. Some studies confirm that HA crystallinity increases when HA coatings are heat-treated (Gu et al., 2003; Huang, Best, Bonfield, & Buckland, 2010). This will be further discussed in a later section.

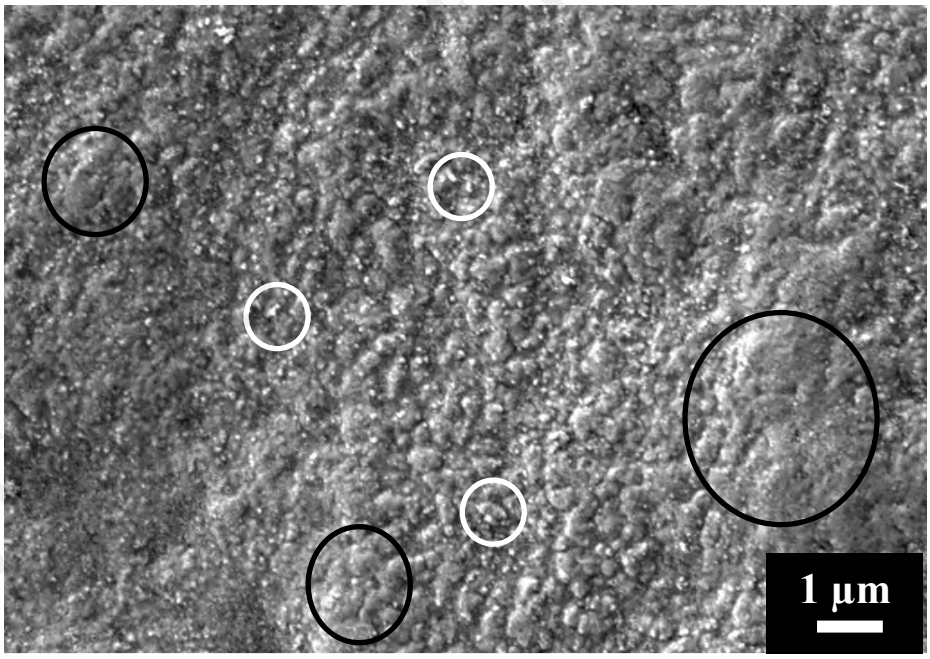

Figure 4.4: Surface morphology of HA layer embedded in SPE sample

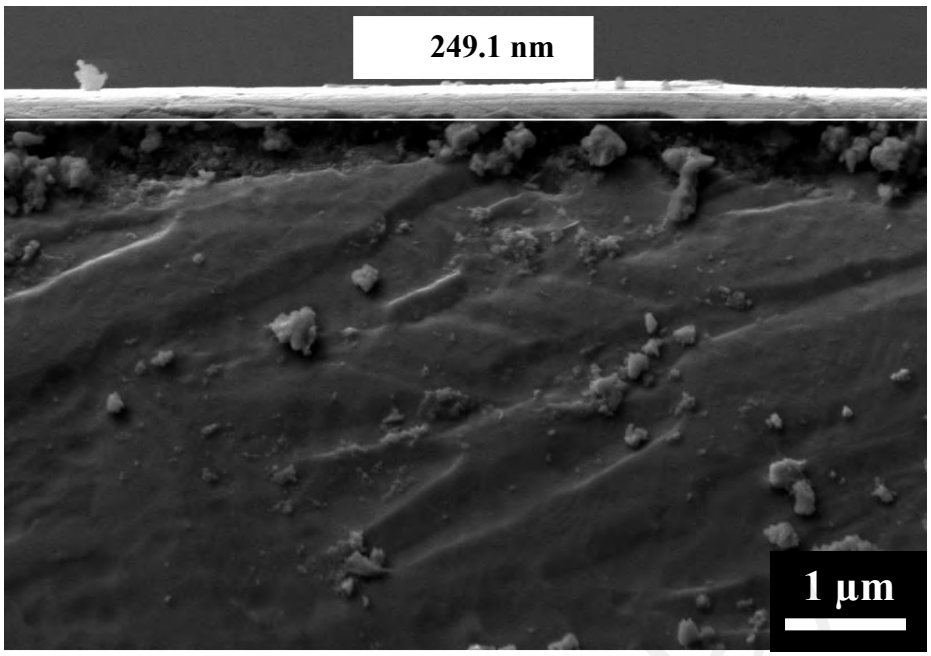

Figure 4.5: Cross-sectional view of HA layer embedded in SPE sample

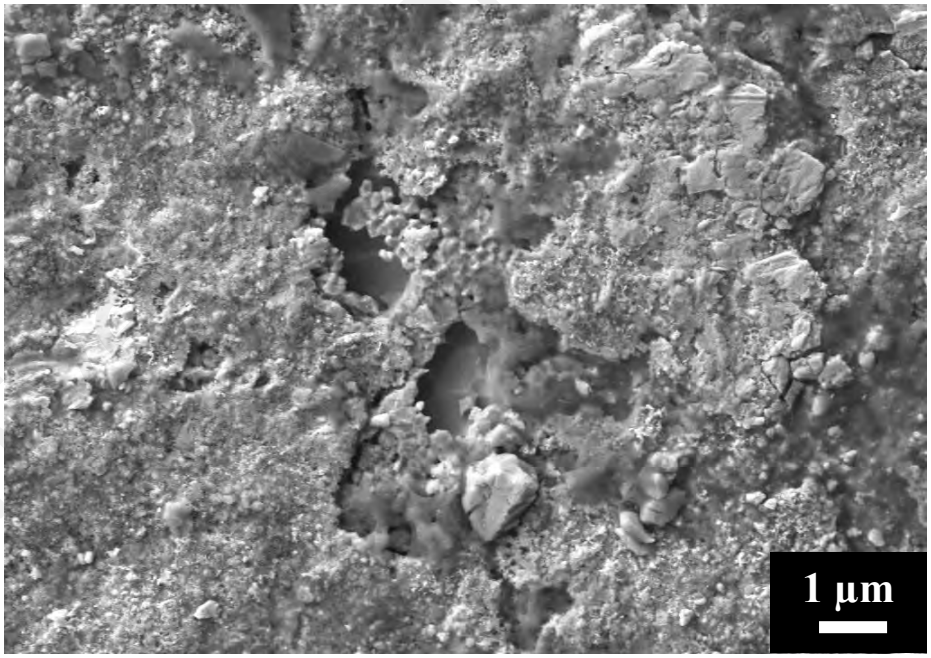

Figure 4.6: Surface morphology of HA layer embedded in SPD sample

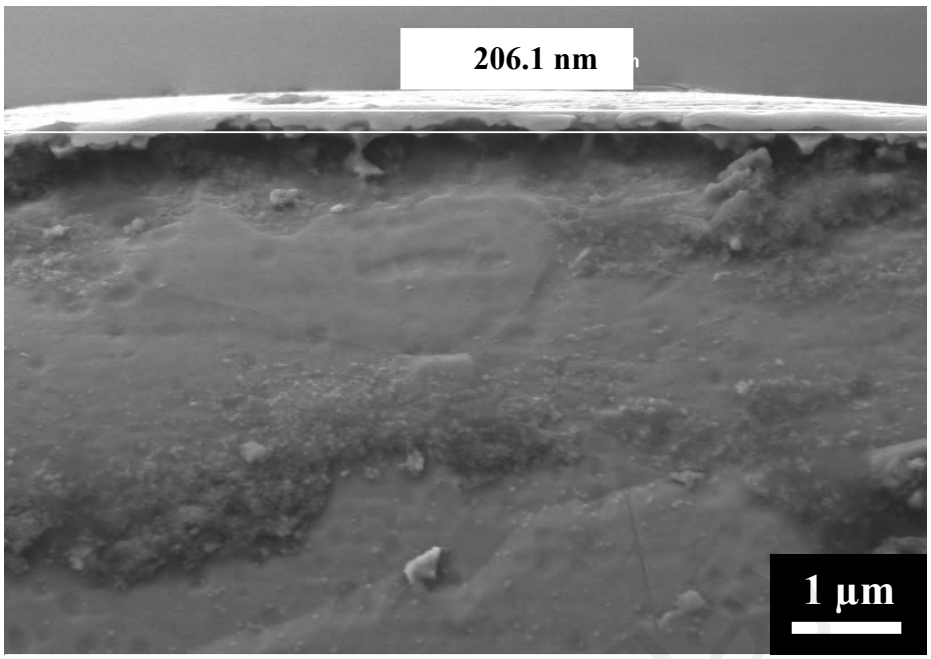

Figure 4.7: Cross-sectional view of HA layer embedded in SPD sample

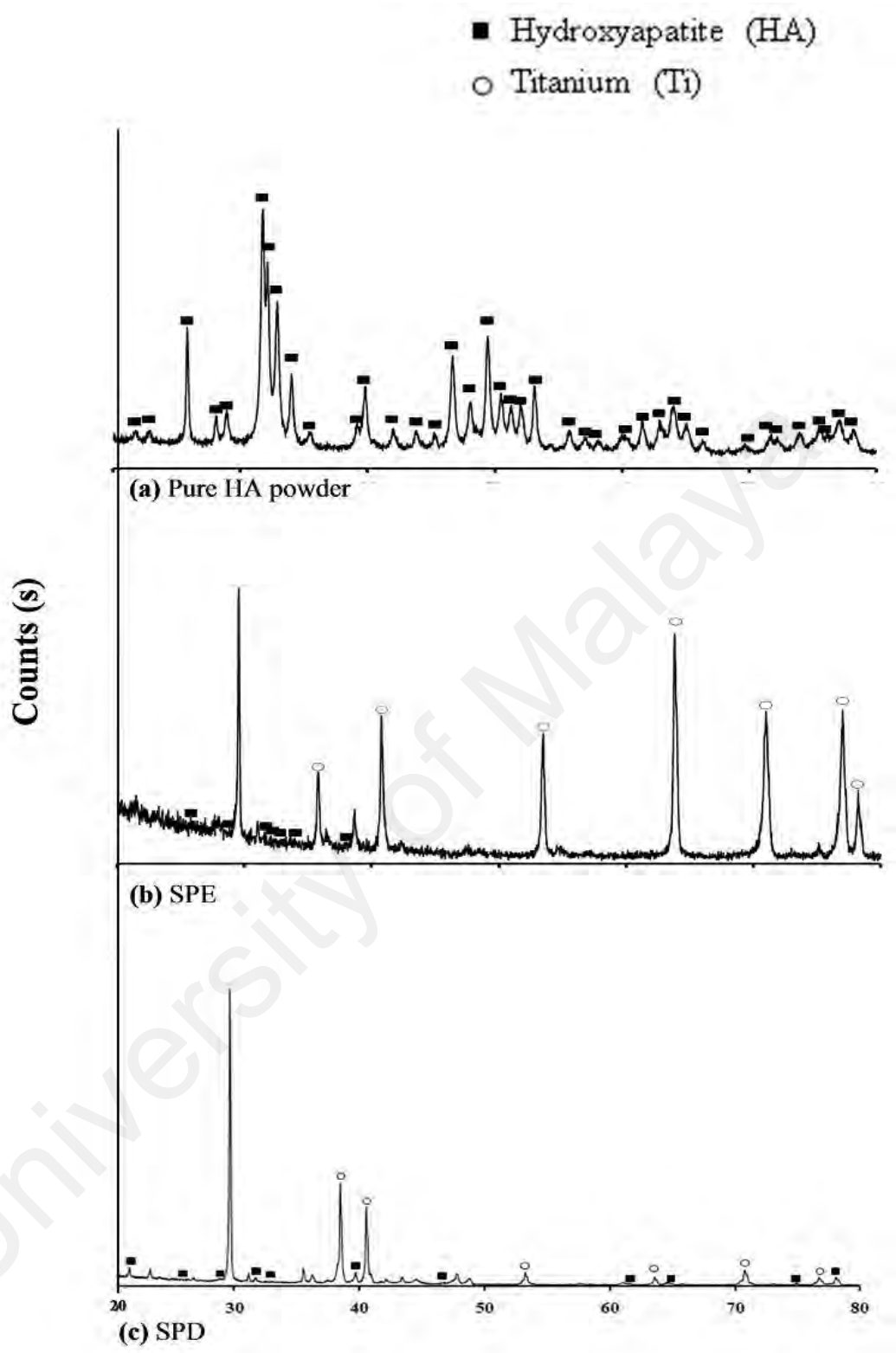

Figure 4.8: X-ray diffractograms of: (a) pure HA powder, (b) SPE sample and (c) SPD sample

4.2 Macroscopic Observation

All rats tolerated the operative procedure well. The SPE and SPD implants remained intact and united subcutaneously at all post-implant time points. As a general observation of the rats, no operative site infections behavioural changes or visible signs of physical/systematic impairment were recognized.

4.2.1 SPE and SPD Bioactivity after Implantation

Bioactivity is widely viewed as an essential requirement for an artificial biomaterial to exhibit chemical bonding to living host tissues upon bone formation, for instance apatite layer formation on the material's surface in any simulated body environment (Forsgren et al., 2007; Yoshida et al., 2012). Therefore, implanted SPE and SPD samples bioactivity was evaluated through the surface morphology and properties of the implanted HA nanolayer in the SPE and SPD samples, respectively.

4.2.1.1 Surface Morphology and Properties of Implanted HA Nanolayer (SPE)

The HA layer thickness and surface morphology of the SPE samples after implantation for various periods of time are illustrated in Figure 4.9 to Figure 4.14. After 1 week of implantation, the HA layer thickness increased to approximately 537.9±27.3 nm (Figure 4.9). A combination of needle-shaped crystal clusters and bone-like structure (spongy bone) appeared on the entire surface as a newly-grown HA layer (Figure 4.10). It was found that some areas were only covered with spongy or needle-shape structures while other areas were covered with a mixture of both structures. Micropores were also recognizable more on the spongy area and a well-interconnected macro-porous structure was identified only on the needle-shape structure. The spongy structure appeared upon initiation of new HA layer growth (Stergioudi, Choleridis, Paulidou, Smyrnaios, & Michailidis, 2015). The HA layer thickness increased to approximately 737.6±40.8 nm (Figure 4.11) and 874.8±37 nm (Figure 4.13) when the

implantation time increased to 5 and 12 weeks, respectively. The SPE surface morphology evoked the formation of abundant rough apatite structures after 5 weeks of subcutaneous implantation (Figure 4.12). On week 12, the overall structure was the same as on week 5, but apatite structure growth was apparent, as illustrated by the rougher globular apatite structure with very fine micropores (Figure 4.14).

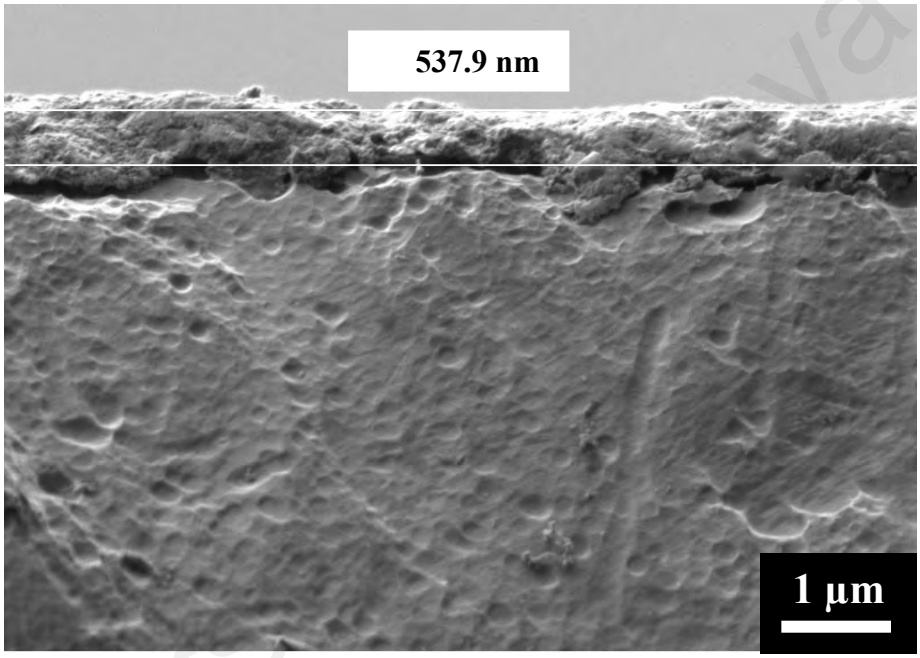

Figure 4.9: Cross-sectional view of SPE sample after 1 week of implantation

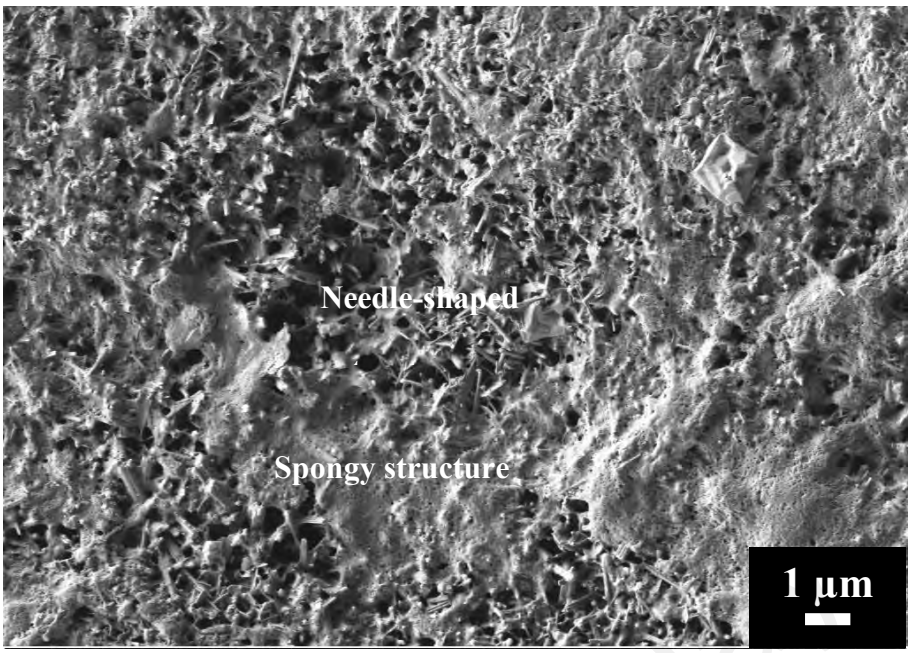

Figure 4.10: Surface morphology of the SPE sample after 1 week of implantation.

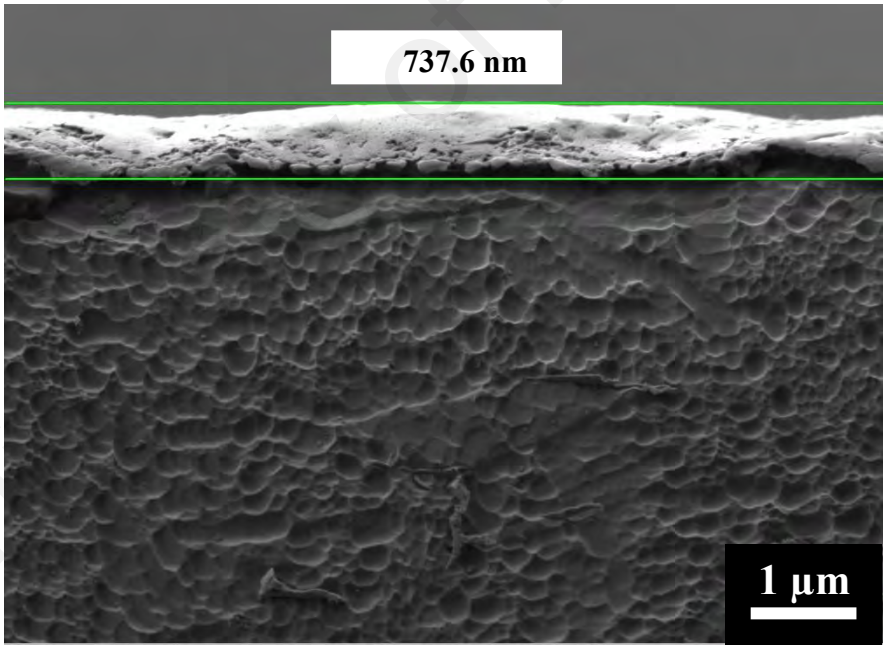

Figure 4.11: Cross-sectional view of SPE sample after 5 weeks of implantation

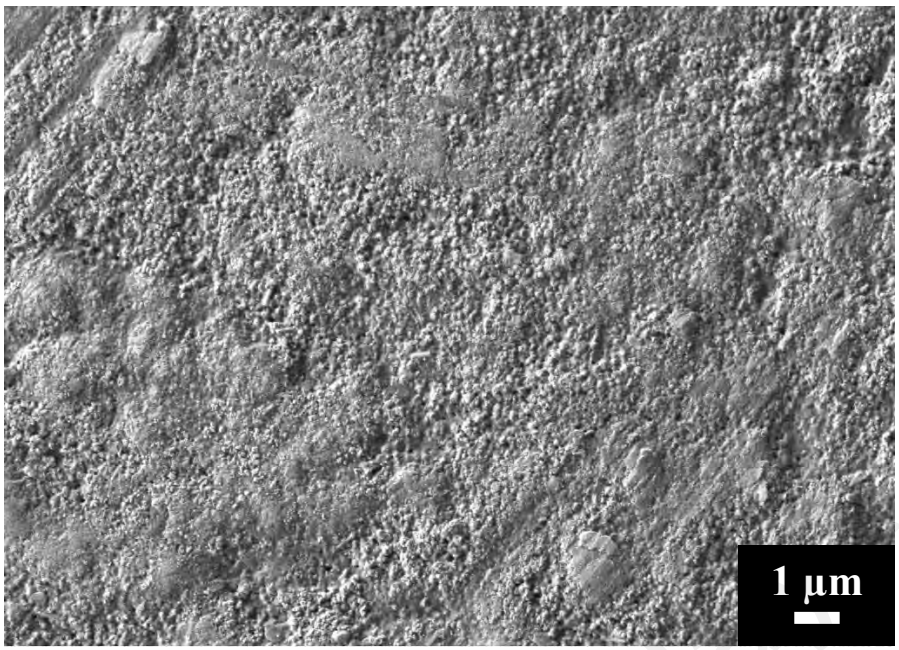

Figure 4.12: Surface morphology of SPE sample after 5 weeks of implantation

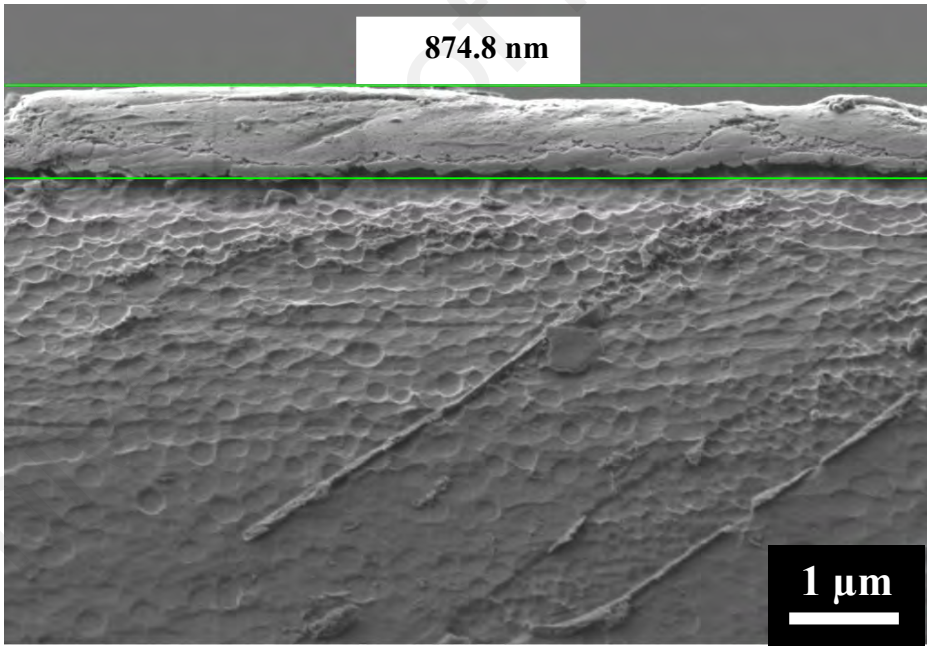

Figure 4.13: Cross-sectional view of SPE sample after 12 weeks of implantation

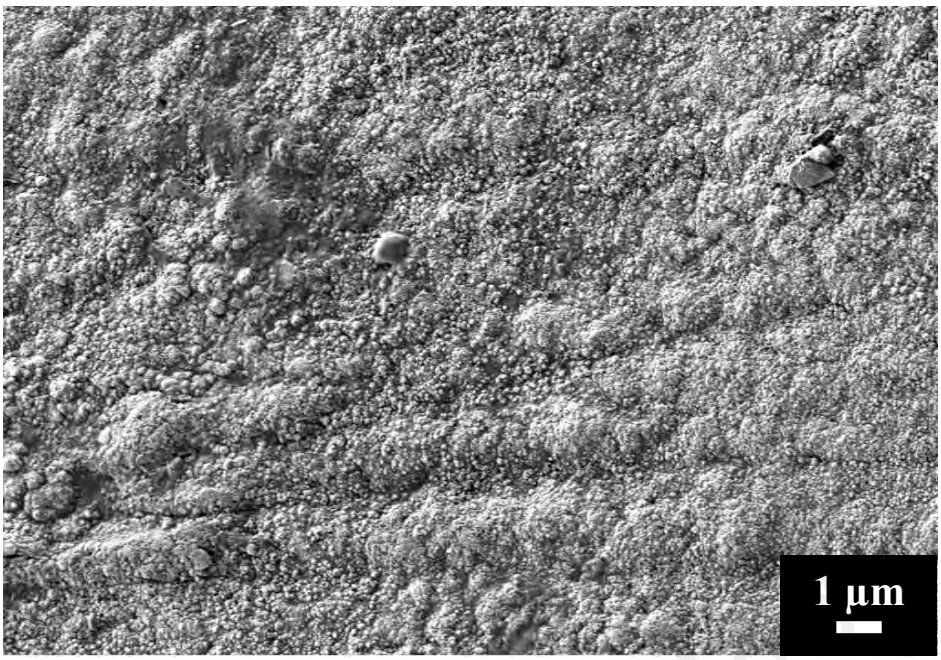

Figure 4.14: Surface morphology of SPE sample after 12 weeks of implantation

4.2.1.2 Surface Morphology and Properties of Implanted HA Nanolayer (SPD)

Cross-sectional and surface morphology images of the SPD samples after implantation on weeks 1, 5 and 12 are shown in Figure 4.15Figure 4.20. At 1 week after implantation, the surface morphology of the sample (Figure 4.16) was similar to that of the SPE sample after 5 weeks of implantation. At this stage, a needle-shape structure was observed after 1 week of implantation of SPE is not in the appearance. The HA layer thickness increased drastically to 731.8±50.6 nm (Figure 4.15). By 5 weeks of implantation, the surface morphology was generally the same as in earlier weeks, but the spongy structure was still quite noticeable as marked by the black arrows (Figure 4.18). This suggests that HA layer growth continued. The HA layer thickness here was approximately 1139.8±70.2 nm (Figure 4.17). After 12 weeks of implantation, the surface morphology showed no signs of a spongy structure (Figure 4.20). The HA layer thickness also only exhibited marginal growth, as seen in Figure 4.19 (1162.6±91.3 nm). This indicates that HA layer growth stabilized, and no more growth was expected.

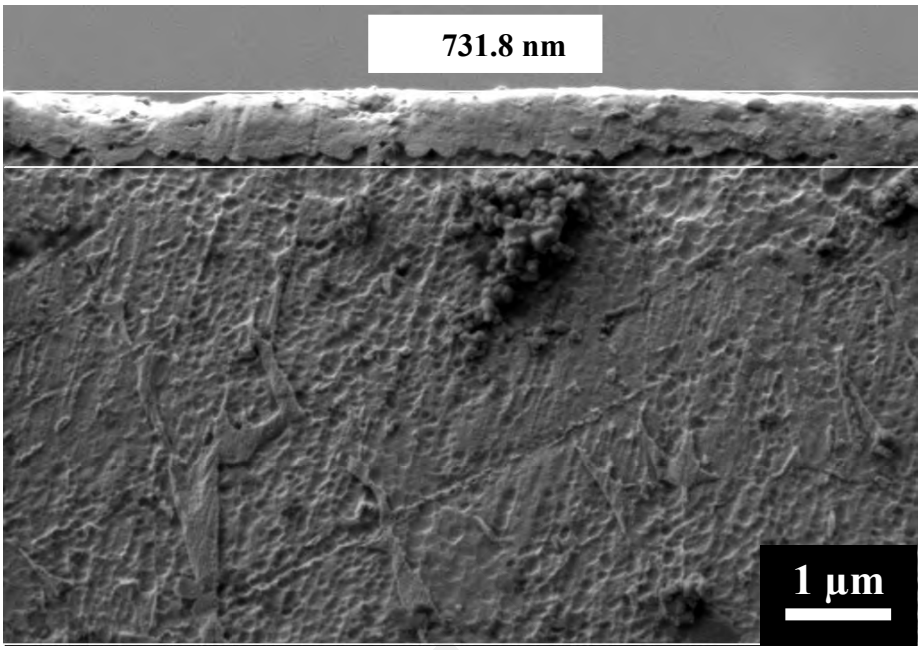

Figure 4.15: Cross-sectional view of SPD sample after 1 week of implantation

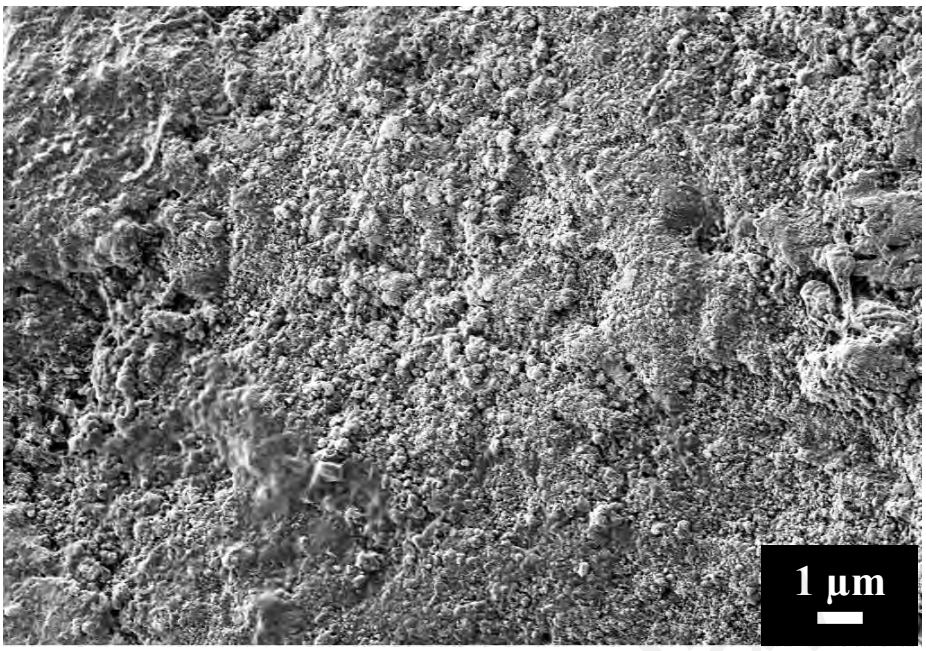

Figure 4.16: Surface morphology of SPD sample after 1 week of implantation

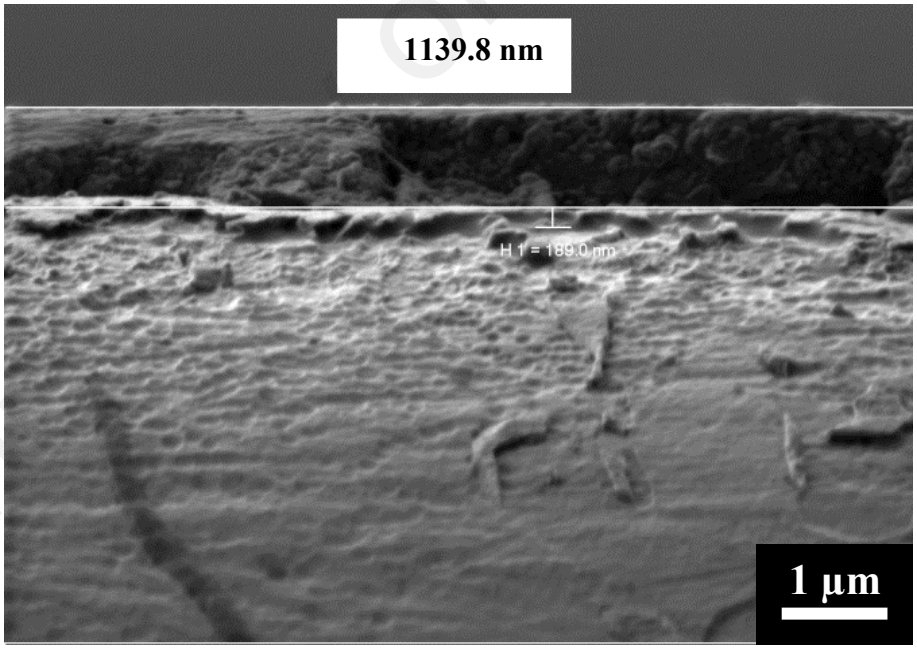

Figure 4.17: Cross-sectional view of SPD sample after 5 weeks of implantation

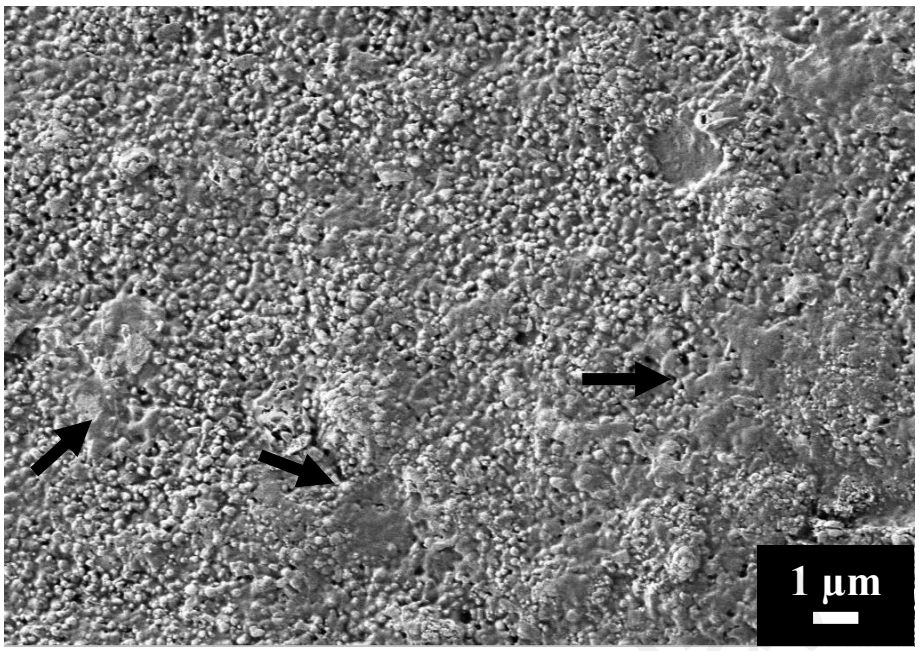

Figure 4.18: Surface morphology of SPD sample after 5 weeks of implantation

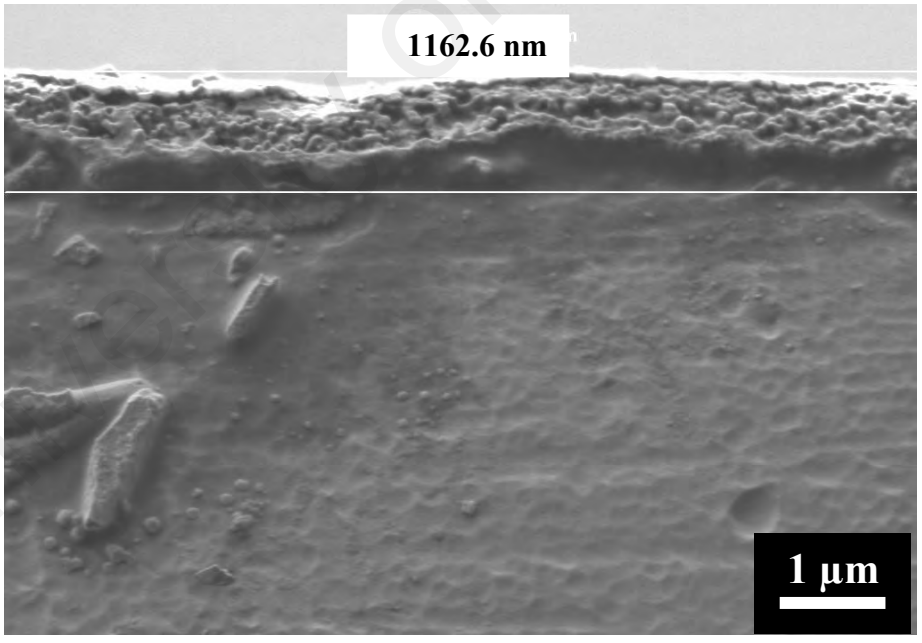

Figure 4.19: Cross-sectional view of SPD sample after 12 weeks of implantation

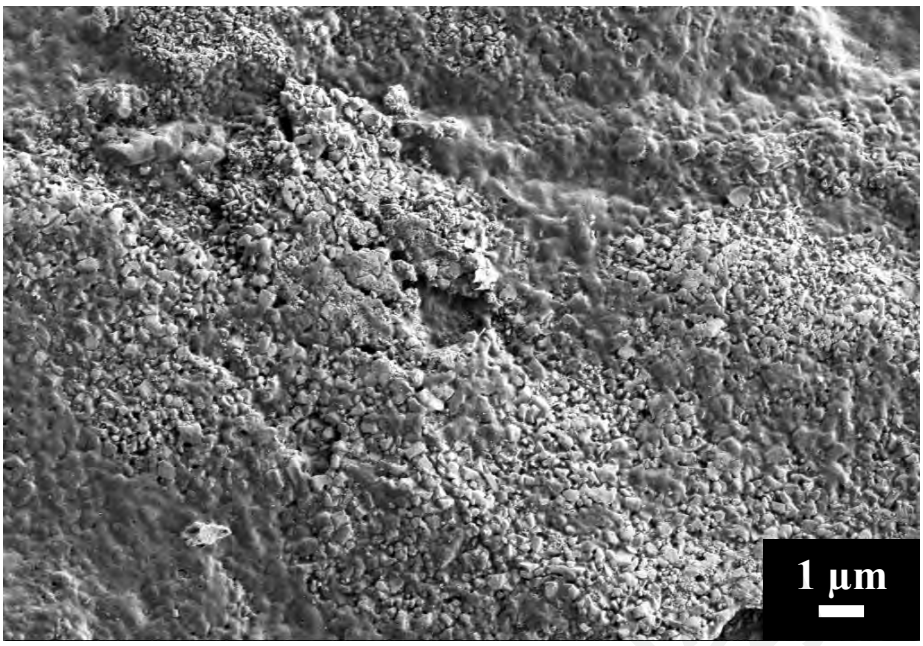

Figure 4.20: Surface morphology of SPD sample after 12 weeks of implantation

4.2.2 Stability of Implanted HA Nanolayer

Figure 4.21 summarizes the HA layer thickness growth with implantation time for both SPE and SPD samples. It can be clearly distinguished that despite a thinner initial HA layer before implantation (206.1±5.8 nm), the SPD sample experienced much faster growth than the SPE sample (initial HA layer thickness of 249.1±0.6 nm). Figure 4.21 indicates that the HA layer growth in SPE from week 1 to 5 was about 200 nm, whereas for SPD the growth was much greater with about 431 nm. The p was less than 0.05 for SPE and SPD at weeks 1,5 and 12. This suggests the importance of having a higher amount of HA in the initial condition in order to achieve rapid crystallized HA growth during implantation. The results also reveal that even after the new crystallized HA layer formed and covered the initial HA layer, new HA layer growth was strongly dependent on the HA amount in the initial condition (before implantation). In this regard, some studies have reported that HA coatings with high degrees of crystallinity

demonstrate more direct contact *in vivo* (Overgaard, Bromose, Lind, Bunger, & Soballe, 1999; Tahmasbi Rad, Solati-Hashjin, Osman, & Faghihi, 2014).

Figure 4.22 illustrates the XRD patterns of the SPE and SPD samples after 1 and 12 weeks of implantation. Obviously, the HA peaks significantly increased after implantation. The HA line peaks for the SPD samples were stronger than for SPE. The results confirm that the initial (deformed) HA layer was able to enhance the samples' bioactivity. The TiO_2 and Ti_6O peaks appeared in this condition due to the effect of body fluid reaction to the sample.

Figure 4.23 shows the surface hardness values for the substrate and sample before and after implantation. The substrate hardness was about 321±28.8 HV. Following the SPE and SPD processes, the hardness values increased to 661±0.4 HV and 585±6.6 HV respectively. For both samples, the hardness decreased with implantation time although the HA layer thickness increased (Figure 4.21). This is because the new HA layer that grew on the initial HA layer was more porous than, and not as dense as the initial layer. The decrease in hardness was more apparent in the SPD sample.

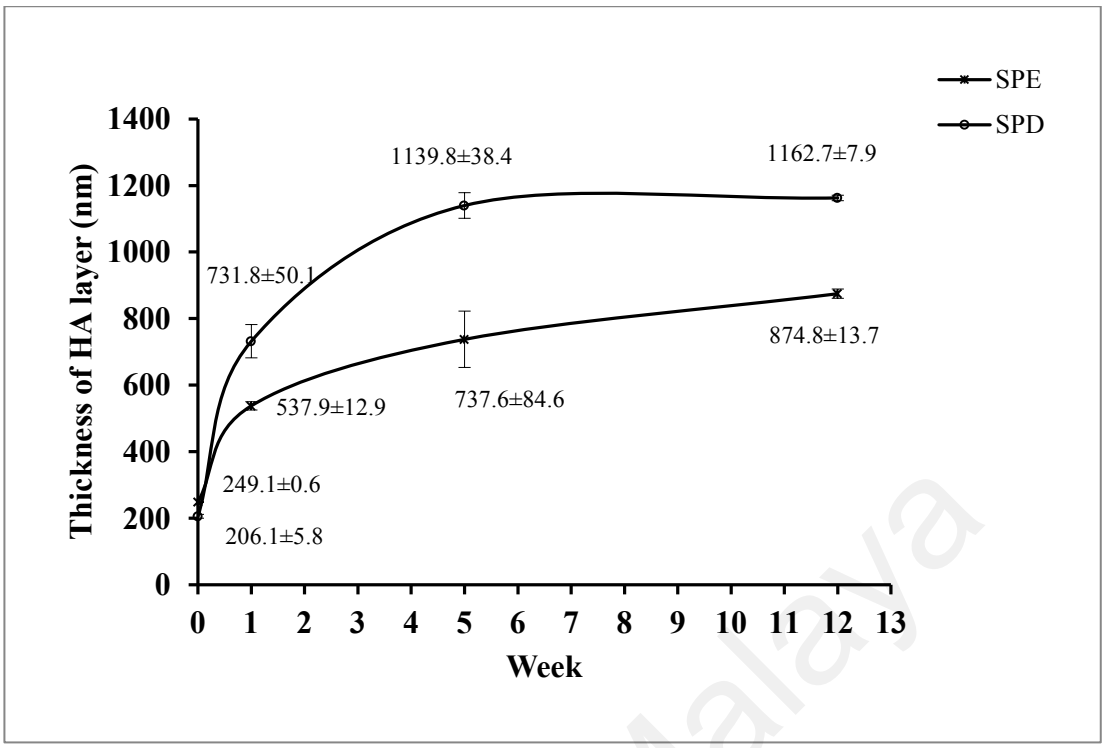

Figure 4.21: HA layer thickness for SPD and SPE samples at different time points after implantation ($p < 0.05$). Each value is the average of five tests; values are given as the mean± standard deviation

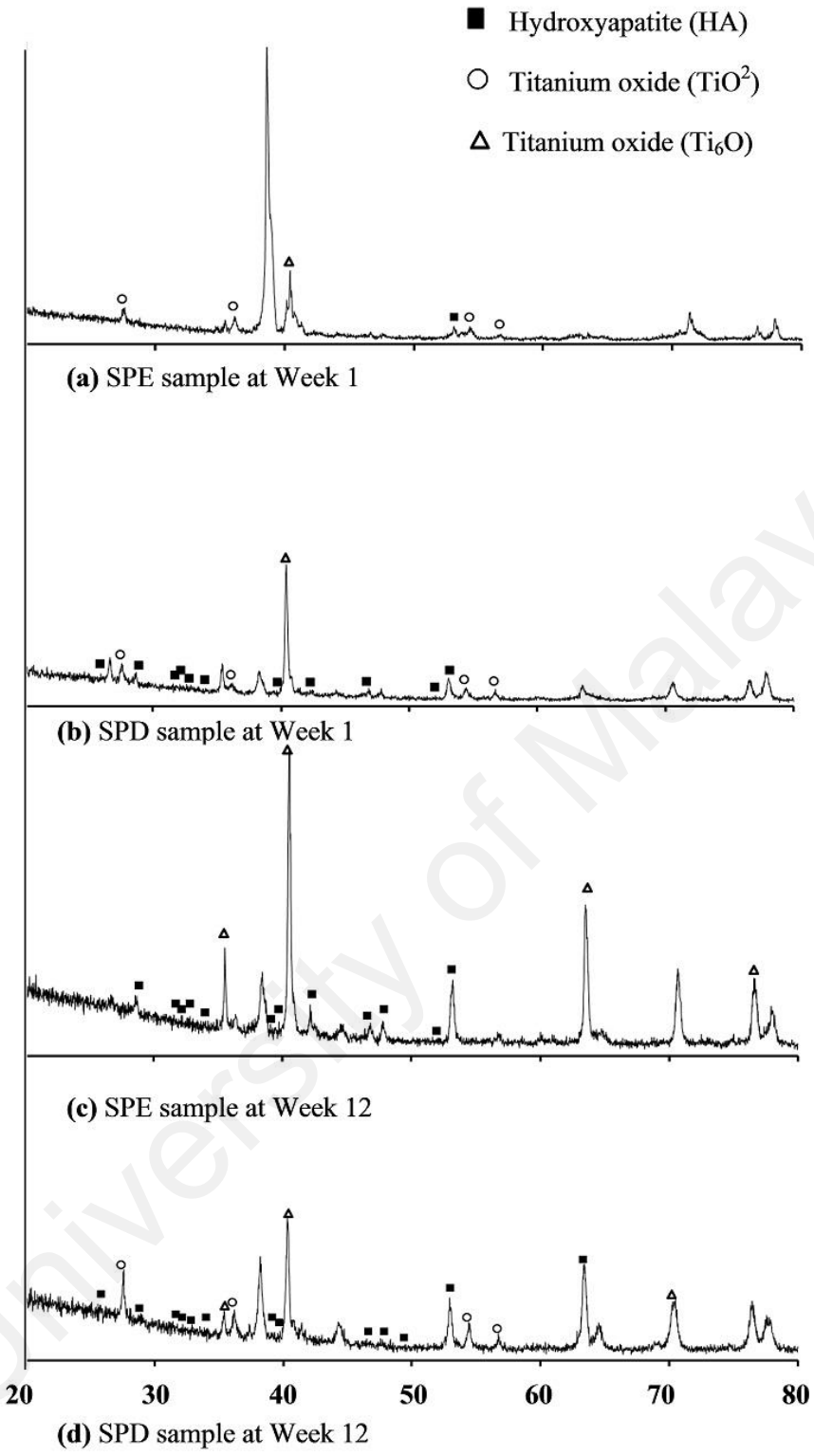

Figure 4.22: X-ray diffractograms of samples at different time points after implantation: (a) SPE sample at Week 1, (b) SPD sample at Week 1, (c) SPE sample at Week 12 and (d) SPD sample at Week 12

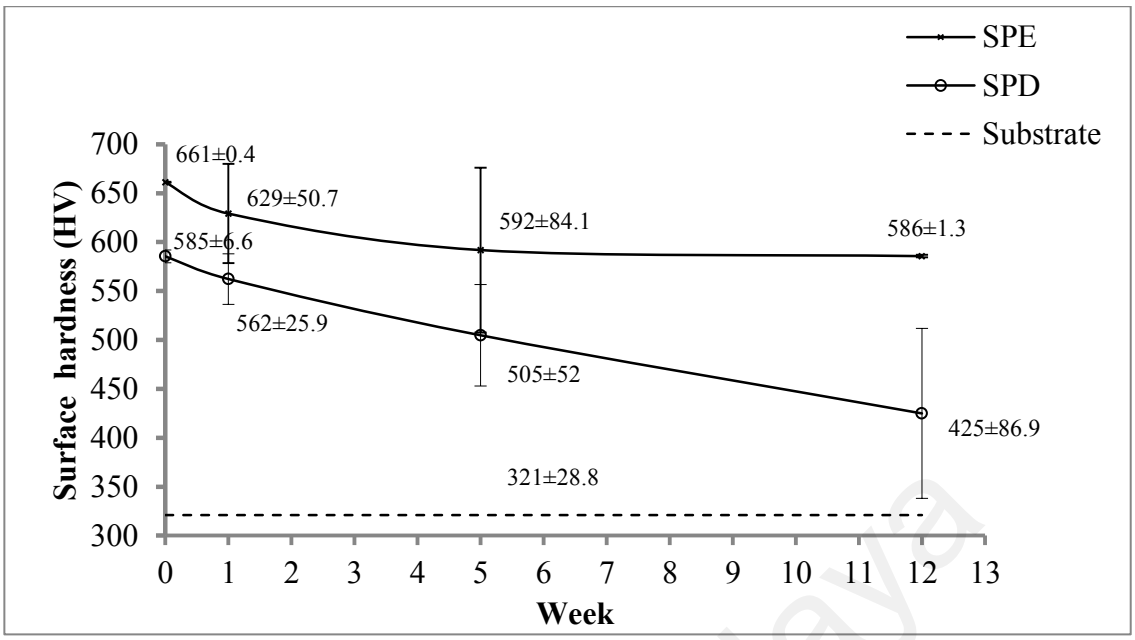

Figure 4.23: Surface hardness of SPE and SPD samples at different time points after implantation. Each value is the average of five tests; values are given as the mean± SD

4.2.3 Stability of As-Received Ti-6Al-4V in *In Vivo* Condition

For comparison purposes, the as-received titanium alloy samples were exposed to the same *in vivo* condition for 5 and 12 weeks. As seen in Figure 4.24, after 5 weeks the surface of the as-received sample was almost like the original condition. After 12 weeks, the formation of dark patches was observed on the titanium alloy surface (Figure 4.25). Higher magnification of the dark patches (Figure 4.26) revealed spongy-like microstructures similar to the ones formed in the SPE and SPD samples discussed earlier in sections 4.2.1.1 and 4.2.1.2. However, it took about 12 weeks for the spongy-like microstructures to form and they were not homogenous throughout the surface.

According to the preceding results, both SPE and SPD samples functioned appropriately in *in vivo* condition throughout testing. Even after 1 week of implantation new HA layers grew more significantly on both samples as compared to 12 weeks for the as-received sample, indicating that the HA embedded layers reacted positively to the

body system. The bioactivity rate measured in terms of new HA layer growth was better in the SPD sample than SPE, because the HA crystallinity in the initial layer was higher.

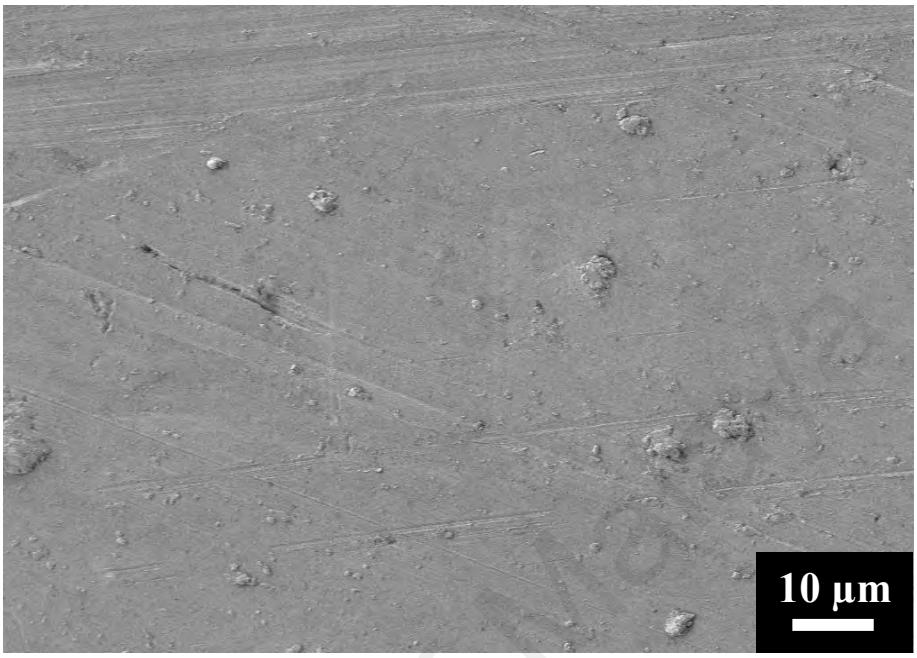

Figure 4.24: Surface morphology of as-received Ti-6Al-4V sample after 5 weeks of implantation

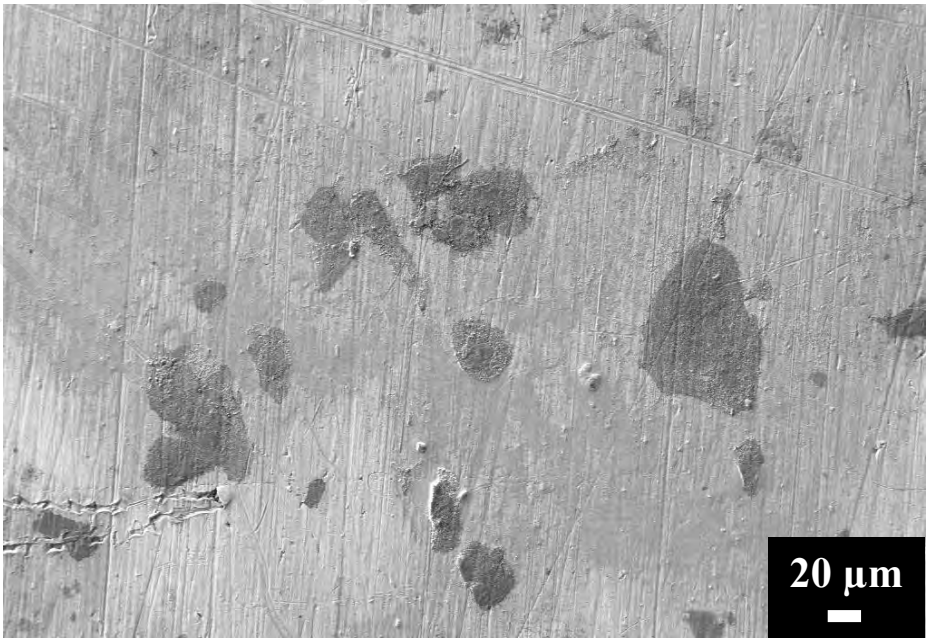

Figure 4.25: Surface morphology of as-received Ti-6Al-4V sample after 12 weeks of implantation

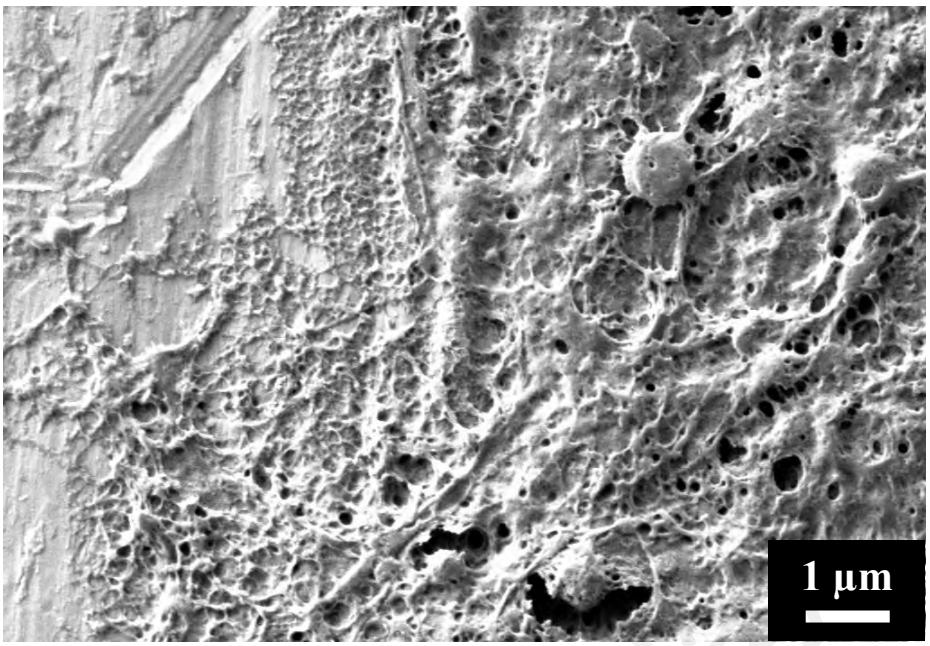

Figure 4.26: Surface morphology of as-received Ti-6Al-4V sample after 12 weeks of implantation at magnification of 10 000×

4.3 Biocompatibility of SPE and SPD Samples

It is important to assess the biocompatibility of a designed biomaterial to identify the nature and degree of interaction between the biomaterial and host tissue. Basically, biocompatibility consists of two elements: (a) biosafety, i.e., appropriate host response, not only systemic but also local (the surrounding tissue) and the absence of cytotoxicity, mutagenesis and/or carcinogenesis, and (b) biofunctionality, i.e., the ability of the material to perform the specific task intended (Morais, Papadimitrakopoulos, & Burgess, 2010; Shakya & Kumar, 2016).

4.3.1 SPE

Histological optical microscope images of each SPE sample implanted in subcutaneous tissue after 1 and 12 weeks post-surgery are shown in Figure 4.27 and Figure 4.28. The locations where the samples were implanted are marked by P. At week 1, an intense inflammation response (marked by arrows) in the SPE implant site section with mild fibrous connective tissue was observed (Figure 4.27). The figure also shows

finger-like fibrous tissue structures appearing to encroach the empty space left by the SPE implant, in an attempt to fill the space (marked by arrow heads). After week 12, less severe inflammation was observed around the implantation site (Figure 4.28).

Figure 4.27: Micrographs of rat subcutaneous tissue response to SPE implant at week 1 (20×)

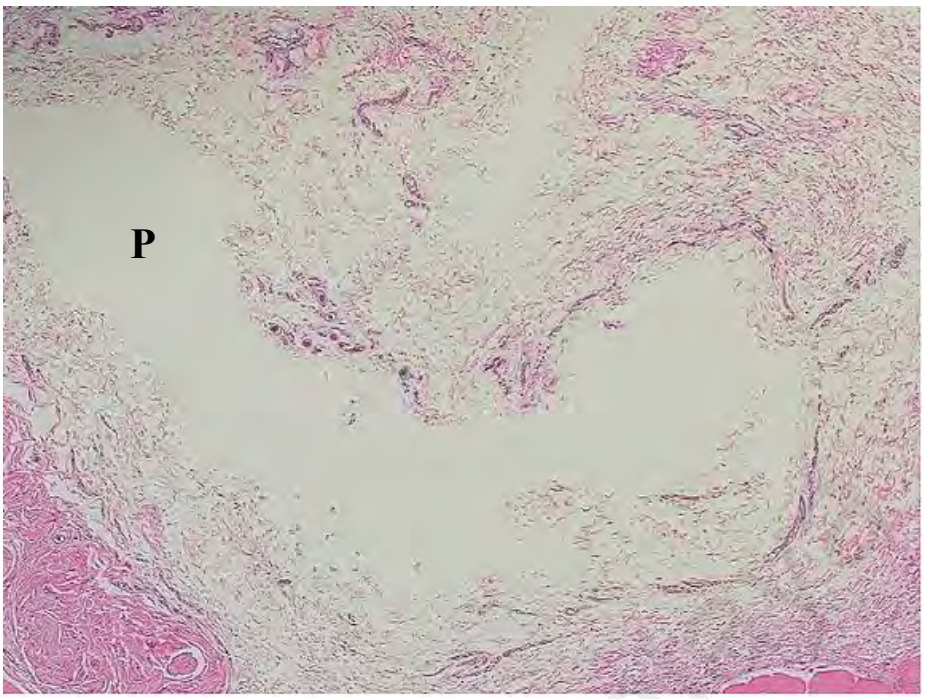

Figure 4.28: Micrograph of rat subcutaneous tissue response to SPE implant at week 12 (20×)

4.3.2 SPD

Figure 4.29 and Figure 4.30 represent micrographs of rat subcutaneous tissue response to the SPD implant. After week 1 of implantation (Figure 4.29), the areas surrounding the implant areas showed mild inflammation with numerous inflammatory cells consisting mainly of neutrophils. There were many new capillaries (marked by arrow heads) within the moderately thick, loose and fibrous tissue (marked by arrows). After week 12 (Figure 4.30) the inflammation subsided. The surrounding areas were characterized by thick fibrous tissue proliferation, indicating initial re-arrangement and organization (marked by arrows). The fibrous tissue seems to have encroached and filled the space left by the removed implant (marked by arrow heads).

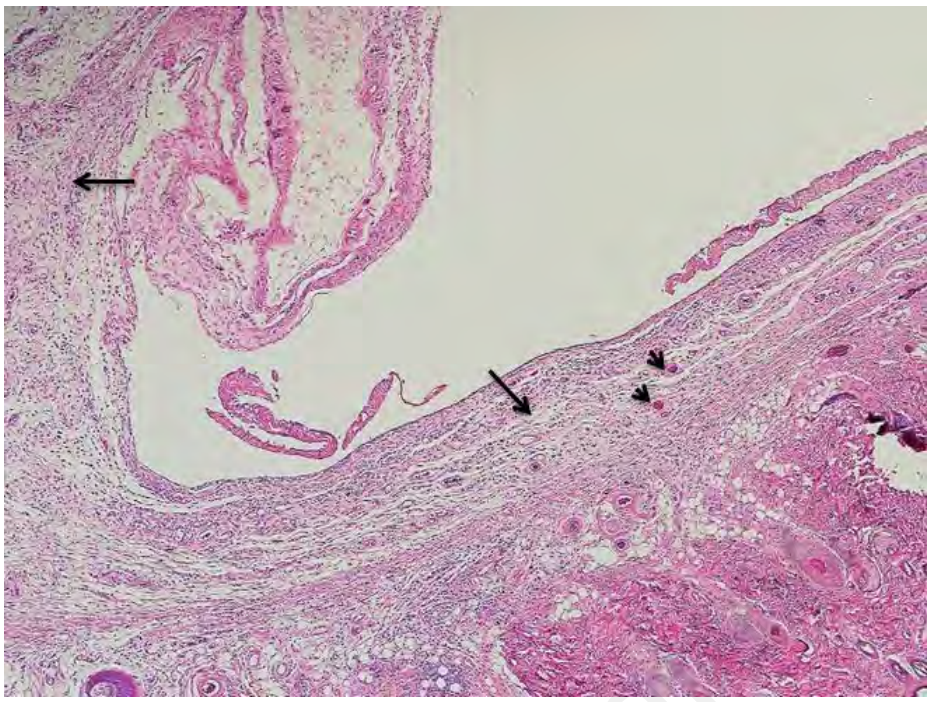

Figure 4.29: Micrograph of rat subcutaneous tissue response to SPD implant at week 1 (20×)

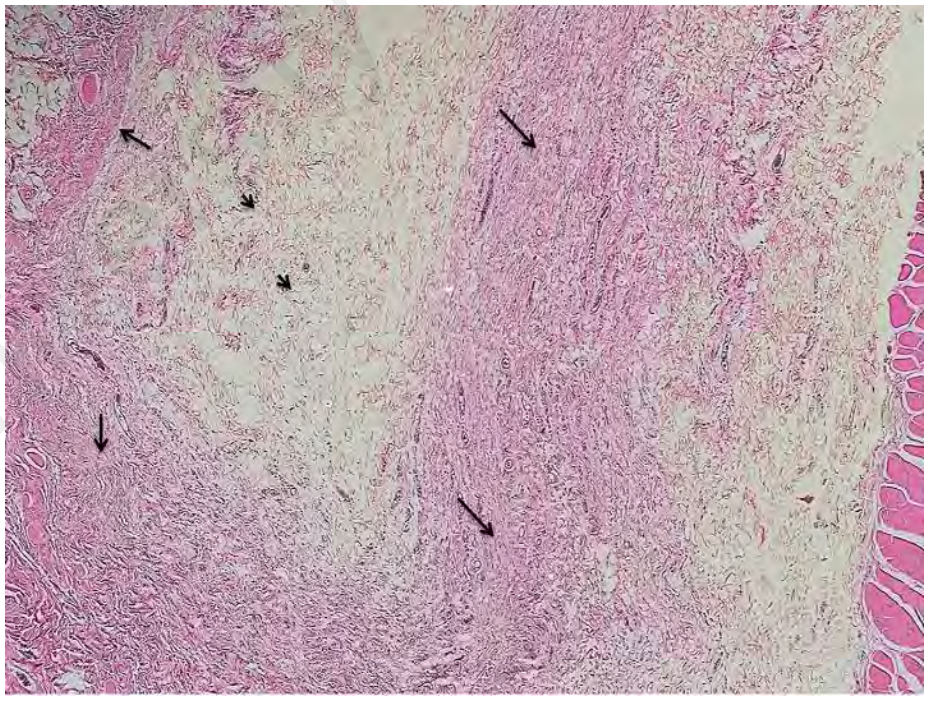

Figure 4.30: Micrograph of rat tissue response to SPD implant at week 12 (20×)

4.3.3 Biocompatibility of As-Received Ti-6Al-4V

The as-received implant did not exhibit any bioactivity even after 5 weeks of implantation, as described in section 4.2.3. Therefore, the microscopic histological observation for the as-received sample is based on 12 weeks of implantation. According to Figure 4.31, a thin, compact layer of well-organized fibrous tissue immediately surrounded the implant. A less organized, thick layer of fibrous tissue with less severe inflammation further surrounded the well-organized fibrous tissue layer. However, the proliferation of fibrous tissue was much milder compared with the SPE and SPD samples. It is well-known that fibrous tissue formation is very important, since it is an early tissue that populates a healing wound and is often also a major tissue that adheres to implant devices (Morais et al., 2010).

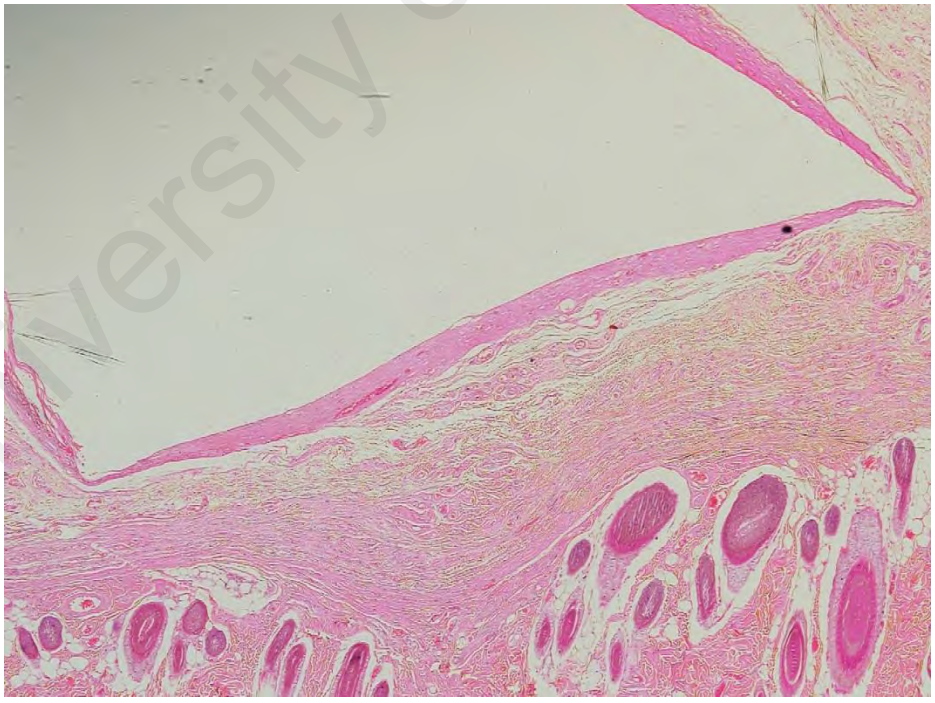

Figure 4.31: Micrograph of rat subcutaneous tissue response to as-received Ti-6Al-4V at 12 weeks (20×)

Based on the histological results, the tissue reactions to all samples (SPE, SPD and as-received) suggested reasonable compatibility, since tissue necrosis was totally absent and there was no evidence of extended acute inflammatory response. Although intense inflammatory reaction to the SPE sample was initially evident, the reaction subsided after longer implantation time. It is acknowledged that soft tissue inflammatory response to the implant in early implantation stages is normal and determines the stability and biocompatibility of the implanted device (Fulzele, Satturwar, & Dorle, 2003; Sato et al., 2008). However, after 12 weeks of implantation, fibrous tissue proliferated significantly, especially in the SPD sample, where the space left by the removed implant was almost completely filled by fibrous tissue. This suggests that the more bioactive HA layer accelerated the body system's response to the SPD sample.

4.4 Durability of the Implanted SPE and SPD Samples during Wear Testing

Figure 4.32 and Figure 4.33 illustrate schematics of the HA layers for SPE and SPD before and after implantation, which were summarized in sections 4.2.1.1 and 4.2.1.2. For SPE (Figure 4.32), the HA layer was 249.1±0.6nm thick following embedment. Due to the newly-formed HA layer, the HA layer increased to 537.9±27.3 nm and 874.8±37 nm after implantation for 1 and 12 weeks respectively. For SPD (Figure 4.33), the HA layer was 206.1±5.8 nm after superplastic deformation. After 1 and 12 weeks of implantation, the thickness increased to 731.8±30.8 nm and 1162.6±91.2 nm, respectively.

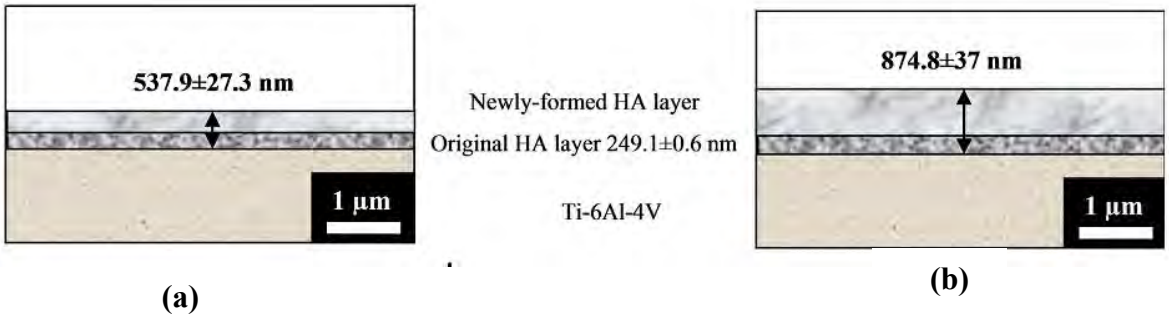

Figure 4.32: HA layers of SPE sample (a) before and (b) after implantation

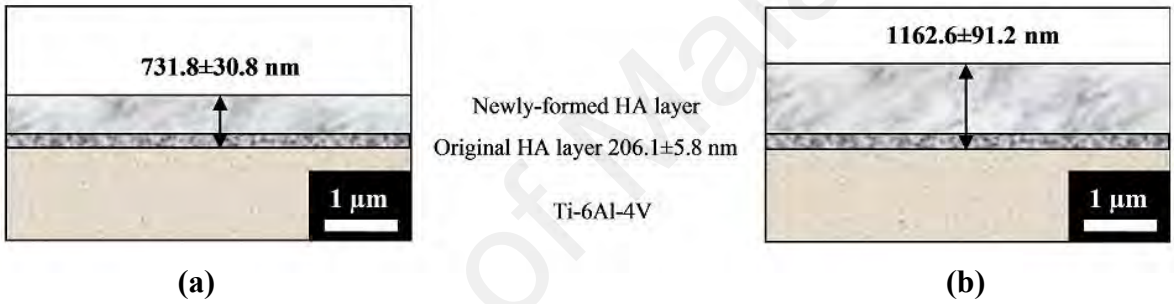

Figure 4.33: HA layers of SPD sample (a) before and (b) after implantation

4.4.1 Wear Testing of Implanted SPE Samples

Figure 4.34 Figure 4.39 present the surface morphology of the SPE implants before and after implantation at low and high magnification. As explained in section 4.1.2, after embedment the implant surface exhibited well-melted splat morphology (marked by black arrows) with very fine, globular un-melted HA (marked by white arrows) (Figure 4.35). After 1 week of implantation and exposure to wear, the HA surface experienced non-uniform surface removal (white arrows), where areas that spalled off the original HA surface were determined (Figure 4.36). However, as seen in the higher magnification image (Figure 4.37), it seems the spalled area was still covered by the original HA layer. This is because, the morphology of the smoother surface was nearly

the same as that of the SPE implant before implantation as shown in Figure 4.34. Moreover, EDX analysis confirmed that the surface contained HA elements of Ca and P (Figure 4.40 and Figure 4.41). After 12 weeks of implantation and after wear, the surface area showed no un-uniform surface removal and it looked smooth with some signs of scratches as a result of sliding against cloth (Figure 4.38). At higher magnification (Figure 4.39), the surface clearly showed the morphology of a newly-formed HA layer. However, the apatite formation structure agglomerated and the macroporous structure was not uniform as the SPE morphology after implantation, as described in section 4.2.1.1.

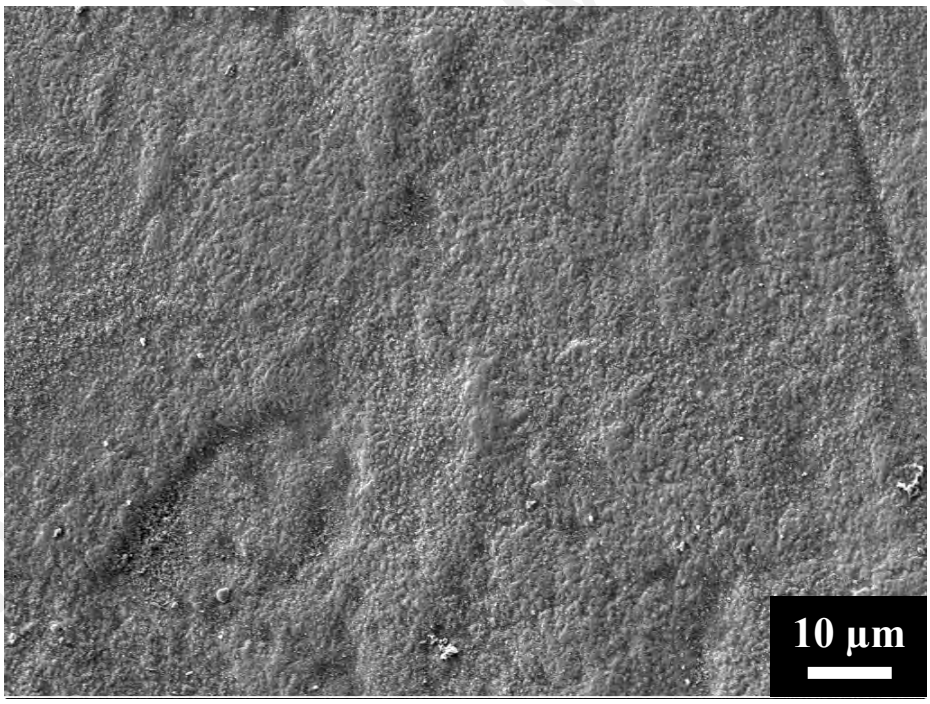

Figure 4.34: Surface morphology of SPE implant at low magnification (1000×)

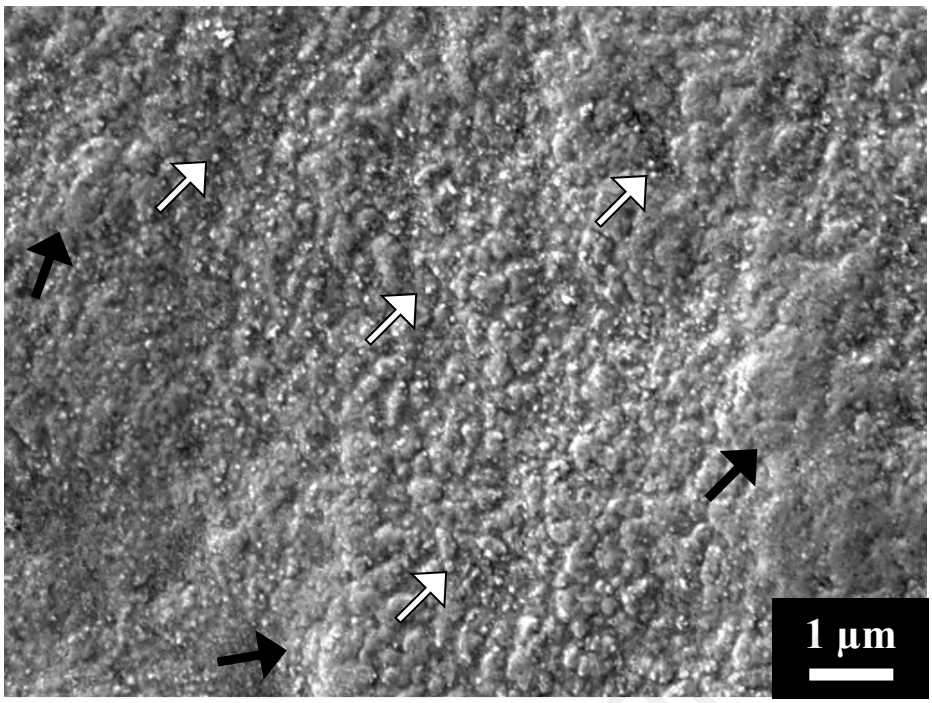

Figure 4.35: Surface morphology of SPE implant before implantation at high magnification (10000×)

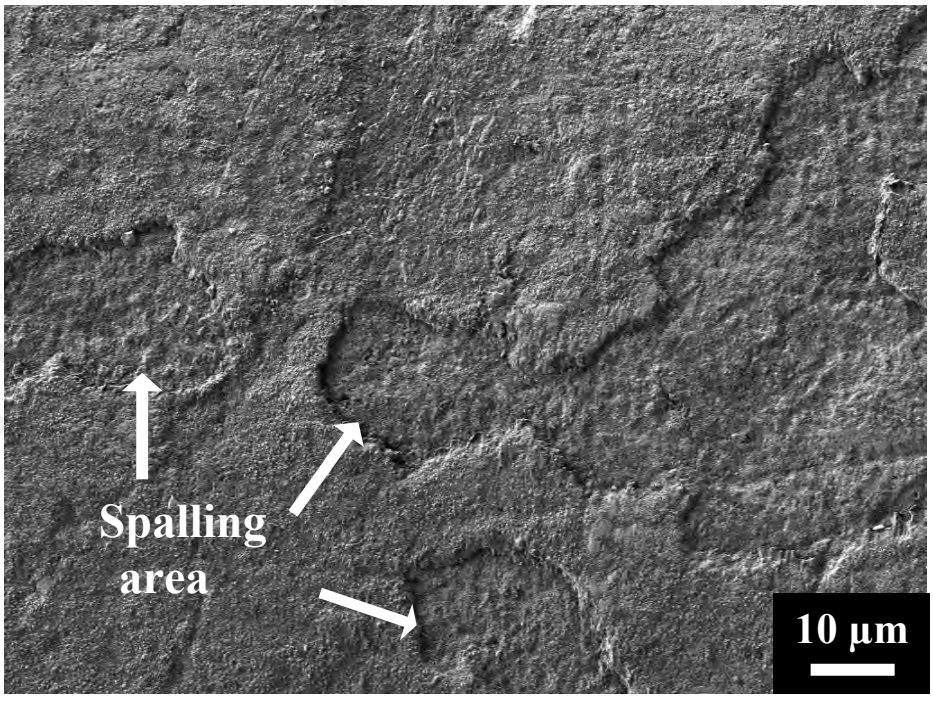

Figure 4.36: Worn surface morphology of SPE implant after 1 week of implantation at low magnification (1000×)

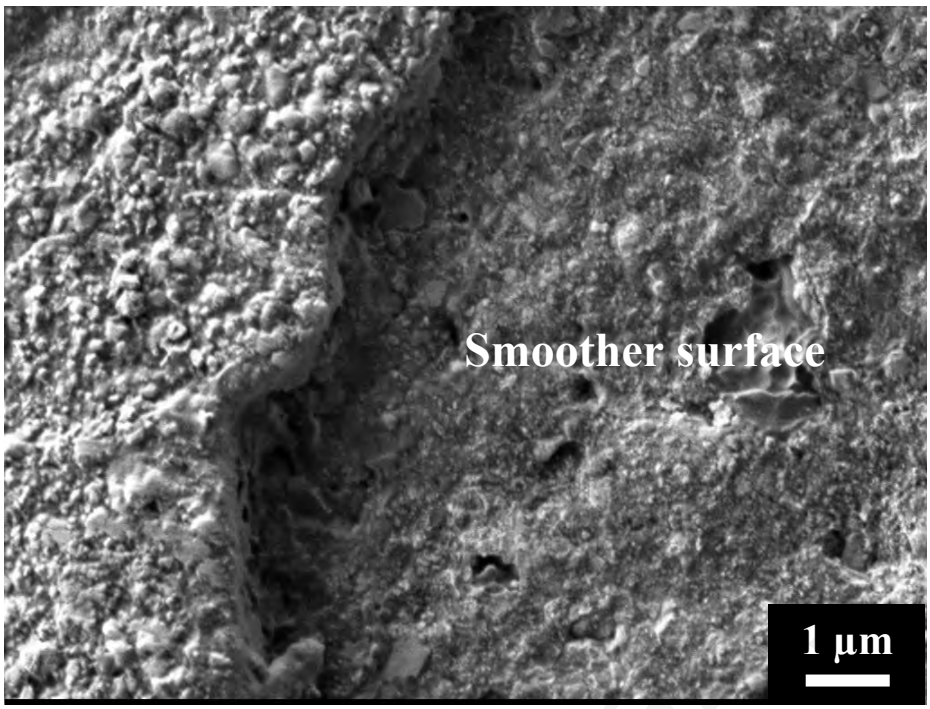

Figure 4.37: Worn surface morphology of SPE implant after 1 week of implantation at high magnification (10000×)

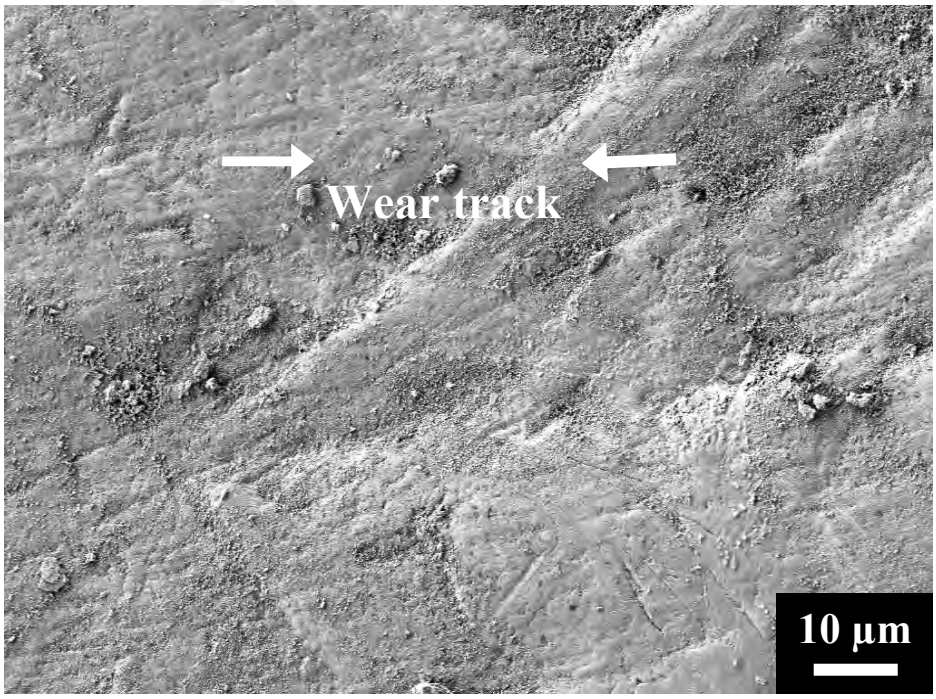

Figure 4.38: Worn surface morphology of SPE implant after 12 weeks of implantation at low magnification (1000×)

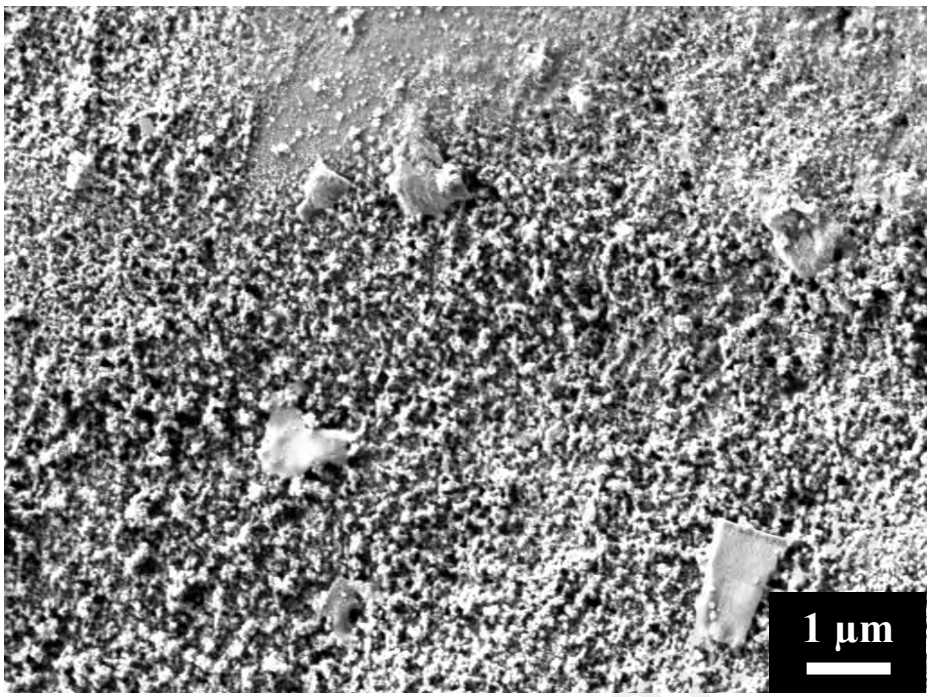

Figure 4.39: Worn surface morphology of SPE implant after 12 weeks of implantation at high magnification (10000×)

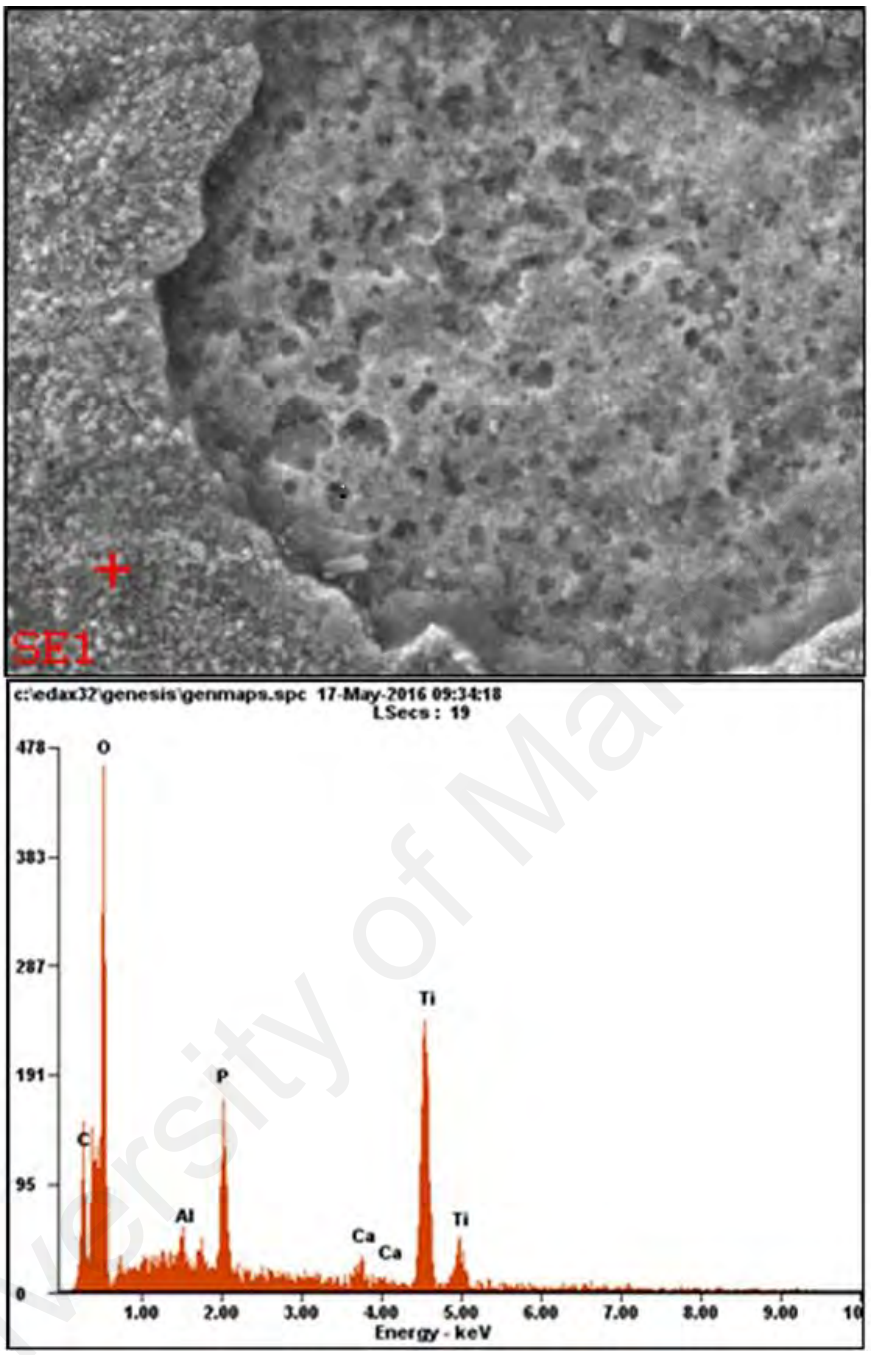

Figure 4.40: EDX spectrum of worn SPE surface at 1 W, with focus on the non-spalled area of the newly-formed HA layer

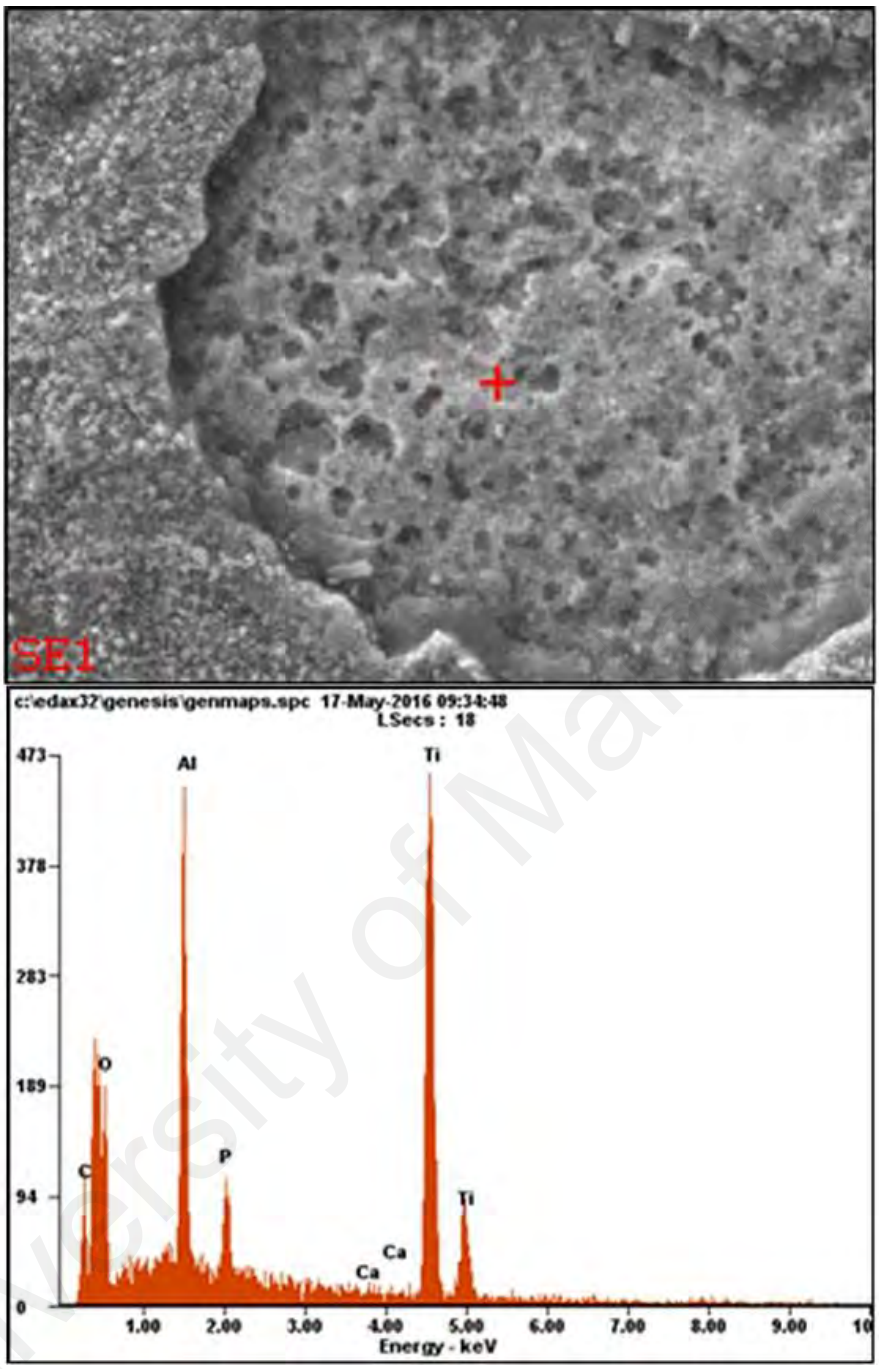

Figure 4.41: EDX spectrum of worn SPE surface at 1 W, with focus on the spalled area of the newly-formed HA layer

4.4.2 Wear testing of implanted SPD samples

Figure 4.42 to Figure 4.47 illustrate the surface morphology of the SPD implant before and after implantation at low and high magnification. After the SPD process (Figure 4.43) the surface was relatively rough, contained cracks and experienced delamination due to a further 30% superplastic deformation. After 1 week of implantation and exposure to wear (Figure 4.44), a rough and spongy structure was still noticeable (marked by white arrows) and the surface removal structure did not appear. At higher magnification, the surface was still clearly covered by the newly-formed HA layer (Figure 4.45). After 12 weeks of implantation, the worn surface morphology at low and high magnification (Figure 4.46 and Figure 4.47) was more or less similar to that at 1 week of implantation, as shown in Figure 4.16.

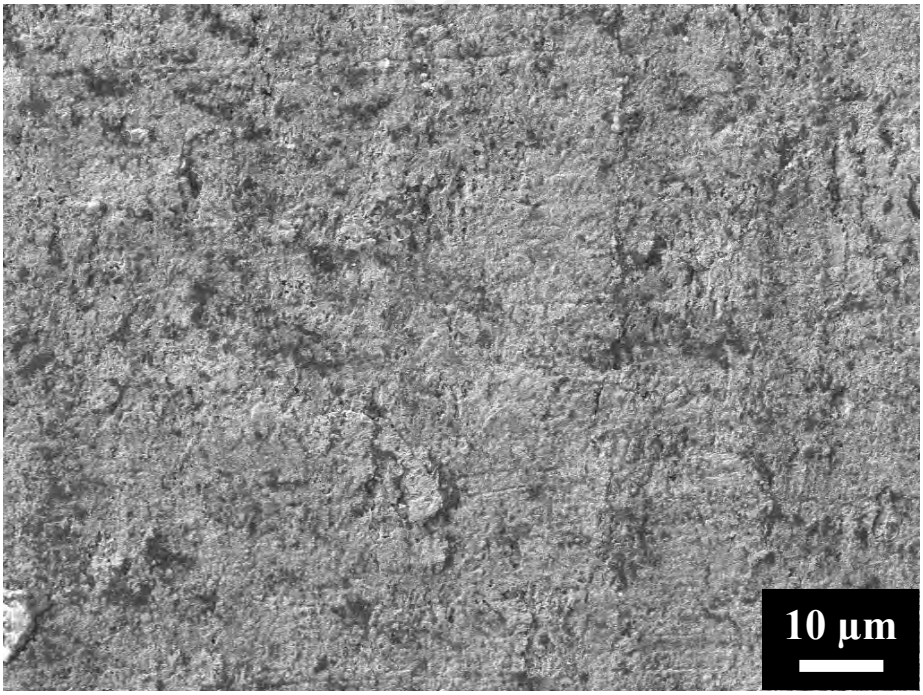

Figure 4.42: Surface morphology of SPD implant at low magnification (1000×)

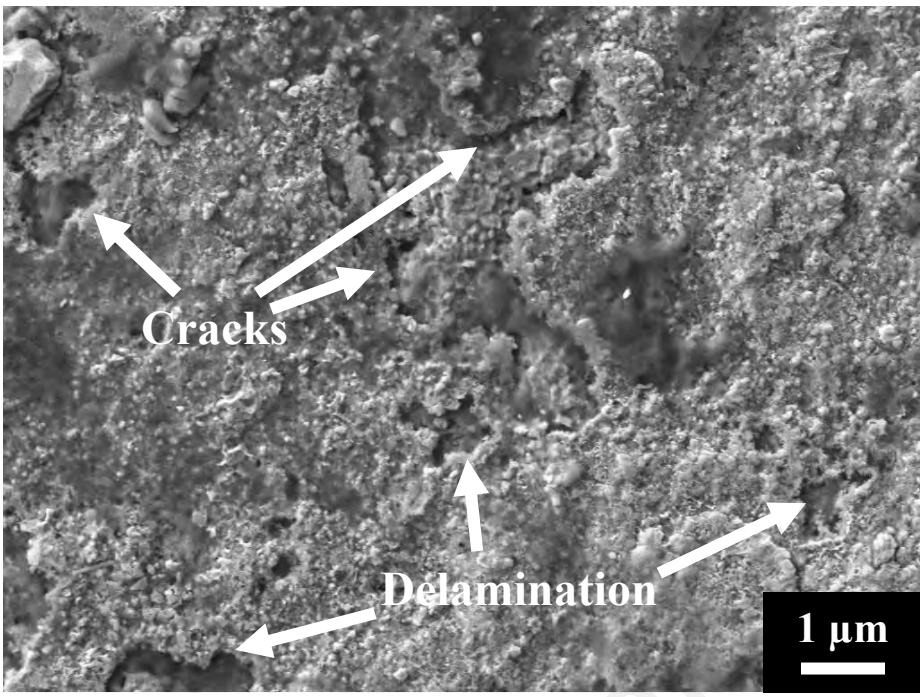

Figure 4.43: Surface morphology of SPD implant at high magnification (10000×)

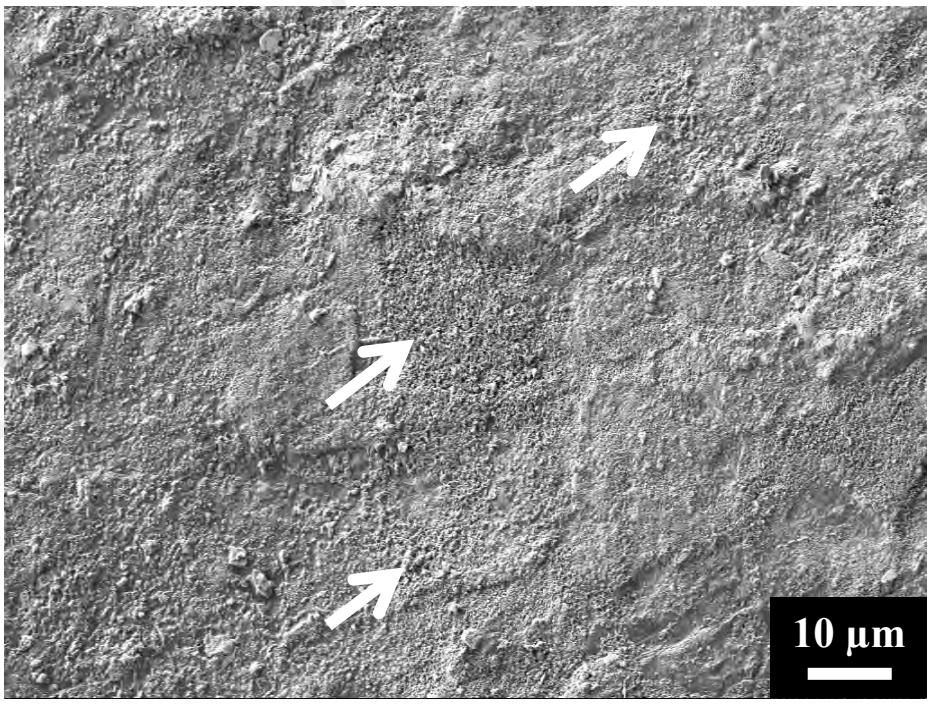

Figure 4.44: Worn surface morphology of SPD implant after 1 week of implantation at low magnification (1000×)

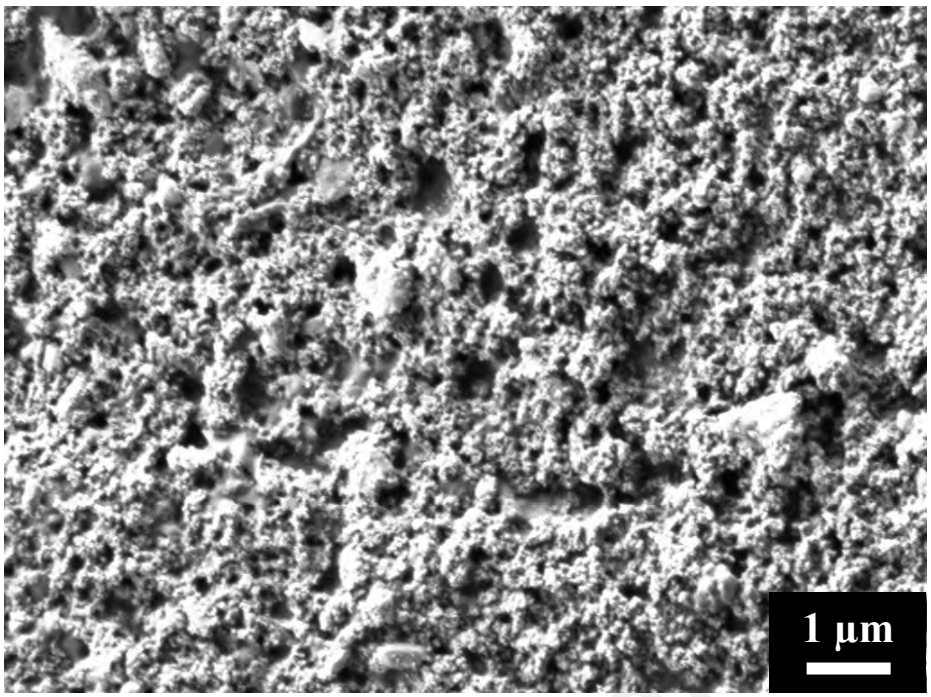

Figure 4.45: Worn surface morphology of SPD implant after 1 week of implantation at high magnification (10000×)

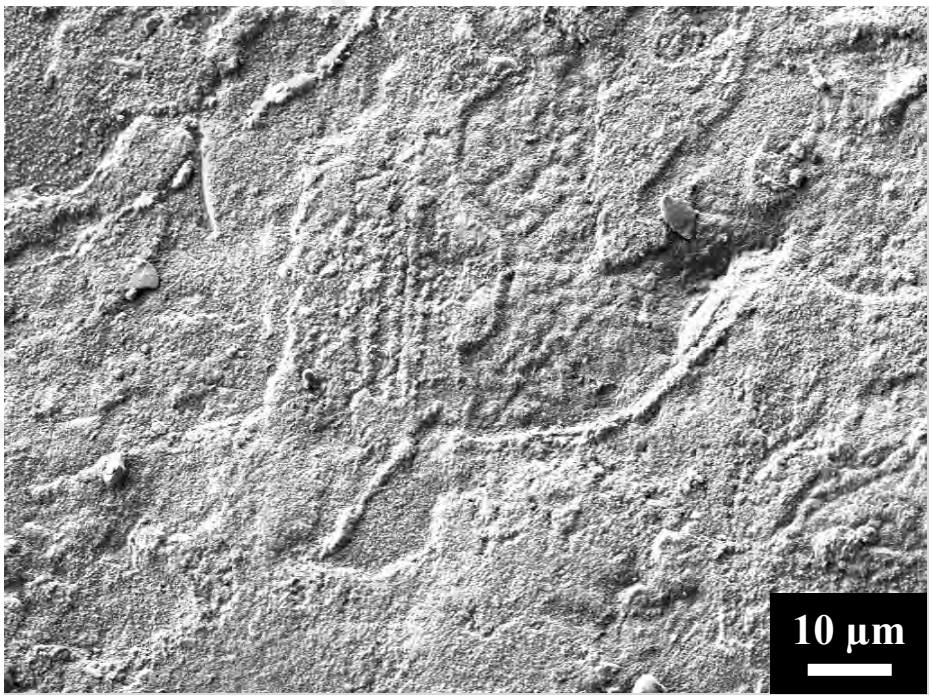

Figure 4.46: Worn surface morphology of SPD implant after 12 weeks of implantation at low magnification (1000×)

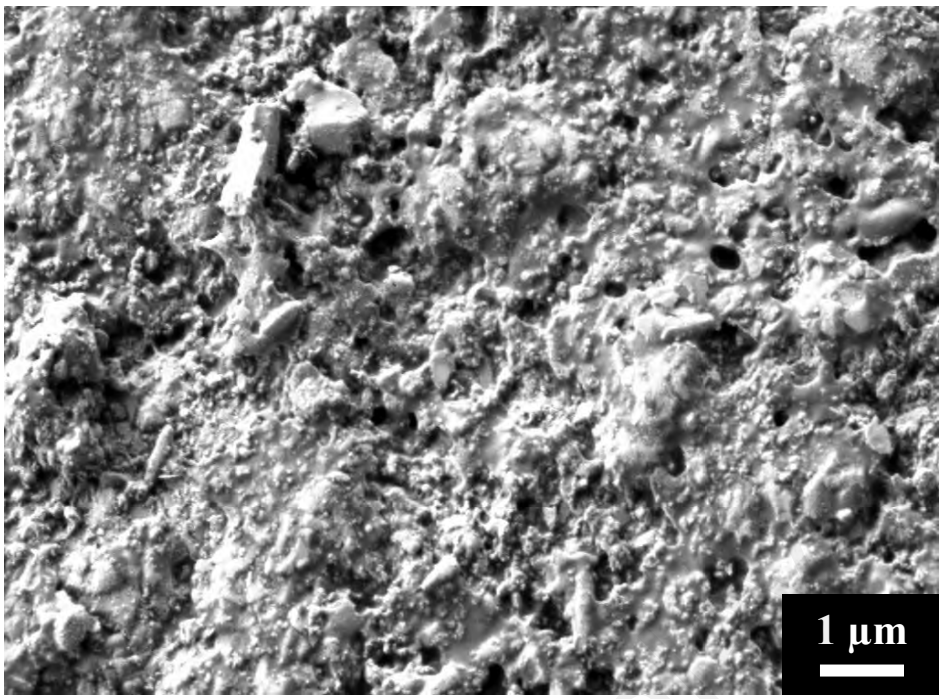

Figure 4.47: Worn surface morphology of SPD implant after 12 weeks of implantation at high magnification (10000×)

Figure 4.48 summarizes the HA layer thickness of the SPE and SPD samples before and after wear testing. For SPE, HA surface removal from the sample at 1 week of implantation clearly reached that of the after-embedment HA layer, where almost all of the newly-formed HA layer was removed (from 537.9±27.3 to 239.9±57.1 nm). In the 12week sample, the HA surface removal occurred within the newly-formed HA layer (from 874.8±37 to 415.3±41.1 nm). For SPD, HA layer removal in both 1 and 12week samples was within the newly-formed HA layer. HA layer removal was from 731.8±50.8 to 269.3±68.7 nm and 1162.6±91.3 to 444.3±45.1 nm for 1 and 12 weeks of implantation, respectively. A p below 0.05 was achieved for the SPE and SPD samples before and after wear testing at 1 and 12 weeks.

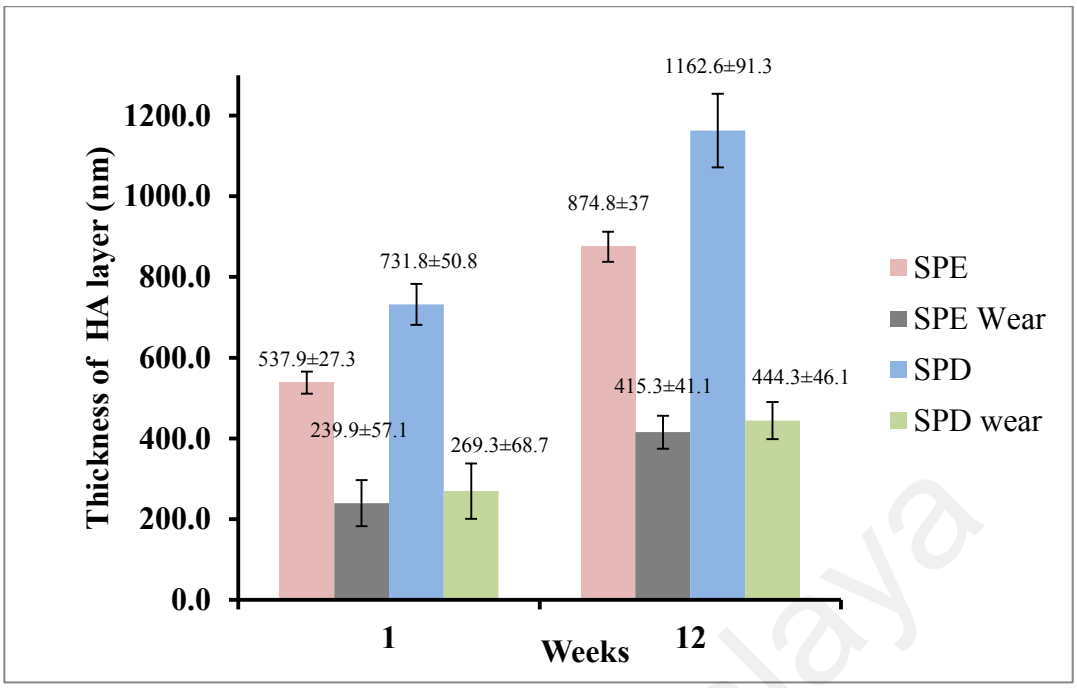

Figure 4.48: HA layer thicknesses in SPD and SPE samples before and after wear testing ($p < 0.05$). Each value is the average of five tests; the values are given as the mean± standard deviation

According to the results, both SPE and SPD samples were able to withstand the durability test (wear test in this study) to some extent. For SPE, although the newly-formed HA layer in the implantation sample at 1 week was almost completely removed after the wear test, as the sample was implanted in the tissue for up to 12 weeks, the newly-formed HA layer on top of the existing HA layer became adequately strong to withstand wear. As for SPD, even after a week, the newly-formed HA layer strengthened adequately.

The implant biocompatibility and HA layer durability were strongly related to the ability of the new HA layer to grow on top of the original HA layer. The SPD sample demonstrated that it is a suitable candidate for future medical implant applications.

CHAPTER 5: CONCLUSION AND RECOMMENDATIONS

5.1 Conclusion

From this study, the following conclusions are derived:

1. An implant comprising as-received Ti-6Al-4V embedded with hydroxyapatite (HA) was produced successfully by two different coating methods, namely Superplastic Embedment (SPE) and Superplastic Deformation (SPD). Dense HA layers with 249.1±0.6 nm and 206.1±5.8 nm thickness and 661±0.4 HV and 585±6.6 HV surface hardness formed on the SPE and SPD samples, respectively. XRD characterization confirmed that the HA crystallinity improved after experiencing deformation (SPD).
2. The bioactivity of as-received Ti-6Al-4V, SPE and SPD samples was analysed after implanting them subcutaneously on the backs of SD rat models for 1, 5 and 12 weeks. For the SPE and SPD samples, the newly formed HA layer was able to grow on the initial HA layer even after a week of implantation. The growth of the newly formed HA layer was strongly dependent on the degree of initial HA layer crystallinity. The SPD sample showed much faster growth of the newly formed HA layer compared with SPE, because the degree of HA crystallinity in the initial layer was higher. The surface hardness values for SPE and SPD samples after 12 weeks of implantation decreased to 586±1.3 HV and 425±86.9 HV respectively. This is because the newly formed HA layer was basically more porous than the initial HA layer. However, the values were still higher than the substrate alloy (321±28.8 HV).
3. According to histological evaluations, tissue necrosis was completely absent and there was no evidence of extended acute inflammation for all samples. The SPD sample exhibited the best biocompatibility because the space left by implant removal was almost completely filled by fibrous tissue, suggesting that the body

system's response to the SPD sample was accelerated by the more bioactive HA layer.

4. The wear test suggests that both SPE and SPD samples were able to withstand the durability testing to some extent, with the SPD sample having adequately strengthened the newly-formed HA layer, indicating the best durability test result.

The bioactivity, biocompatibility and durability results confirmed the potential of the SPD sample for medical implant applications.

5.2 Recommendations

Recommendations for future research are listed as follows:

1. It is known the Ti-6Al-4V is an alloy highly reactive to nature. Hence future experiments should be carried out in vacuum condition during the embedment process.
2. Since implants are applied more to bone areas, the biocompatibility of SPE and SPD implants in joint reconstruction can also be accessed in large animals like rabbits or sheep.
3. The durability of the newly-formed HA layers of SPE and SPD can be evaluated perfectly by using fatigue tests.

REFERENCES

Alabort, E., Putman, D., & Reed, R. C. (2015). Superplasticity in Ti–6Al–4V: Characterisation, modelling and applications. *Acta Materialia, 95*, 428-442.

Apachitei, I., Lonyuk, B., Fratila-Apachitei, L. E., Zhou, J., & Duszczyk, J. (2009). Fatigue response of porous coated titanium biomedical alloys. *Scripta Materialia, 61*(2), 113-116.

Balazic, M., Kopac, J., Jackson, M. J., & Ahmed, W. (2007). Review: titanium and titanium alloy applications in medicine. *International Journal of Nano and Biomaterials, 1*(1), 3-34.

Bigi, A., Fini, M., Bracci, B., Boanini, E., Torricelli, P., Giavaresi, G., . . . Giardino, R. (2008). The response of bone to nanocrystalline hydroxyapatite-coated Ti13Nb11Zr alloy in an animal model. *Biomaterials, 29*(11), 1730-1736.

Bohner, M., & Lemaitre, J. (2009). Can bioactivity be tested in vitro with SBF solution? *Biomaterials, 30*(12), 2175-2179.

Britannica, T. E. o. E. (2016). Encyclopedia Britannica *Titanium (Ti)*.

Brown, B. R. (2000). A Theory for Stretchiness. *Physics and Astronomy, 6*(10).

Chen, J., Bly, R. A., Saad, M. M., AlKhodary, M. A., El-Backly, R. M., Cohen, D. J., . . . Soboyejo, W. O. (2011). In-vivo study of adhesion and bone growth around implanted laser groove/RGD-functionalized Ti-6Al-4V pins in rabbit femurs. *Materials Science and Engineering: C, 31*(5), 826-832.

Chen, J., Mwenifumbo, S., Langhammer, C., McGovern, J. P., Li, M., Beye, A., & Soboyejo, W. O. (2007). Cell/surface interactions and adhesion on Ti-6Al-4V: Effects of surface texture. *Journal of Biomedical Materials Research Part B: Applied Biomaterials, 82B*(2), 360-373.

Chen, J., Tong, W., Cao, Y., Feng, J., & Zhang, X. (1997). Effect of atmosphere on phase transformation in plasma-sprayed hydroxyapatite coatings during heat treatment. *Journal of Biomedical Materials Research, 34*(1), 15-20.

Cheng, T., Chen, Y., & Nie, X. (2013). Insertion torques influenced by bone density and surface roughness of HA–TiO2 coatings. *Thin Solid Films, 549*, 123-130.

Cheong, B. H., Lin, J., & Ball, A. A. (2001). Modelling of hardening due to grain growth for a superplastic alloy. *Journal of Materials Processing Technology, 119*(1–3), 361-365.

Collier, J. P., Surprenant, V. A., Mayor, M. B., Wrona, M., Jensen, R. E., & Surprenant, H. P. (1993). Loss of hydroxyapatite coating on retrieved, total hip components. *The Journal of Arthroplasty, 8*(4), 389-393.

D., W., & Callister, J. (2003). *Materials science and engineering an introduction*. United States of America: John Wiley & Sons, Inc.

Darimont, G. L., Cloots, R., Heinen, E., Seidel, L., & Legrand, R. (2002). In vivo behaviour of hydroxyapatite coatings on titanium implants: a quantitative study in the rabbit. *Biomaterials, 23*(12), 2569-2575.

de Jonge, L. T., Leeuwenburgh, S. C. G., van den Beucken, J. J. J. P., te Riet, J., Daamen, W. F., Wolke, J. G. C., . . . Jansen, J. A. (2010). The osteogenic effect of electrosprayed nanoscale collagen/calcium phosphate coatings on titanium. *Biomaterials, 31*(9), 2461-2469.

Ding, R., Guo, Z. X., & Wilson, A. (2002). Microstructural evolution of a Ti–6Al–4V alloy during thermomechanical processing. *Materials Science and Engineering: A, 327*(2), 233-245.

Edington, J. W., Melton, K. N., & Cutler, C. P. (1976). Superplasticity. *Progress in Materials Science, 21*(1–2), 61-170.

Efunda. (2016). Titanium Alloys. *Efunda*.

Encyclopedia of Materials Science and Engineering: Co - E. (1986). Pergamon.

Fathi, M. H., Hanifi, A., & Mortazavi, V. (2008). Preparation and bioactivity evaluation of bone-like hydroxyapatite nanopowder. *Journal of Materials Processing Technology, 202*(1–3), 536-542.

Forsgren, J., Svahn, F., Jarmar, T., & Engqvist, H. (2007). Formation and adhesion of biomimetic hydroxyapatite deposited on titanium substrates. *Acta Biomaterialia, 3*(6), 980-984.

Froes, F. H., & Bomberger, H. B. (2012). The Beta Titanium Alloys. *JOM, 37*(7), 28-37.

Fukuda, A., Takemoto, M., Saito, T., Fujibayashi, S., Neo, M., Yamaguchi, S., . . . Nakamura, T. (2011). Bone bonding bioactivity of Ti metal and Ti–Zr–Nb–Ta alloys with Ca ions incorporated on their surfaces by simple chemical and heat treatments. *Acta Biomaterialia, 7*(3), 1379-1386.

Fulzele, S. V., Satturwar, P. M., & Dorle, A. K. (2003). Study of the biodegradation and in vivo biocompatibility of novel biomaterials. *European Journal of Pharmaceutical Sciences, 20*(1), 53-61.

Gallagher, L. (2004). Enhancement of Cryogenically Treated Lacrosse Shafts. from http://www.learningace.com/doc/53096/c8affd000f8b0f06607e9dc0b17b1a0f/independent-study-paper-cryogenics

Garriga-Majo, D., Paterson, R. J., Curtis, R. V., Said, R., Wood, R. D., & Bonet, J. (2004). Optimisation of the superplastic forming of a dental implant for bone augmentation using finite element simulations. *Dental Materials, 20*(5), 409-418.

Ghosh, A. K., & Hamilton, C. H. (1979). Mechanical behavior and hardening characteristics of a superplastic Ti-6AI-4V alloy. *Metallurgical Transactions A, 10*(6), 699-706.

Giuliano, G. (2008). Constitutive equation for superplastic Ti–6Al–4V alloy. *Materials & Design, 29*(7), 1330-1333.

Gu, Y. W., Khor, K. A., & Cheang, P. (2003). In vitro studies of plasma-sprayed hydroxyapatite/Ti-6Al-4V composite coatings in simulated body fluid (SBF). *Biomaterials, 24*(9), 1603-1611.

Guo, M.-L., Liu, J., Tan, M.-J., & Chua, B.-W. (2014). Microstructure Evolution of Ti-6Al-4V during Superplastic-like Forming. *Procedia Engineering, 81*, 1090-1095.

Hefti, L. D. (2007). Innovations in the Superplastic Forming and Diffusion Bonded Process. *Journal of Materials Engineering and Performance, 17*(2), 178-182.

Henkel, D. P., & Pense, A. W. (2002). *Structure and Properties of Engineering Materials*: McGraw-Hill.

Hieda, J., Niinomi, M., Nakai, M., Cho, K., Mohri, T., & Hanawa, T. (2014). Adhesive strength of medical polymer on anodic oxide nanostructures fabricated on biomedical β-type titanium alloy. *Materials Science and Engineering: C, 36*, 244-251.

Huang, J., Best, S. M., Bonfield, W., & Buckland, T. (2010). Development and characterization of titanium-containing hydroxyapatite for medical applications. *Acta Biomaterialia, 6*(1), 241-249.

Jamlus, S. A., Jauhari, I., & Khalid, H. M. (2014). Mechanical and biological stability of superplastically embedded HA nanolayer deformed at high temperature. *Materials Science and Engineering: C, 43*(0), 566-572.

Karanjai, M., Kumar, B. V. M., Sundaresan, R., Basu, B., Rama Mohan, T. R., & Kashyap, B. P. (2008). Fretting wear study on Ti–Ca–P biocomposite in dry and simulated body fluid. *Materials Science and Engineering: A, 475*(1–2), 299-307.

Kaya, C. (2008). Electrophoretic deposition of carbon nanotube-reinforced hydroxyapatite bioactive layers on Ti–6Al–4V alloys for biomedical applications. *Ceramics International, 34*(8), 1843-1847.

Kim, Y. H., Lee, J.-M., & Hong, S. S. (2001). Optimal design of superplastic forming processes. *Journal of Materials Processing Technology, 112*(2–3), 166-173.

Kurzweg, H., Heimann, R. B., Troczynski, T., & Wayman, M. L. (1998). Development of plasma-sprayed bioceramic coatings with bond coats based on titania and zirconia. *Biomaterials, 19*(16), 1507-1511.

Lakstein, D., Kopelovitch, W., Barkay, Z., Bahaa, M., Hendel, D., & Eliaz, N. (2009). Enhanced osseointegration of grit-blasted, NaOH-treated and electrochemically hydroxyapatite-coated Ti–6Al–4V implants in rabbits. *Acta Biomaterialia, 5*(6), 2258-2269.

Layman, T. (1961). *Metals Handbook*. OH: American Society for Metals: Metals Park.

Lee, H.-S., Yoon, J.-H., Park, C. H., Ko, Y. G., Shin, D. H., & Lee, C. S. (2007). A study on diffusion bonding of superplastic Ti–6Al–4V ELI grade. *Journal of Materials Processing Technology, 187–188*, 526-529.

Lee, Y.-S., Lee, S.-Y., & Lee, J.-H. (2001). A study on the process to control the cavity and the thickness distribution of superplastically formed parts. *Journal of Materials Processing Technology, 112*(1), 114-120.

Leyens, C., & Peters, M. (2003). *Titanium and Titanium Alloys: Fundamentals and Applications* Retrieved from http://onlinelibrary.wiley.com/doi/10.1002/3527602119.fmatter/pdf

Li, H., Khor, K. A., & Cheang, P. (2007). Adhesive and bending failure of thermal sprayed hydroxyapatite coatings: Effect of nanostructures at interface and crack propagation phenomenon during bending. *Engineering Fracture Mechanics, 74*(12), 1894-1903.

Liang, H., Shi, B., Fairchild, A., & Cale, T. (2004). Applications of plasma coatings in artificial joints: an overview. *Vacuum, 73*(3–4), 317-326.

Lin, D.-J., Chuang, C.-C., Chern Lin, J.-H., Lee, J.-W., Ju, C.-P., & Yin, H.-S. (2007). Bone formation at the surface of low modulus Ti–7.5Mo implants in rabbit femur. *Biomaterials, 28*(16), 2582-2589.

Matsushita, M., Ogiyama, H., Suko, T., & Matsuda, S. (2009). Study on solid-phase welding of duplex stainless steel with carbon steel based on superplasticity and consideration of the cyclic fatigue fracture behavior. *Materials Chemistry and Physics, 114*(2–3), 599-603.

Mohamad Dom, A. H., Jauhari, I., Yazdanparast, S., & Khalid, H. M. (2010). Embedment of HA/Ti composite on superplastic titanium alloy (Ti–6Al–4V). *Materials Science and Engineering: A, 527*(21–22), 5831-5836.

Morais, J. M., Papadimitrakopoulos, F., & Burgess, D. J. (2010). Biomaterials/Tissue Interactions: Possible Solutions to Overcome Foreign Body Response. *The AAPS Journal, 12*(2), 188-196.

Nakahigashi, J., & Yoshimura, H. (2002). Superplasticity and Its Application of Ultra-Fine Grained Ti-6Al-4V Alloy Obtained through Protium Treatment. *MATERIALS TRANSACTIONS, 43*(11), 2768-2772.

Nandi, S. K., Kundu, B., Mukherjee, J., Mahato, A., Datta, S., & Balla, V. K. (2015). Converted marine coral hydroxyapatite implants with growth factors: In vivo bone regeneration. *Materials Science and Engineering: C, 49*, 816-823.

Nie, X., Leyland, A., & Matthews, A. (2000). Deposition of layered bioceramic hydroxyapatite/TiO2 coatings on titanium alloys using a hybrid technique of micro-arc oxidation and electrophoresis. *Surface and Coatings Technology, 125*(1–3), 407-414.

Nieh, T. G., & Wadsworth, J. (1997). Microstructural characteristics and deformation properties in superplastic intermetallics. *Materials Science and Engineering: A, 239–240*, 88-96.

Overgaard, S., Bromose, U., Lind, M., Bunger, C., & Soballe, K. (1999). The influence of crystallinity of the hydroxyapatite coating on the fixation of implants. Mechanical and histomorphometric results. *J Bone Joint Surg Br, 81*(4), 725-731.

Park, C. H., Ko, Y. G., Park, J.-W., & Lee, C. S. (2008). Enhanced superplasticity utilizing dynamic globularization of Ti–6Al–4V alloy. *Materials Science and Engineering: A, 496*(1–2), 150-158.

Pilling, J., & Ridley, N. (1989). Superplasticity in crystalline solids. *Inst. Book/Inst. of metals*.

Ramdan, R. D., Jauhari, I., Hasan, R., & Masdek, N. R. N. (2008). The role of strain rate during deposition of CAP on Ti6Al4V by superplastic deformation-like method using high-temperature compression test machine. *Materials Science and Engineering: A, 477*(1–2), 300-305.

Sato, Y., Yokoyama, A., Kasai, T., Hashiguchi, S., Ootsubo, M., Ogino, S.-i., . . . Tohji, K. (2008). In vivo rat subcutaneous tissue response of binder-free multi-walled carbon nanotube blocks cross-linked by de-fluorination. *Carbon, 46*(14), 1927-1934.

Scemama, C., David, B., Bensidhoum, M., & Hamadouche, M. (2014). Osseointegration of polyethylene implants coated with titanium and biomimetically or electrochemically deposited hydroxyapatite in a rabbit model. *International Orthopaedics, 38*(8), 1739-1744.

Shakya, A., & Kumar, A. (2016). Biocompatibility of Macroporous Cryogel Materials *Supermacroporous Cryogels* (pp. 199-218): CRC Press.

Siegert, K., & Werle, T. (1994). Physical Mechanism of Superplasticity *TALAT Lecture 3802* Institut für Umformtechnik, Universität Stuttgart

Song, W.-H., Jun, Y.-K., Han, Y., & Hong, S.-H. (2004). Biomimetic apatite coatings on micro-arc oxidized titania. *Biomaterials, 25*(17), 3341-3349.

Srinivasa Raghavan, K. (1984). Superplasticity. *Bulletin of Materials Science, 6*(4), 689-698.

Stergioudi, F., Choleridis, A., Paulidou, E., Smyrnaios, E., & Michailidis, N. (2015). Novel production and characterization of porous calcium phosphate suitable for bone tissue engineering applications. *Ceramics International, 41*(3, Part A), 3822-3832.

Surmenev, R. A., Surmeneva, M. A., & Ivanova, A. A. (2014). Significance of calcium phosphate coatings for the enhancement of new bone osteogenesis – A review. *Acta Biomaterialia, 10*(2), 557-579.

Tahmasbi Rad, A., Solati-Hashjin, M., Osman, N. A. A., & Faghihi, S. (2014). Improved bio-physical performance of hydroxyapatite coatings obtained by electrophoretic deposition at dynamic voltage. *Ceramics International, 40*(8, Part B), 12681-12691.

Takemoto, M., Fujibayashi, S., Neo, M., Suzuki, J., Kokubo, T., & Nakamura, T. (2005). Mechanical properties and osteoconductivity of porous bioactive titanium. *Biomaterials, 26*(30), 6014-6023.

Tian, Z. R. (2008). Nanotechnology for improving bone implants. *BONE Zone, 7*(10), 78-80.

Vanderhasten, M., Rabet, L., & Verlinden, B. (2008). Ti–6Al–4V: Deformation map and modelisation of tensile behaviour. *Materials & Design, 29*(6), 1090-1098.

Wang, G., & Fu, M. W. (2007). Maximum m superplasticity deformation for Ti–6Al–4V titanium alloy. *Journal of Materials Processing Technology, 192–193*, 555-560.

Wang, H., Eliaz, N., Xiang, Z., Hsu, H.-P., Spector, M., & Hobbs, L. W. (2006). Early bone apposition in vivo on plasma-sprayed and electrochemically deposited hydroxyapatite coatings on titanium alloy. *Biomaterials, 27*(23), 4192-4203.

Wang, J., Chao, Y., Wan, Q., Zhu, Z., & Yu, H. (2009). Fluoridated hydroxyapatite coatings on titanium obtained by electrochemical deposition. *Acta Biomaterialia, 5*(5), 1798-1807.

Wang, X.-h., Li, J.-s., Hu, R., Kou, H.-c., & Zhou, L. (2013). Mechanical properties of porous titanium with different distributions of pore size. *Transactions of Nonferrous Metals Society of China, 23*(8), 2317-2322.

Watari, F., Yokoyama, A., Omori, M., Hirai, T., Kondo, H., Uo, M., & Kawasaki, T. (2004). Biocompatibility of materials and development to functionally graded implant for bio-medical application. *Composites Science and Technology, 64*(6), 893-908.

Yang, Y.-C., & Yang, C.-Y. (2013). Mechanical and histological evaluation of a plasma sprayed hydroxyapatite coating on a titanium bond coat. *Ceramics International, 39*(6), 6509-6516.

Yao, Z. Q., Ivanisenko, Y., Diemant, T., Caron, A., Chuvilin, A., Jiang, J. Z., . . . Fecht, H. J. (2010). Synthesis and properties of hydroxyapatite-containing porous titania coating on ultrafine-grained titanium by micro-arc oxidation. *Acta Biomaterialia, 6*(7), 2816-2825.

Yazdan Parast, S., Jauhari, I., & Asle Zaeem, M. (2011). Implantation of HA into Superplastic Ti-6Al-4V: Kinetics and Mechanical Behaviors of Implanted Layer. *Metallurgical and Materials Transactions A, 42*(1), 219-226.

Yildiz, F., Yetim, A. F., Alsaran, A., & Efeoglu, I. (2009). Wear and corrosion behaviour of various surface treated medical grade titanium alloy in bio-simulated environment. *Wear, 267*(5–8), 695-701.

Yip, C. S., Khor, K. A., Loh, N. L., & Cheang, P. (1997). Thermal spraying of Ti・6Al・4V/hydroxyapatite composites coatings: powder processing and post-spray treatment. *Journal of Materials Processing Technology, 65*(1‐3), 73-79.

Yoshida, Y., Kuroda, K., Ichino, R., Hayashi, N., Ogihara, N., & Nonaka, Y. (2012). Influence of surface properties on bioactivity and pull-out torque in cold thread rolled Ti rod—Development of bioactive metal-forming technology. *CIRP Annals - Manufacturing Technology, 61*(1), 579-582.

LIST OF PUBLICATIONS AND PAPERS PRESENTED

Khalid, H. M., Jauhari, I., Jamlus, S. A., & Dom, A. H. M. (2012). High temperature deformation of Ti alloy superplastically embedded with HA. *Materials Science and Engineering: A, 534*(0), 37-42. doi: http://dx.doi.org/10.1016/j.msea.2011.11.027

Khalid, H., Jauhari, I., & Dom, A. (2012). Development of Nanolayer Hydroxyapatite (HA) on Titanium Alloy via Superplastic Deformation Method. *Metallurgical and Materials Transactions A, 43*(10), 3776-3785. doi: 10.1007/s11661-012-1185-6

Khalid, H. M., Hasan, S. N., & Jauhari, I. (2016). Mechanical behaviour of nanolayer hydroxyapatite (HA) coating developed through superplastic embedment of titanium (Ti) alloy (Ti6Al4V). *Materials Chemistry and Physics, 177*, 314-321. doi: http://dx.doi.org/10.1016/j.matchemphys.2016.04.032

Hidayah Mohd, K., Iswadi, J., Haryanti Azura Mohamad, W., & Suhaeb Abdulrazzaq, M. (2017). Bioactivity and mechanical stability of Ti–6Al–4V implants superplastically embedded with hydroxyapatite in rats. *Biomedical Materials, 12*(1), 015019.

APPENDIX

Appendix 1: Surgical process flow

The procedure of subcutaneous implantation on the backs of Sprague Dawley (SD) rat models contains 7 steps. Before surgery, male SD rats 8weeks old and weighing approximately 250 g were used. The procedure steps are listed below

i) The rats were anaesthetized via intramuscular administration of Ketamine 50mg/kg and Xylazine 5mg/kg (mixed in the same syringe) before the surgical procedure.

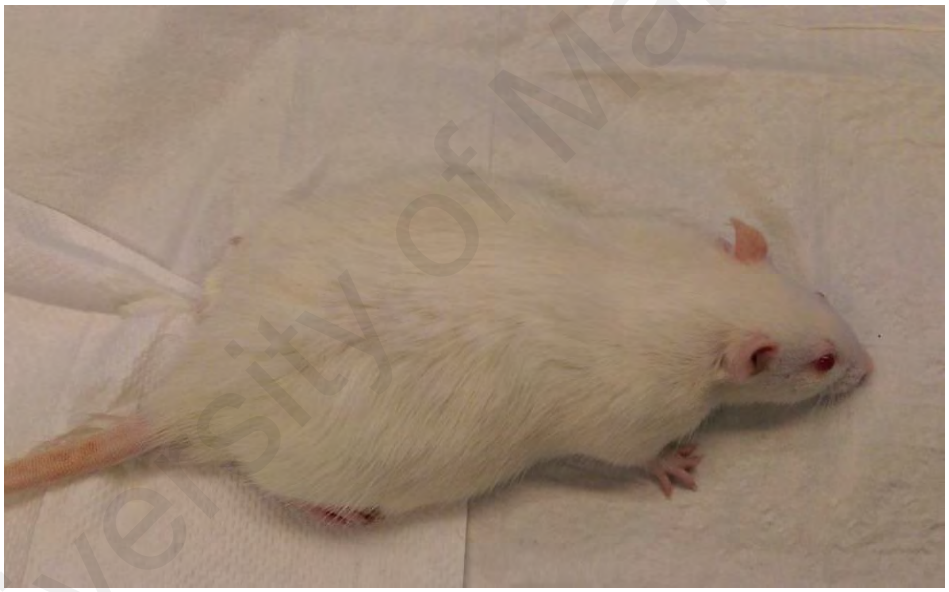

ii) Size of 2cm × 4cm of fur on the dorsum area was completely shaved by using Gillet razor blades.

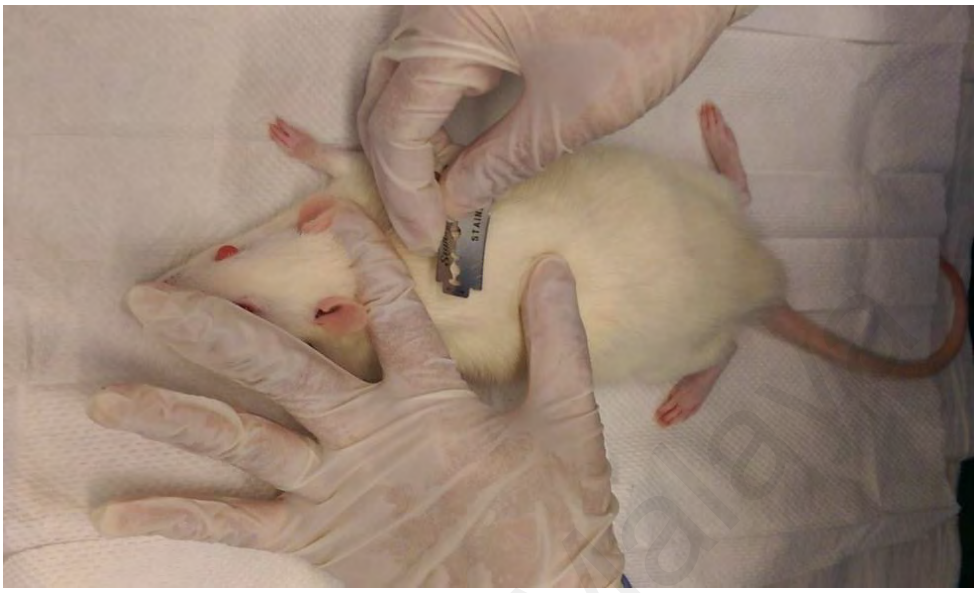

iii) The area for surgery was cleaned with betadine solution (10%).

iv) A small transverse dorsal incision of approximately 1 cm was made.

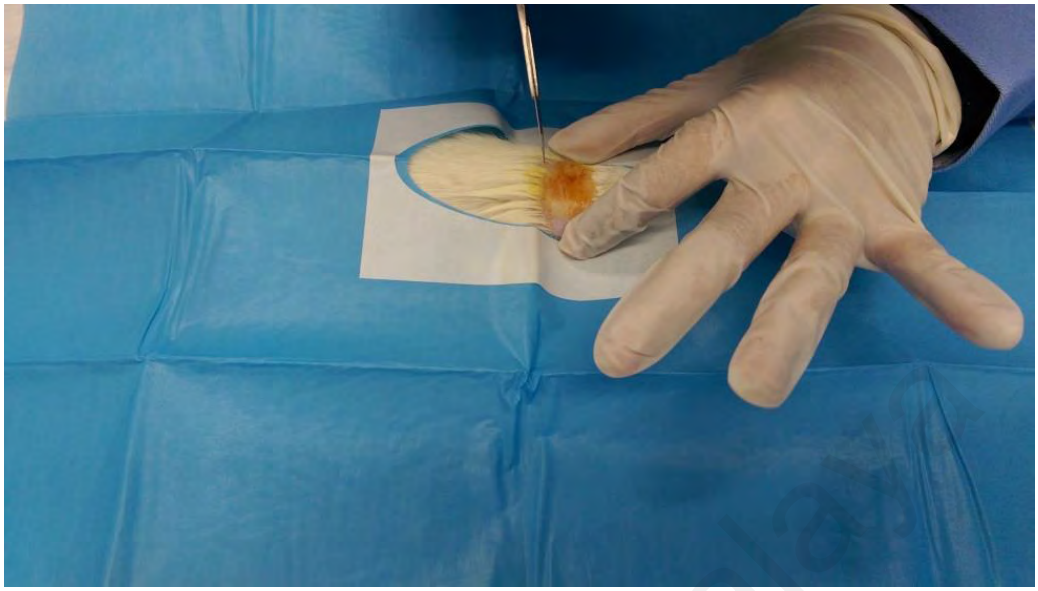

v) The substitution layer was spread to create a pocket by using dissecting scissors.

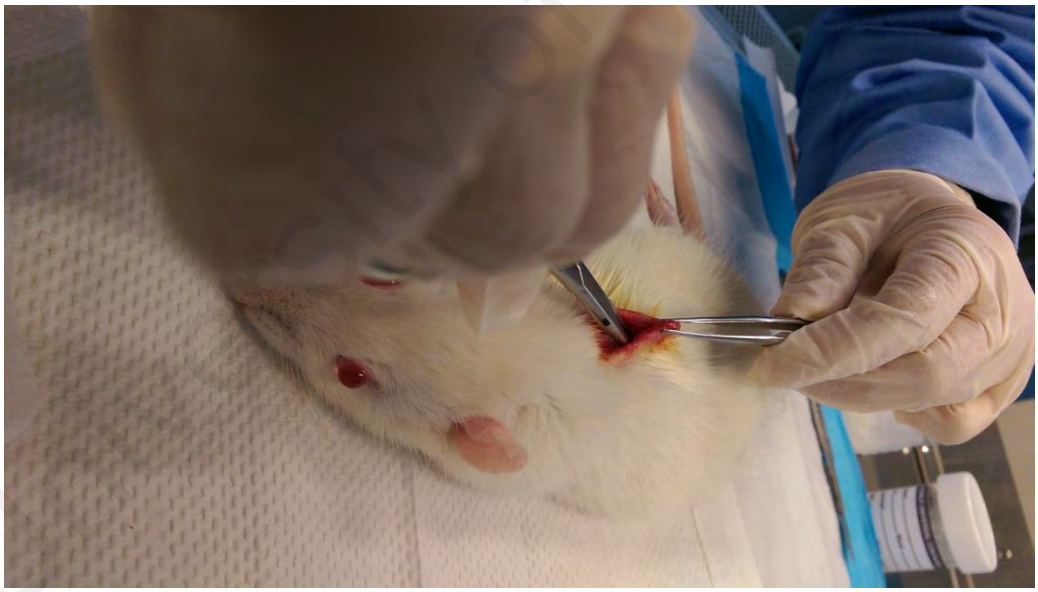

vi) The respective implant was then removed from the covering and inserted into the incision.

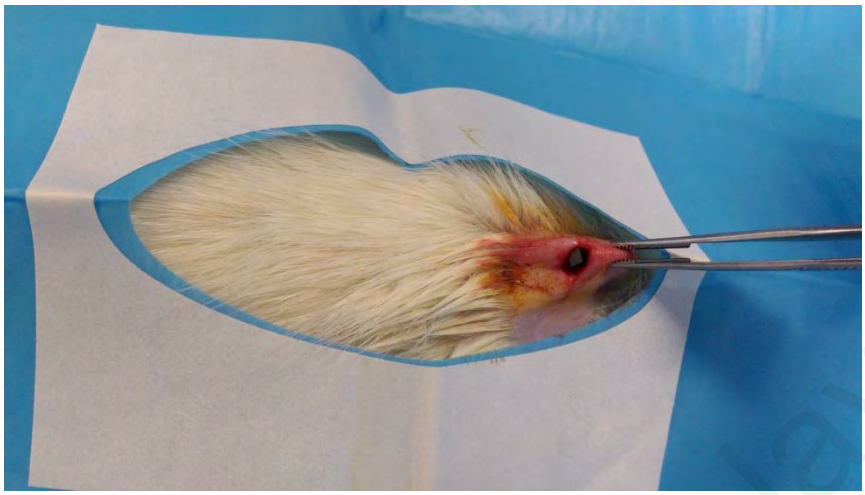

vii) Each incision was closed by intermittent suturing (0.5 cm apart) using surgical nylon thread and No. 4 suture.

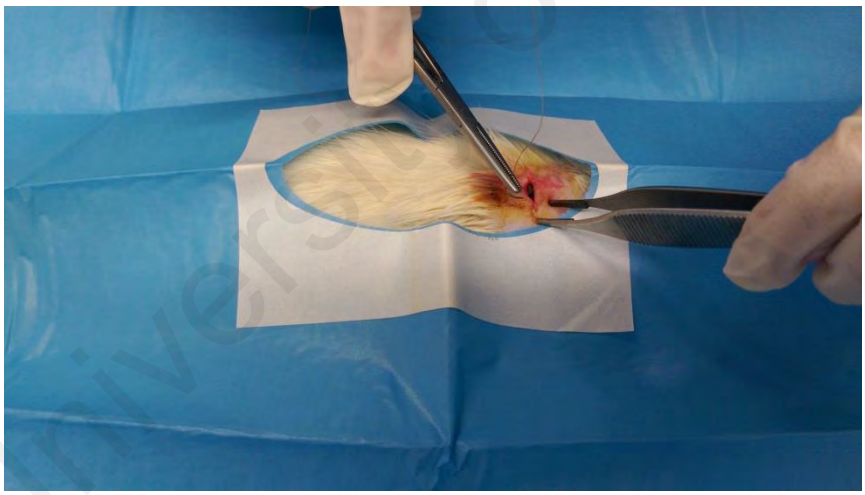

viii) Antibiotic (Kombitrim, which is a combination of Trimethoprim and Sulfadiazine) and Meloxicam as analgesics were administered post operatively for 3 consecutive days based on the animal's weight.

The rats were sequentially euthanized with CO_2 at specific times after the surgery.